ANALYSIS AND DESIGN OF CONFORMAL FREQUENCY SELECTIVE SURFACES

A THESIS SUBMITTED TO
THE GRADUATE SCHOOL OF NATURAL AND APPLIED SCIENCES
OF
MIDDLE EAST TECHNICAL UNIVERSITY

BY

AKIN DALKILIÇ

IN PARTIAL FULFILLMENT OF THE REQUIREMENTS
FOR
THE DEGREE OF MASTER OF SCIENCE
IN
ELECTRICAL AND ELECTRONICS ENGINEERING

JUNE 2014

Approval of the thesis:

ANALYSIS AND DESIGN OF CONFORMAL FREQUENCY SELECTIVE SURFACES

submitted by **AKIN DALKILIÇ** in partial fulfillment of the requirements for the degree of **Master of Science in Electrical and Electronics Engineering Department, Middle East Technical University** by,

Prof. Dr. Canan Özgen
Dean, Graduate School of **Natural and Applied Sciences** _____

Prof. Dr. Gönül Turhan Sayan
Head of Department, **Electrical and Electronics Eng.** _____

Assoc. Prof. Dr. Lale Alatan
Supervisor, **Electrical and Electronics Eng. Dept.,METU** _____

Examining Committee Members:

Prof. Dr. Nilgün Günalp
Electrical and Electronics Eng. Dept.,METU _____

Assoc. Prof. Dr. Lale Alatan
Electrical and Electronics Eng. Dept.,METU _____

Prof. Dr. Gönül Turhan Sayan
Electrical and Electronics Eng. Dept.,METU _____

Prof. Dr. Gülbin Dural
Electrical and Electronics Eng. Dept.,METU _____

Can Barış Top, Ph.D.
ASELSAN _____

Date: **11.06.2014**

I hereby declare that all information in this document has been obtained and presented in accordance with academic rules and ethical conduct. I also declare that, as required by these rules and conduct, I have fully cited and referenced all material and results that are not original to this work.

Name, Last name: Akın DALKILIÇ

Signature:

ABSTRACT

ANALYSIS AND DESIGN OF CONFORMAL FREQUENCY SELECTIVE SURFACES

Dalkılıç, Akın
M. Sc., Department of Electrical and Electronics Engineering
Supervisor: Assoc. Prof. Dr. Lale Alatan

June 2014, 112 pages

An efficient analysis and design approach for conformal frequency selective surface (FSS) structures is developed. The design methodology involves the analysis of both the planar and curved FSS structures. First, planar unit cell analysis of conformal FSS models are accomplished for normal and oblique incidence cases. To prove conformal applicability of planar designs, a semi-finite analysis method is utilized. This method is based on solution of a singly periodic curved FSS structure of semi-cylinder shape possessing periodicity, curved element arrangement and finite model conditions together. The model is finite in curved direction and infinite along the axis of the cylinder. Semi-finite model analysis is a powerful solution tool to determine both transmission and reflection responses of conformal FSS structures. With the introduced design methodology for conformal FSS implementations, a narrow band FSS radome operating in Ku-band and a wide band FSS model serving as a band-pass spatial filter for X-band (8.2-12.4 GHz) signals are designed. FSS performances are verified with both planar single element unit cell solutions and semi-finite analyses of curved and planar structures. Planar prototypes of narrowband FSS model are fabricated and measured. Reasons for discrepancies between simulated and measured filtering characteristics are investigated and explained.

KEYWORDS: Frequency Selective Surface (FSS), Conformal FSS, RCS reduction, Coupled Aperture FSS, Wide band FSS

ÖZ

KONFORMAL FREKANS SEÇİCİ YÜZEYLERİN ANALİZ VE TASARIMI

Dalkılıç, Akın
Yüksek Lisans, Elektrik ve Elektronik Mühendisliği Bölümü
Tez Yöneticisi: Doç. Dr. Lale Alatan

Haziran 2014, 112 sayfa

Konformal frekans seçici yüzey (FSY) yapıları için etkin bir analiz ve tasarım yaklaşımı geliştirilmiştir. Tasarım yöntemi hem düzlemsel hem de eğimli FSY elemanlarının analizini içermektedir. İlk aşamada konformal FSY modellerinin düzlemsel birim hücre analizleri dik ve farklı açılarda yayın geldiği durumlar için gerçekleştirilmektedir. Düzlemsel modellerin konformal yüzeylerde uygulanabilirliğini kanıtlamak için yarı-sonlu analiz yöntemi kullanılmıştır. Temel olarak bu yöntem tek yönde periyodik, bükümlü, yarım silindir şeklindeki FSY yapısının periyodiklik, konformal eleman ve sonlu model koşullarının etkilerini içerecek şekilde çözümünü ifade etmektedir. Kullanılan model kavisli olduğu yönde sonlu, boylamsal yönde ise sonsuz uzunluktadır. Yarı-sonlu model analizi, konformal FSY yapılarının geçirgenlik ve yansıma performanslarının tespit edilebileceği güçlü bir çözüm aracıdır. Konformal FSY uygulamaları için bildirilen tasarım yöntemi ile Ku-bantta çalışan dar bantlı FSY radom ile X-bant (8.2-12.4 GHz) frekanslarının tamamını kapsayan geniş bantlı bant-geçiren bir FSY yapısı tasarlanmıştır. FSY performansları hem düzlemsel tek eleman birim hücre çözümüyle hem de yarı-sonlu analiz yöntemi ile düzlemsel ve eğimli modeller için doğrulanmıştır. Dar bantlı FSY modelinin düzlemsel prototiplerinin üretimi ve ölçümleri alt yapı koşullarının el verdiği ölçüde gerçekleştirilmiştir. Benzetim sonucu beklenen filtreleme performansı ile ölçümler arasındaki uyumsuzlukların sebepleri incelenmiş ve açıklanmıştır.

ANAHTAR KELİMELER: Frekans Seçici Yüzey (FSY), Konformal FSY, RKA azaltımı, Bağlaşık Açıklıklı FSY, Geniş Bantlı FSY

To Nazlım,

ACKNOWLEDGEMENTS

I would like to express my sincere gratitude to my advisor, Assoc. Prof. Dr. Lale Alatan, for her guidance, support and technical suggestions throughout the study.

I would like to express my gratitude to Dr. Can Barış Top providing invaluable support for both theoretical and practical topics throughout the study.

I am grateful to ASELSAN A.Ş. for the financial and technical opportunities provided for the completion of this thesis.

I would also like to express my sincere appreciation for Erdinç Erçil, Doğanay Doğan, Egemen Yıldırım, Mehmet Emre Demir and Onur Cem Erdoğan for their valuable friendship, motivation and help.

I would like to thank TÜBİTAK for providing financial support during the study.

For their understanding my spending lots of time on this work, I sincerely thank to my family.

TABLE OF CONTENTS

LIST OF TABLES

TABLES

LIST OF FIGURES

FIGURES

CHAPTER 1

INTRODUCTION

1.1 Preface

With advancing techniques in radar technologies, the invisibility of radar systems has become one of the major challenging topics over the years beginning with the spectacular progress after World War II [1]. To have almost invisible radar systems, RCS is the key parameter which has to be kept at minimum. RCS defines the scattering characteristics of a target. In other words, it is a measure of the reflected signals in the direction of receiving antenna. There are two cases for scattering: monostatic and bistatic. Monostatic scattering refers to backscattering, which means the transmitter and receiver antennas are at the same position. In bistatic cases, the transmitter and receiver are at different locations. RCS of a target is determined by different factors like polarization, angle of incidence, angle of observation, target geometry, electrical properties of target and frequency of operation [2]. Different methods are developed in order to have low observable targets. The major two methods to reduce the RCS of a target are "modifying the shape" and "using materials". The adjustment of the reflecting surface is implemented in order to reflect the incoming signal to other directions avoiding back scattering. Thus, the RCS of the target can be reduced significantly. However, the modification of the target surface is generally limited by other fundamental requirements of the operating systems like aerodynamic qualifications for flying air platforms. The materials are used to absorb the incoming wave and weaken the power of the reflecting signal resulting to low RCS. Generally, the shaped surfaces

and absorbing materials are treated together to maximize the effect in reducing the target RCS. Nevertheless, the absorber materials cannot be used over the radiating apertures. Thus, the use of FSS is required in order to lessen the RCS of the radiating structures. Frequency selective surfaces can be defined as any periodic structure, generally in two dimensions, which is modeled as metallic patches over dielectrics or apertures in metals and exhibits band-stop or band-pass characteristics, respectively. Frequency selective surfaces have a very wide range for many applications from the optic region to microwave frequencies. FSS are generally used in radar or telecommunication systems in order to reduce radar cross section (RCS) or to provide a dual-band operation for reflector antennas. Furthermore, FSS are also used in various applications like circuit analog absorbers, filters, polarizers and some recent applications such as RFID tags [3], robotic guided paths, photonic bandgap structures [4], collision avoidance, EMI protection [5] and secure building applications [6]. An interesting use of FSS on fabrics for wearable applications is mentioned in [7]. The first conceptual work about “periodic surfaces” was patented by Marconi and Franklin in 1919 [8]. FSS studies starting with Marconi and Franklin's invention have been continued by many researchers up to now. There has been a great interest in these structures especially since 1960's. However, the name “Frequency Selective Surface” was patented for the first time by Yee in 1993 [9]. The definitions and discussions about FSS phenomena are clearly declared by Munk, guru of FSS, in [1]. The first concept which should be understood is "Periodic Surface" since it constitutes the nature of FSS structures. A periodic surface consists of identical elements of infinite arrays in one or two dimensions. The factors affecting the performance of FSS structures can be listed as:

- Type of elements (patches vs. slots),
- Shape of elements,
- Dimensions of elements,
- Inter element spacing,
- Array configuration (i.e. rectangular, triangular, hexagonal etc.),

- Alignment of elements in multi-layer structures.

Moreover, the electrical properties of the substrate material also determine the performance of FSS. Therefore, there are numerous combinations of various parameters in order to reach an optimum solution for a specific problem.
Informative technical details about type and shape of FSS elements will be presented in the following sections.

1.1.1. Type of Elements: Patches and Slots (Apertures)

FSS structures are constructed with any of two types of elements: metallic patches on dielectric slabs or slots in metals. The metallic patches exhibit a capacitive behavior and low pass filtering characteristics (see Figure 1- 1.a). If the patches and apertures are replaced as shown in Figure 1- 1.b, the structure can be made inductive, which results in high-pass filtering properties [10]. In order to govern desired filtering characteristics, capacitive and inductive models can be arranged together.

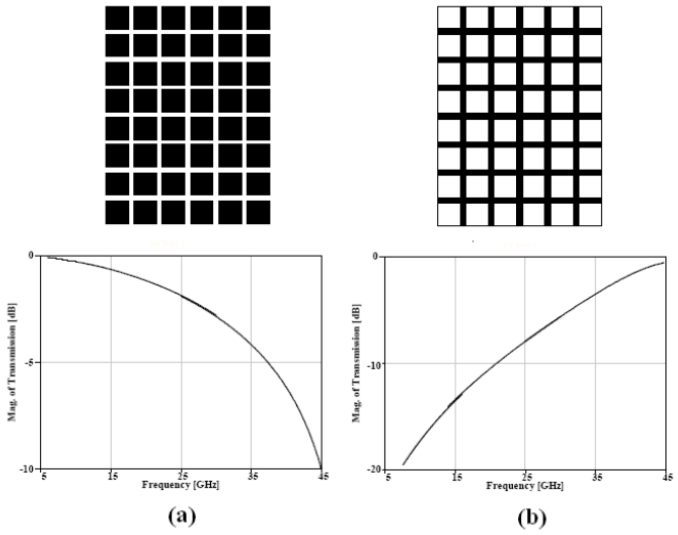

Figure 1- 1 Transmission characteristics and models of FSS with respect to electrical properties: (a) Capacitive (b) Inductive [10]

By modification and utilization of different element types together, different filtering characteristics like low-pass, high-pass, band-pass and band-stop, can be

obtained. As mentioned above, if the elements are pure capacitive, corresponding is a low-pass filter. Reversely, if the elements are pure inductive, a high-pass characteristics comes up. The size of patches in Figure 1- 1.a is greater than the size of the apertures, which results a high capacitance and a negligible inductance with respect to the capacitance. In Figure 1- 1.b, the same situation is present for the apertures against small patches which creates an almost pure inductive medium. These characteristics are modified by making the inter-element apertures between the patches comparable and vice versa. In this way, FSS elements can be arranged in order to include both capacitive and inductive properties together. If patches are modified in this manner a band-stop filtering effect is observed. Similarly, due to the duality principle, apertures can be utilized in order to achieve band-pass performance.

1.1.2. Shape of Elements

Munk groups FSS elements according to their shapes in four main categories (see Figure 1- 2), which are namely;

1. The center connected or N-poles
2. The loop types
3. Solid interior or plate types
4. Combinations

The center connected or N-poles types include single dipole, three-legged, anchor, the Jerusalem cross and square spiral elements. Single dipole is the basic form for the other types of elements. Simple dipoles are arrayed in two dimensionally periodic sense which demonstrate a band-stop characteristics when illuminated.

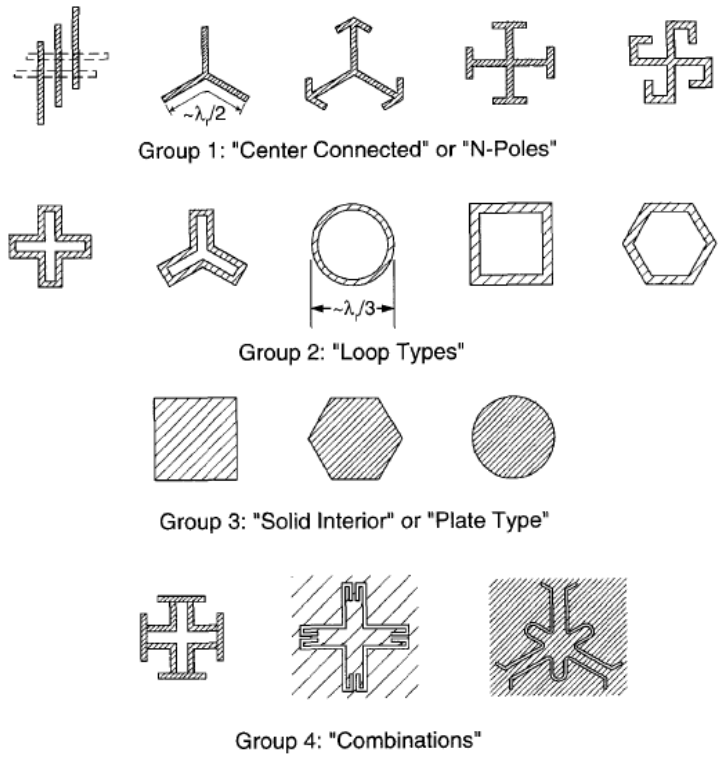

Figure 1- 2 Classification of FSS elements [1]

A patent for FSS was granted in 1974 to Munk for his work about the stabilization of FSS performance against oblique incidence [11]. Munk determined that the spacings between the unit cell elements must be smaller than 0.4*λ so as to preserve the FSS characteristics for different scan angles. Furthermore, in order to provide small inter-element spacing, he claimed that the elements should be miniaturized. The most commonly used method to miniaturize a resonance structure is to load it either capacitively or inductively. As shown in Figure 1- 3, the dipole elements (Figure 1- 3.a) are loaded by a shorted two wire segment (Figure 1- 3.b) which supplies the required inductance to obtain the resonance frequency of half wavelength dipole elements in smaller sizes. The characteristics of the unloaded dipole elements are very sensitive to the angle of impinging waves as seen in Figure 1- 4. When the shorted loading segment is inserted between smaller dipole elements, the stabilization is observed to increase significantly.

According to Munk, the reason is the impedance of the shorted dipole elements which is much higher compared to the mutual impedance. Thus, the effect of the mutual impedance, which normally changes with the scan angle and modifies the behavior, is diminished. The loaded model has narrow-band characteristics since the impedance of the shorted dipoles varies dramatically with frequency. Therefore, Munk suggests that kind of FSS elements for applications where wide scanning and minimum bore-sight error are desired.

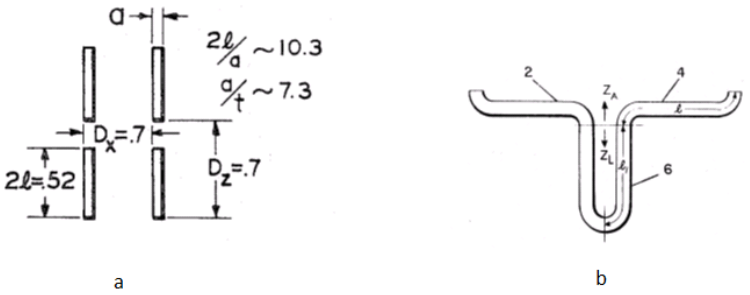

Figure 1- 3 Dipole elements a) Regular half wavelength dipoles b) Loaded dipoles [11]

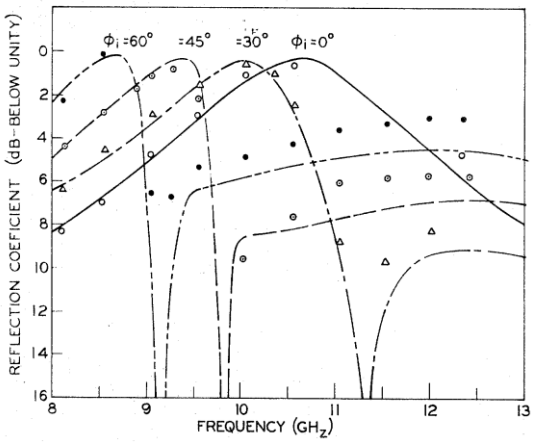

Figure 1- 4 Reflection curves of standard dipoles for different angles of incidence [11]

The band reject performance of the single dipoles is poor since secondary resonance frequencies occur in oblique incidence cases for parallel polarization. This situation may cause transmission of undesired signal of stop-frequency for parallel polarization cases. The unloaded tripole element improves the bandwidth performance with respect to single dipoles. The smaller inter-element spacing is another advantage of the unloaded tripoles. However, the second harmonic excited by parallel polarization still occurs for these elements. The anchor elements are constructed by tuning the tripole element with an end capacitance. The modification results in a broader bandwidth and smaller spacing. Nevertheless, the null due to the parallel polarization incidence cannot be terminated. The Jerusalem cross consists of crossed dipoles loaded at the ends similar to anchor elements. The capacitive loading decreases the fundamental resonance frequency. The second harmonic null shifts upward in frequency. For Jerusalem cross, another null also takes place in upper band, which is defined as "free space grating lobe" by Munk [1]. The last member of "center connected" elements is the square spiral. The interesting feature of the square spiral element is its dual filtering characteristics. In other words, the element can be used as either band-pass or band-stop filter due to the higher null position in frequency.

The second group of elements called “loop types” consists of three or four-legged, circular, square and hexagonal loops. The invention of the four legged loaded element by Munk in [11], aims to decrease the inter-element spacing in order to strengthen the stability against oblique incidence and to increase the bandwidth of operation. Since the model is symmetric in two orthogonal axes, both vertical and horizontal polarizations are filtered equally. As a natural consequence, the same equivalent circuit model parameters apply for both polarizations

The three-legged loaded element is modeled as a consequence of the four-legged element. The bandwidth and stability performance is more powerful with respect to unloaded model. The three legged loaded element has a wider broadband than the four legged elements since the inter-element spacing is significantly smaller which can be observed from Figure 1- 5.

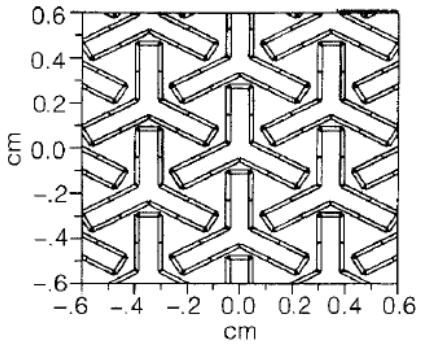

Figure 1- 5 Array of three-legged loaded FSS elements [1]

The hexagonal loop element is better than the other members of loop family in terms of the location of the first null which occurs at a higher frequency like the square spiral of the first group. Solid interior FSS elements contain the circular, triangular, square, hexagonal plates or the apertures of the corresponding shapes for the reflecting or transmitting characteristics, respectively. According to Munk, the main disadvantage of this group is the size of elements, which should be around $\lambda/2$ and results in a higher inter-element spacing. Thus, these elements are more sensitive to the angle of incidence. However, the weaknesses of plate family can be overcome with either different array models like triangular arrangement or the dielectric loading, which will be explained later in this chapter in details.

The last group of elements is constructed combining the elements of the three groups above. The number of possible combinations is countless. As an example, the modification of four-legged loop element with a Jerusalem type loading can be shown. As a consequence of the capacitive effect of loading, the element sizes and inter-element spacing decrease. Thus, the oblique incidence performance of the four-legged loaded element enhances. Any combination of the elements can be applied in order to benefit the major advantages of different types.

The performance parameters for FSS structures can be listed as follows:

- Bandwidth
- Sensitivity to angle of incidence
- Pass-band flatness
- Selectivity

Bandwidth definition for FSS model can be made with respect to either transmission or reflection performances. In terms of transmission properties, the frequency points where the transmitted signal is 3dB below of maximum transmission value can be defined as a bandwidth criterion. It is also possible to define bandwidth of operation using reflection characteristics of FSS model. In this case, a pre-determined value for reflected signals, i.e. -10 dB, can be regarded as the limits for bandwidth determination. These definitions are valid for band-pass cases. However, for band-stop FSS, duals of the definitions are applicable. For example, 3dB below of resonance reflection of a band-reject FSS can be chosen as bandwidth measure.

In aspects of bandwidth characteristics, FSS can be constructed for narrow or wide band operations. Single element dipoles create a narrow-band filtering behavior. For the applications where a wide spectrum of frequency is required, wideband FSS structures can be employed. When the literature is studied, numerous articles about wideband FSS can be found. For example, Zhou et. al. designed an ultra-wideband FSS consisting of three metallic layers and two very thin dielectric layers [12]. The upper and bottom layers of the model are rectangular patches while the middle layer is a square grid as demonstrated in Figure 1-6.a. The prototype fabrication of the FSS seen in Figure 1-6.b consists of an array of 67x67 unit cells.

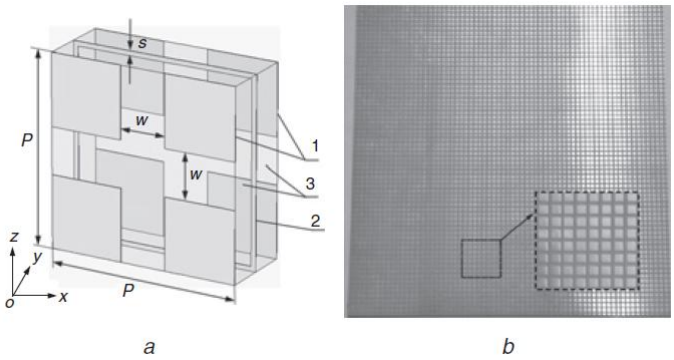

Figure 1-6 Wideband FSS structure a) Three dimensional unit cell model b) Prototype of fabricated FSS [12]

Rather than single band of operation, it is also possible to achieve dual-band filtering responses with FSS structures. Figure 1- 7 demonstrates a dual-band reject FSS which consists of two nested rectangular loops placed on the same surface. The model can be further modified such that a band-pass filtering occurs between two nulls of rejection frequencies.

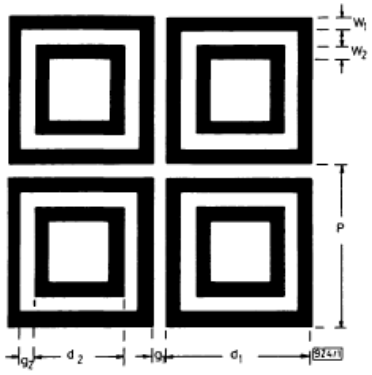

Figure 1- 7 Double square loop FSS model [13]

Another dual-band FSS model described by Yee in [9] consists of three metal layers and two dielectric layers between them. The outer metallic sheets have arrays of apertures while the inner sheet has patches. Yee also suggests the implementation of both low and high frequency FSS arrays on the same metallic sheet as in Figure 1-8. With this configuration, a dual-band frequency selective surface is obtained. When the crossed dipole elements are used, FSS rejects the signals of two predetermined frequencies. If the elements are crossed apertures, FSS transmits the impinging waves of two different wavelengths. The sheets are kept apart from each other using the dielectric substrates.

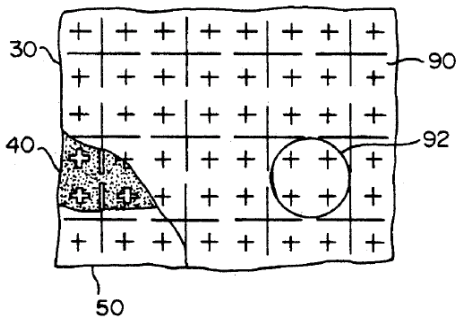

Figure 1-8 Dual-band FSS model [9]

An extension to dual-band FSS could be the concept of "multi-band filtering". The multi-band pass or reject FSS can be designed by applying the different sized elements together or fractal elements. As an example of the recent work about this concept, a tri-band stop FSS developed by Kim and Choi can be shown [14]. In this model, three distinct resonance frequencies are created using the ternary tree shaped loop loaded with a tripole element (see Figure 1-9). Two of the resonance frequencies originate from the loop and the other one from the tripole placed inside the loop.

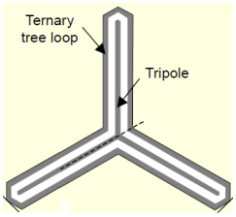

Figure 1-9 Tri-band FSS model [14]

As the design and fabrication technologies improved, new types and applications of FSS structures have arised enormously. Another interesting implementation for FSS structures is the introduction of the fractal elements for multiband operations [15]. Fractal elements have unique properties like small element size due to the confined geometry which creates a long curve in a low space [16]. Thus, the spacings between the fractal elements become closer than the non-fractal ones. The major point about the fractal elements is the self-similarity property which provides multiband behavior [17]. Self-similarity is the replication of the major element at a different scale with iterations (see Figure 1-10). The multiband frequencies change with respect to the replication scale.

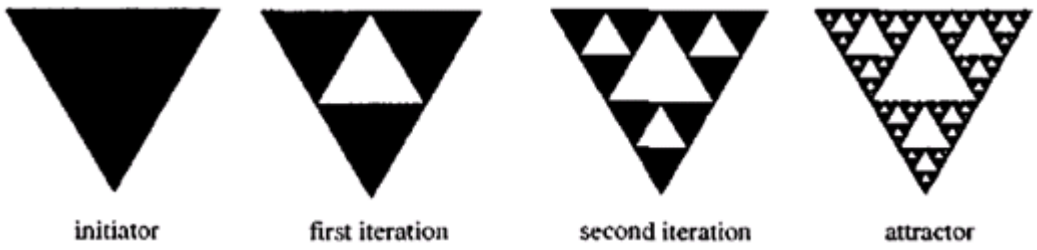

Figure 1-10 Iterations of the Sierpinski FSS [17]

Sensitivity to angle of incidence, top flatness and selectivity properties of FSS structures are directly related with the constructional aspects. Instead of single metal sheet, FSS structures can consist of double metallic layers with dielectric substrates between the FSS layers or superstrates on them, which results "hybrid" structures. The main targets for such modifications to FSS structures are to create a flat-top pass-band and to increase the selectivity with a fast roll-off. First of all, using two cascaded FSS layers as shown in Figure 1- 11 enhances the aforementioned properties (see Figure 1- 12). However, the structure is still weak for the illuminations at different angles of incidences.

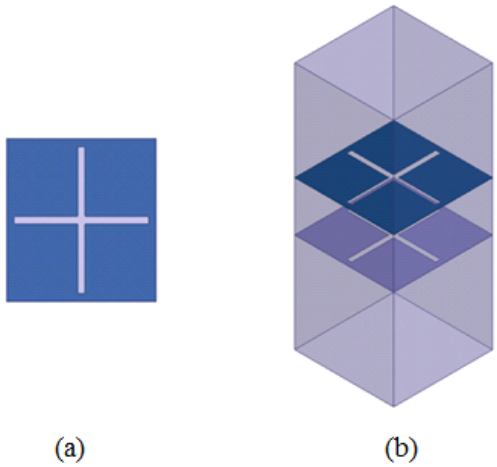

Figure 1- 11 Crossed dipole aperture FSS model: a) Single layer b) Double layer

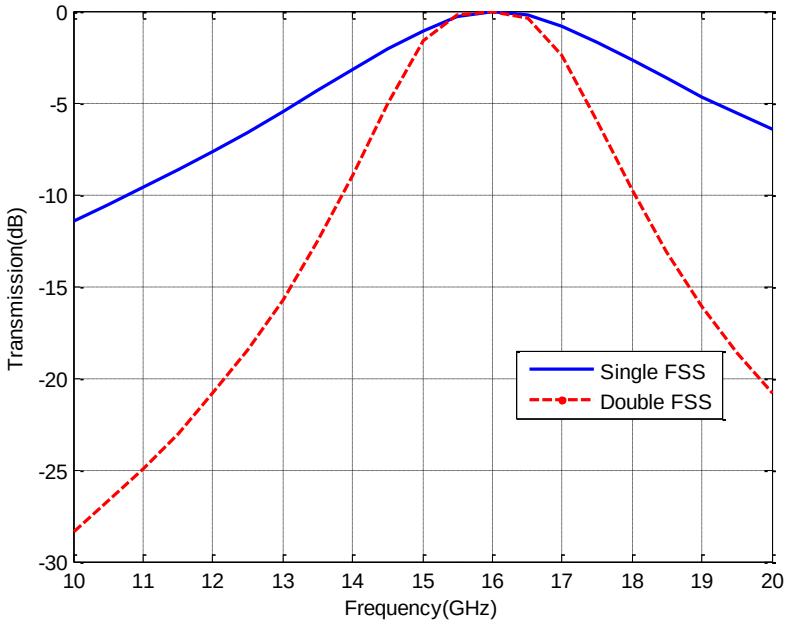

Figure 1- 12 Comparison of transmission performances of single and double layer crossed dipole aperture FSS

Another adaptation is to place dielectric layers of equal thickness and dielectric coefficient on both sides of metallic FSS layer as demonstrated in Figure 1- 13. The single FSS with dielectric layers favors in broadening the bandwidth with respect to the case without dielectric layers. Nevertheless, the model suffers from the rough in-band characteristics. In other words, the flatness cannot be provided with this modification. As observed from Figure 1- 14, the resonance frequency of single FSS layer moves down towards $\frac{f_0}{\sqrt{\varepsilon_r}}$ from f_0.

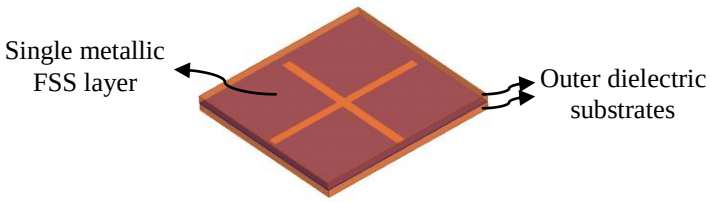

Figure 1- 13 Single crossed dipole aperture FSS with dielectric slabs

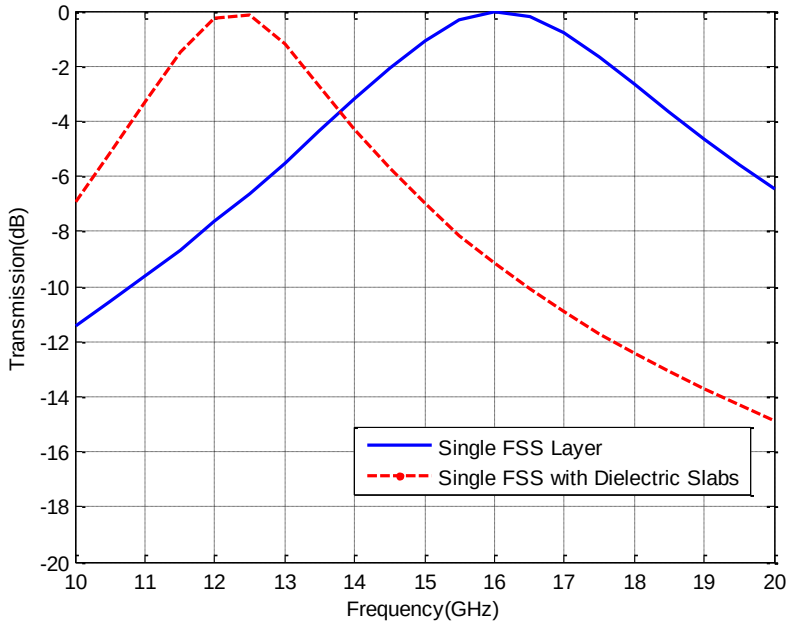

Figure 1- 14 Transmission responses of single FSS layer with and without dielectric slabs

In order to overcome both flatness and selectivity problems with a stable oblique incidence performance, "hybrid" FSS structures can be utilized. According to Munk, a real hybrid FSS consists of two outer dielectric layers, two cascaded metallic FSS sheets and a dielectric slab between them [1]. The outer dielectric layers have the same thickness and dielectric constant and serve for constant bandwidth performance against oblique incidence and polarizations. The middle dielectric layer determines the flatness of transmission curve in the pass band. FSS sheets are responsible for the bandwidth and resonance frequency. The invention patented by Munk called “Space Filter”, a sandwich type FSS consisting of slot metal sheets and dielectric layers, was patented in 1978 [18]. With this invention, Munk claimed that the bandwidth of the FSS remains constant over a wide range of angle of incidence. The new structure includes the cascaded dielectric and metal layers with different thicknesses and models respectively. It is possible to construct a band-pass or band-stop space filter using the corresponding elements, i.e., slots or patches. The drawing in Figure 1-15 exhibits the multilayer hybrid FSS model. The

outermost dielectric layers are used to provide the necessary conductance yielding to constant bandwidth for varying angles of incidence. The intermediate dielectric layer ensures the coupling between the periodic arrays. The total thickness of the FSS is around an odd multiple of one quarter wavelength.

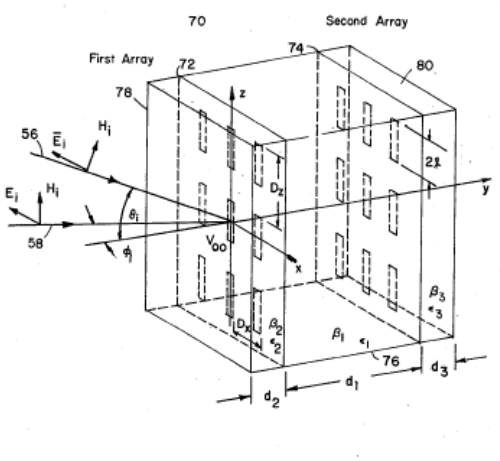

Figure 1-15 The schematic of a multilayer “Space Filter” [18]

Hybrid configuration of crossed dipole aperture FSS is constructed as described above (Figure 1- 16). The transmission response of the hybrid FSS model is observed to be enhanced in terms of band-pass flatness and bandwidth with respect to single metallic layer of crossed dipole aperture FSS (Figure 1- 17). Hybrid model is also more powerful against oblique incidence cases when compared to single layer FSS.

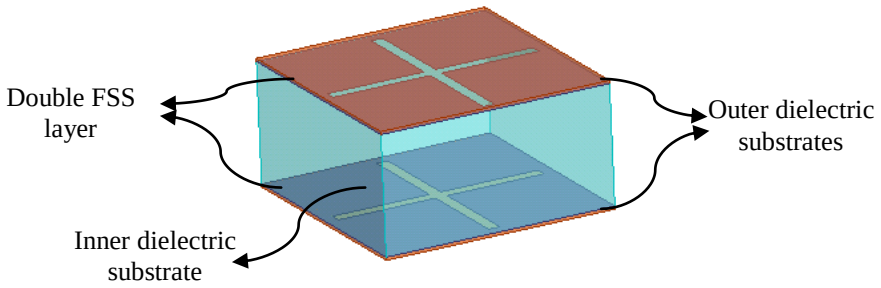

Figure 1- 16 Hybrid FSS configuration of crossed dipole aperture element

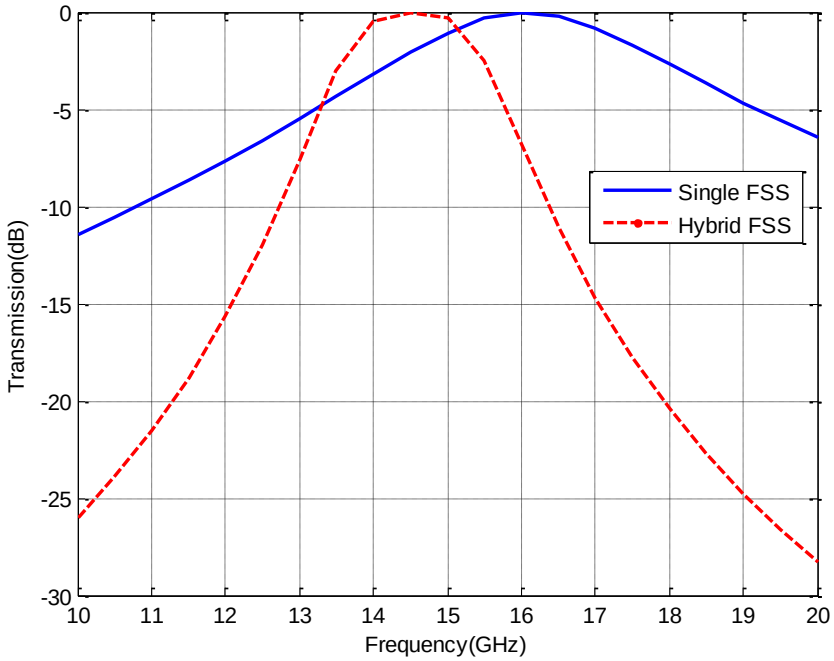

Figure 1- 17 Transmission responses of single layer and hybrid crossed dipole aperture FSS

So far, the characteristics of planar FSS are discussed, however; for some applications like nose radomes on the aircrafts, the nose radome applications on the aircrafts, the angle of incidence of the incoming wave can reach to very high values due to the shape of the radome. Therefore, conformal FSS structures are required in order to decrease the RCS of curved structures successively, while creating no significant effect on the performance of the antenna. Implementation of FSS on curved radomes decreases the out-of-band target RCS of the antenna effectively since the incoming signal is scattered to other directions, not reflected back. Other major application of conformal FSS is the dual band reflector antenna systems. In the dual band reflector systems, a conformal FSS can be designed as a sub-reflector, which reflects the signals of one of the operation frequencies to main reflector and transmits the other (see Figure 1- 18).

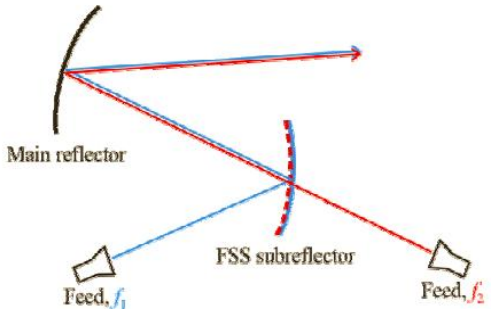

Figure 1- 18 Utilization of conformal FSS in a dual band reflector system [19]

In [20], a multi-layer array approach using open-ended waveguide antenna array combined with FSS structures conformed on a cylindrical surface is presented. A novel fabrication approach for conformal FSS structures on doubly curved bodies is explained in [21]. In this work, cross loop FSS model is implemented on a paraboloid surface with rapid 3D prototyping. Design of a conformal FSS as a sub-reflector in a satellite is studied in [22].

Since the shape of the application surface is limited to one or doubly curved bodies, FSS structures are necessarily to be designed as conformal to implementation surfaces. The researchers have thoroughly studied about FSS problems from 1960's up to date. With the aid of new advanced CPUs, the analysis and design durations have dramatically decreased. Different FSS structures are discovered as the fabrication and analysis techniques are improved. However, still, there are challenging topics about FSS to be intensively investigated and improved. One of these challenging issues, which is also the main concentration of this thesis, is the application of FSS structures to conformal bodies. The conformal application brings extra difficulties different from the classical planar problems. In planar problems, the main assumption in the analytical solutions, periodicity in two dimensions, is almost preserved. The effect of the elements at the end of the arrays can be neglected for large arrays of FSS. However, in curved FSS, the periodicity cannot be kept in two dimensions. On singly curved bodies like cylinders, only the periodicity in longitudinal dimension is conserved. Thus, after a planar unit cell

solution, one has to prove the design with a curved structure analysis. There are some extra difficulties in designing conformal FSS. For example, the stable performance against angle of incidence is a must for conformal implementations since the incident wave can impinge on the surface of a curved FSS structure at very large angles. Thus, FSS model has to maintain its characteristics under these conditions. The orientation and registration of the elements on a curved surface also play a key role in the performance of FSS. The development of a complete methodology for the design and efficient determination of the performances of conformal FSS structures is the main target of the thesis.

In this thesis, the design and analysis methods of the FSS structures for the conformal bodies are explored. Starting from the planar unit cell models with different requirements, semi-finite curved FSS models are constructed and analyzed using HFSS® of ANSYS [23].

The fabrication and measurements of the FSS structures for planar structures are realized in order to prove the designs and complete the study.

1.2 Organization of the Thesis

In Chapter 2, overview on FSS analysis methods is demonstrated. Different solution approaches are investigated stating the advantages and disadvantages of each method with respect others. The analysis methods utilized in this thesis to obtain FSS characteristics are also explained starting from planar solutions to conformal ones step by step.

The design and analysis of a FSS with coupled aperture disk elements are implemented in Chapter 3. FSS parameters are determined using unit cell model. The oblique incidence performance is also tested with that unit cell solution in HFSS. A semi-finite model is constructed which provides both to observe the effects of finite arraying and take advantage of unit cell solutions for a fast analysis. Planar and curved FSS models are constructed using semi-finite analysis

method. The constructed curved model is finite in the curved direction of the cylinder while it is infinite in the longitudinal direction, which is so called "semi-finite". Filtering performance of FSS model is also verified with a finite doubly curved model in HFSS®.

In the 4th chapter, the design of a wide-band conformal FSS is introduced. The design process and verification of performance using the semi-finite model approach of Chapter 3 are also implemented for wide band FSS model.

The fabrication and measurements of planar prototypes of coupled hybrid FSS are presented in Chapter 5. The construction of the setups for the appropriate measurements is detailed. The results of simulations and measurements are compared and possible reasons of discrepancies are discussed. New fabrication approaches are also presented at the end of this chapter.

In the last chapter of the thesis, the conclusion remarks about this work are given with the possible future studies about conformal FSS structures, which can move the knowledge and abilities one more step away.

CHAPTER 2

ANALYSIS METHODS FOR FSS STRUCTURES

2.1 Overview of Analysis Methods

In order to efficiently analyze various FSS problems, different solution methods may be applicable. The analysis methods used to design and improve the performance of the FSS structures can be detailed as follows. The pioneers of the FSS design were first applied the mode matching technique, which was normally used for waveguides, to solve the FSS problems. After mode matching analysis, the equivalent circuit approach is adopted to FSS structures from a perspective of transmission lines. Due to the incapabilities of both techniques to handle the problems for the types different from the standard models like rectangular patches and apertures, more accurate numerical methods, such as method of moments, finite element and finite difference methods, are developed.

To start with the mode matching technique, it is applied by calculating the waveguide modes at the discontinuities on a basis of entire domain [24]. The procedure includes equating the expansions of fields to the boundary conditions of the discontinuity region [25]. When the scattered fields are desired to be calculated from periodic structures, the expansion into Floquet modes is required. In mode matching technique, the appropriate basis and test functions are used to find the unknowns of the problem, i.e., amplitudes of the fields. The transmission and reflection parameters are directly gathered in terms of field amplitudes into the S-matrix of the layer. The multiple layer problems are also possible to be handled with mode matching technique in a manner of cascaded networks. In [26], the numerical

analysis of an arbitrarily shaped FSS with a combination of mode matching and S-matrix methods is revealed.

Another method derived for FSS analysis is the circuit equivalent method which was firstly applied by Anderson [27]. To him, the method is best fitted for the periodic, free standing, thin and perfectly conducting metal structures where the dimensions are smaller than the wavelength of the impinging wave. The impedance between the strips is described as inductive if the polarization of the wave is parallel with respect to strip alignment. Shunt capacitive elements exist if the polarization is perpendicular. The oblique incidence cases for the equivalent circuits of gridded square and double square FSS are analyzed up to 45^{o} referenced to the normal [28]. The method is repeated with a novel attitude for the ring patch FSS in [29]. The equivalent network parameters for ring elements under oblique incidence are determined and the transmission characteristics of the analysis and measurements are compared. Some differences between the results are observed by the authors. They attribute the disagreement mainly to the test environment and the weak accuracy of the circuit equivalent method than other full wave numerical solutions. If the FSS model is easy to model by lumped elements, the equivalent circuit approach can be employed to solve such kind of problems. When the FSS model gets complicated, i.e. hybridized, multilayer or conformal designs , the circuit equivalent method becomes inaccurate when compared to full wave solutions. The main drawbacks of circuit equivalent method can be listed as follows:

- The cross-polarization effects are ignored, i.e., the equivalent circuit parameters are valid for only co-pol illumination.
- Method is incapable to handle FSS problems with large angle incidence.
- The coupling between the adjacent FSS elements is not consulted.
- Analytical solutions of FSS parameters exist for a limited number of element types.

Hence, the circuit equivalent method is not adequate to solve all FSS problems. However, if one will work with a well-known FSS model like rectangular loop or the Jerusalem cross, whose parameters are defined analytically, circuit equivalent approach can be a good starting point to observe the effects of any parameter quickly.

Method of Moments (MoM) can be utilized for the solution of the operator equations of the induced currents or fields defined on an illuminated surface [30]. The characteristics of the FSS structures, i.e., transmission and reflection properties, can be extracted from these solutions [31]. The convergence of the solutions is mainly determined by the basis and test functions. MoM application for FSS brings some difficulties when the medium is multi-layered or a thickness is defined for metal surfaces since it becomes more difficult to handle the Green's functions for 3-D structures [25].

Finite Element Method (FEM) is normally applied for bounded domain structures. The unbounded nature of FSS problems require some specific boundary conditions which eliminate the reflected fields while absorbing the incident and scattered fields appropriately. FEM is easily adapted to complex geometries and anisotropic media [32]. However, the solutions of the FEM equations require a high calculation capacity which is achieved by the high performance work stations.

Finite Difference Time Domain (FDTD) method is implemented in order to obtain broadband responses since a wide band analysis can be gathered in a single simulation. The detailed analysis of FSS with FDTD method is investigated in [33]. An important advantage of FDTD method is that there is no need for any matrix conversion to solve the problems which makes it easier when compared to other methods. However, in FDTD, the data load can be very excessive since storage at any time instant is required.

The general approach to begin an FSS design is the "unit cell" solution. Due to the periodic nature of FSS structures, infinite array approximations are applicable. Unit cell method employs the periodic solution of an FSS model. Unit cell implies for

one period of the FSS. In Figure 2- 1 unit cell sample is demonstrated. In the same figure, full array view is also given.

Using the unit cell model, the performance of an FSS structure under the infinite array conditions can be determined with the help of an electromagnetic simulation software like HFSS®, CST®, etc. [34]. In unit cell analysis, it is possible to create phase difference between the periodic boundaries, which corresponds to the oblique incidence case. The performance of a curved FSS structure has to remain stable under varying angles of incidence. Hence, this feature is required to be tested with the unit cell analysis at first.

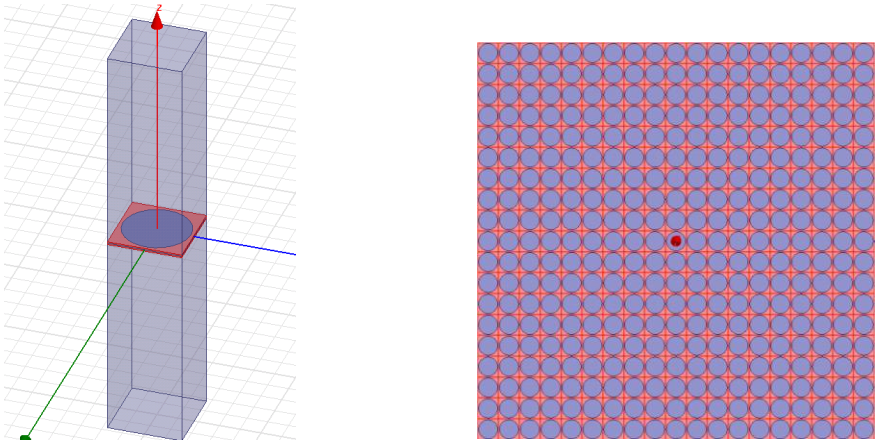

Figure 2- 1 Unit cell (on the left) and finite planar array (on the right) of a disk FSS

Concerning the conformal structures, the FSS array cannot be preserved in linear arrangement. Different array sequencings with respect to various surface topographies like triangular, hexagonal and parallel as shown in Figure 2- 2 are constructed to observe the effects of the corresponding arrangements. For example, the arrangement on a sphere surface can be performed in hexagonal or pentagonal arrays as illustrated in Figure 2- 3.

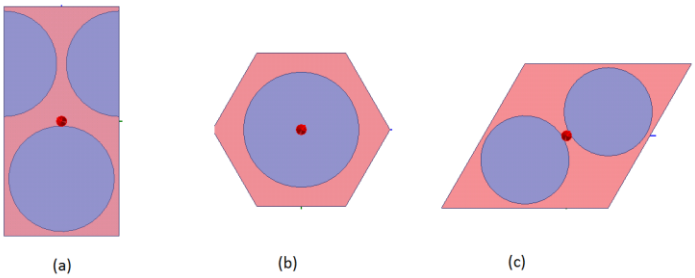

Figure 2- 2 Various unit cell arrangements: (a) Triangular (b) Hexagonal (c) Parallelogram

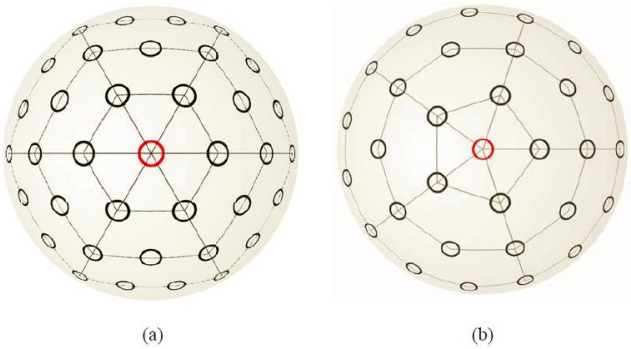

Figure 2- 3 Arrangements of FSS elements on spherical surface: (a) Hexagonal (b) Pentagonal [19]

Hexagonal or pentagonal arrangements of FSS elements on doubly curved structures like spheres cannot provide a full periodicity as in planar cases. The inter-element spacings differ as the elements get away from the poles. Therefore, alternative arrangements on these bodies can be examined in order to maintain the periodic behavior of FSS elements as much as possible. For example, the surface of a doubly curved structure can be coated with the sequences of the FSS elements as demonstrated in Figure 2- 4. Sphere surface can be divided by circles of different radii which are one period apart away from each other. Thus, period between successive FSS sequences on these circles is maintained. On each circle, FSS elements can also be placed periodically. Since the elements are at equal distance from each other on circles with different radii, FSS elements are located as shifted with respect to neighboring sequences. With this configuration, period between

FSS sequences and elements of each sequence can be preserved. However, this method is not applicable for coating full sphere surface perfectly. It is convenient to cover a half sphere which is generally sufficient in aspects of practical applications of FSS radomes.

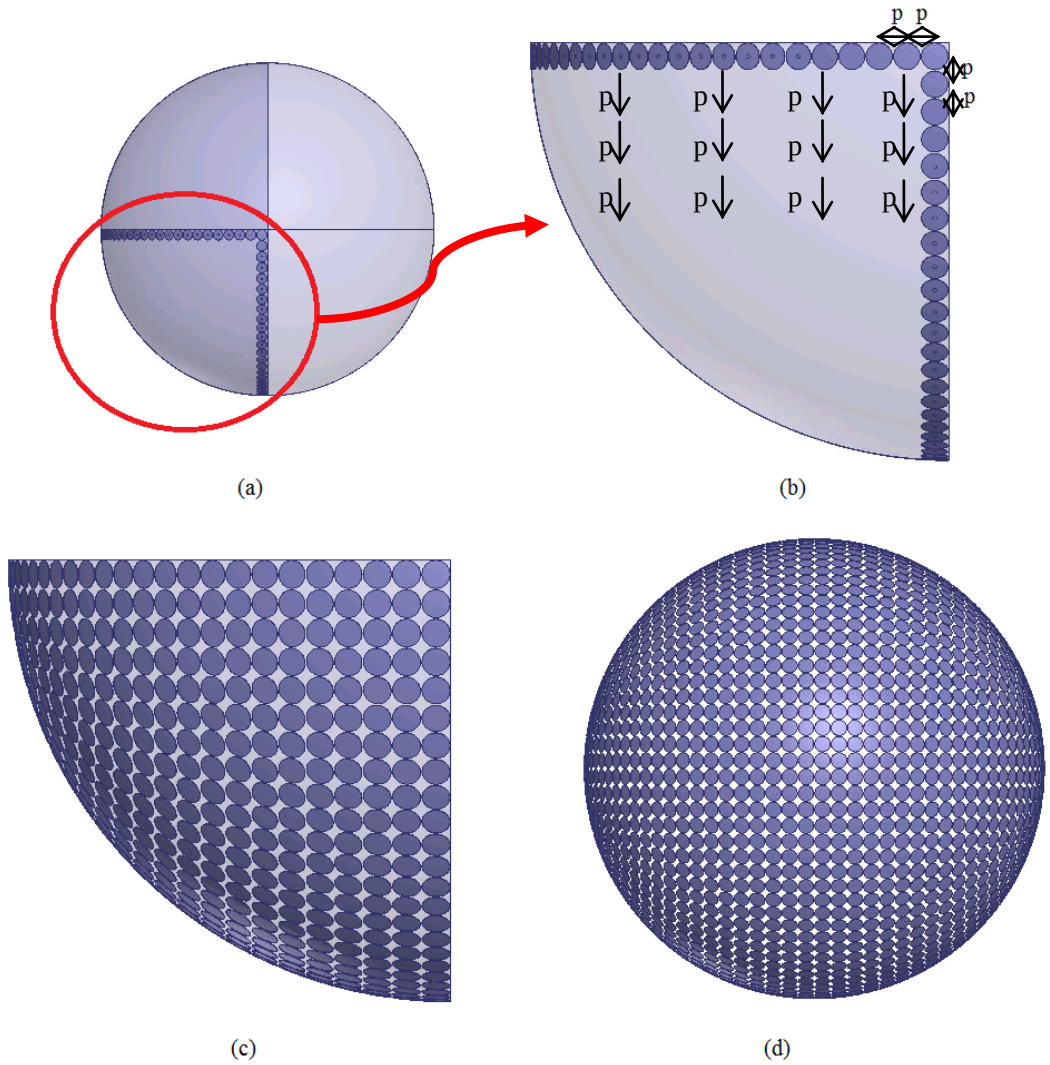

Figure 2- 4 Illustration of element arrangement on sphere with shifted unit cell approach: a) Single sequence placement b) Multiplication of elements on single sequence c) Covered quarter sphere d) Full sphere view

The performance of the related FSS model for such an arrangement can be easily observed with the unit cell solutions. The unit cell models for a sample FSS for this approach is presented in Figure 2- 5. As seen in the figure, different unit cells are designed to determine the corresponding filtering characteristics. Provided that all the unit cell models exhibit filtering performances similar to single element unit cell, this approach is applicable.

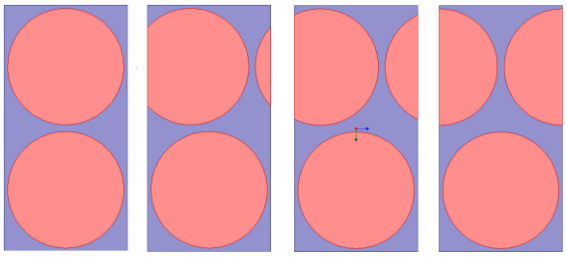

Figure 2- 5 Different unit cell arrangements for the determination of the shifted unit cell performance

The unit cell analysis in FEM based HFSS starts with constructing one period of FSS model. Once the model is created then a vacuum box is built covering the edges of the unit cell model. Then, the boundary conditions are arranged. In Figure 2- 6, assignment of periodic boundary conditions, which are called "master" and "slave" in HFSS terminology, are represented. These boundaries ensure the construction of an infinite array either in one or two dimensions. In Figure 2- 6, the periodicity is in two dimensions. By defining phase differences between the master-slave pairs, the oblique incidence performances of FSS structures are determined.

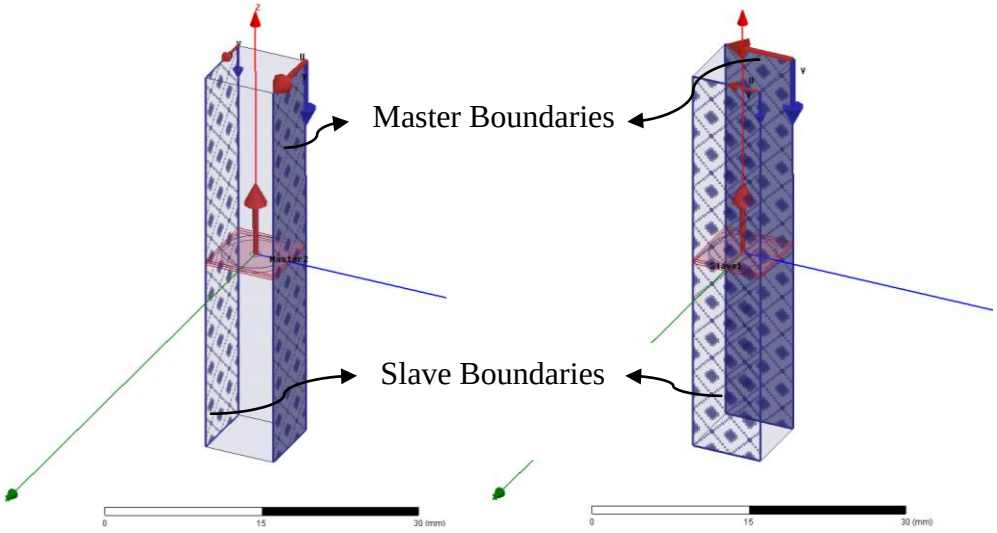

Figure 2- 6 Assignment of "Master" and "Slave" boundary conditions on the walls of vacuum box

The excitation of the unit cell model is accomplished by the Floquet ports as illustrated in Figure 2- 7. Other than the periodic side walls of the unit cell model, at least one open boundary condition which stands for the boundary to infinite space is required. To provide this open boundary condition, Floquet ports are used in HFSS. These ports create Floquet modes, which are plane waves propagating in the direction defined by the frequency, phase difference between the side walls and the model of unit cell. With this configuration, Floquet modes exhibit waveguide mode behaviors, i.e. they have propagation constants and cut-off frequencies. FSS unit cell structures have two Floquet ports since both the transmission and reflection properties of the FSS are performance criteria.

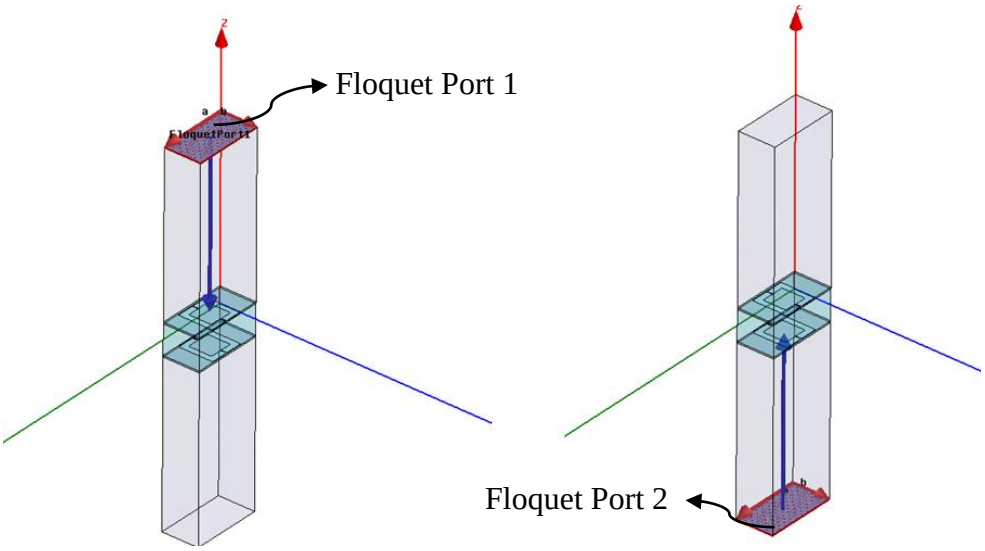

Figure 2- 7 Floquet port assignments for a unit cell FSS model in HFSS

In FSS analysis, the first fundamental modes for TE and TM waves are examined. The other modes are necessarily to be diminished. Thus, the Floquet ports are set apart from each other at a sufficiently long distance where the other evanescent modes disappear until reaching the FSS. In HFSS, there is an option called "Modes Calculator" which shows the attenuation of the higher order modes at unit length (see Figure 2- 8). Using this feature, the length of the vacuum box is arranged in order to provide at least 40-50 dB suppression of the evanescent modes. However, the distance between the unit cell surface and the ports creates a shift in the phase terms of S-parameters. This shift in phase terms can be eliminated by applying the "de-embedding" feature of HFSS. By de-embedding the Floquet ports onto the surface of FSS structure, the exact S-parameters belonging to the analyzed structure are gathered (see Figure 2- 8) .

Once the construction of FSS unit cell is completed, the simulation can be performed after defining the solution setup in HFSS, i.e., frequency range, solution frequency where the meshes are created and the convergence rate of S-parameters. There is an important point for solution frequency that a designer must be careful. Generally, for the analysis of finite structures, the solution frequency is taken as the

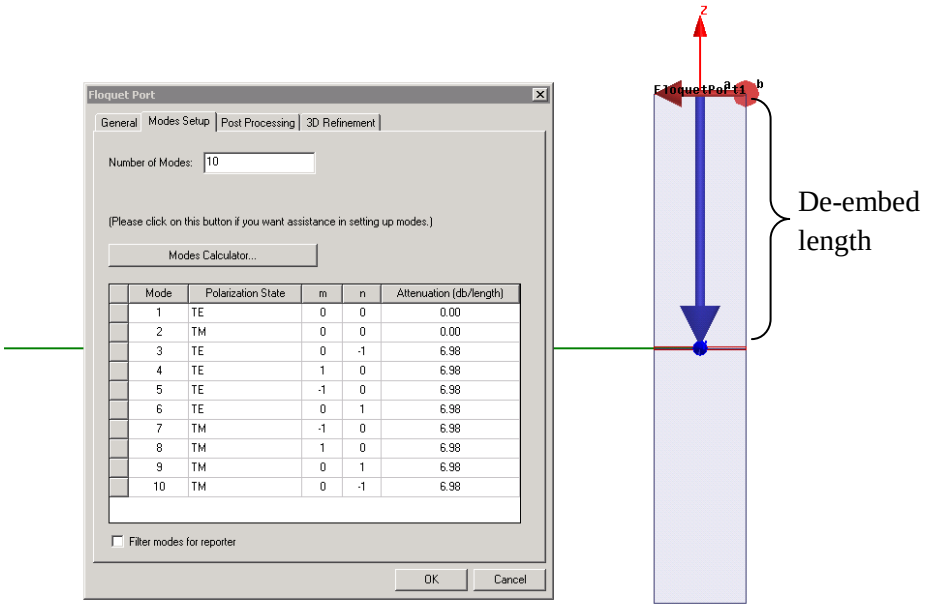

Figure 2- 8 Modes Calculator (on the left) and de-embedding (on the right) properties of HFSS Floquet port setup

upper limit of the interested frequency sweep in order to provide sufficiently small meshes compared to the minimum wavelength of frequency sweep points. However, in resonant structures, the initial solution point must be chosen as the resonance frequency because the most complex mesh arrangement is required for the resonance point. To ensure the resonance frequency of the structure, an iterative way is followed until the solution and observed resonance frequency become equal. With the unit cell analysis, the parameters of the FSS model are optimized very fast and efficiently, i.e., the solution does not create a high calculation load. Moreover, as a scope of this thesis, the oblique incidence performance of the unit cell can be observed easily. Furthermore, the parameter optimization can be continued in the perspective of targeted oblique illumination behavior of the FSS model.

After the parameters of a unit cell that satisfies the design requirements are obtained, the performance of the design needs to be evaluated with a finite model. The infinite periodic array solution of unit cell analysis gives an idea to the designer about the characteristics of the model, however; the results closest to the

fabricated design measurements can be achieved by only finite analysis of the exact structure. The effects of the edge elements can be observed with the simulation of finite models and may create significant difference with the results of the unit cell analysis. The solution for the finite model would create a huge computational load. Therefore, it is sometimes unfeasible to construct and solve the finite model. In such cases, the semi-finite solution can be chosen as the final step of the design process. If the model has symmetry properties, it helps to reduce the size of the problem. Then, a finite conformal solution may be applicable. In HFSS, the exact model can be simulated by using only a half or quarter of the whole structure if the body is symmetric in one or two orthogonal planes with respect to the center, accordingly. The symmetry boundary conditions are assigned on the related walls. The assignment is employed according to the direction of E-field vector of the source. The wall whose plane is normal to E-field vector is selected as PEC boundary. Similarly, the wall with parallel plane is assigned as PMC boundary. A sample finite model and its symmetry boundaries are presented in Figure 2- 9.

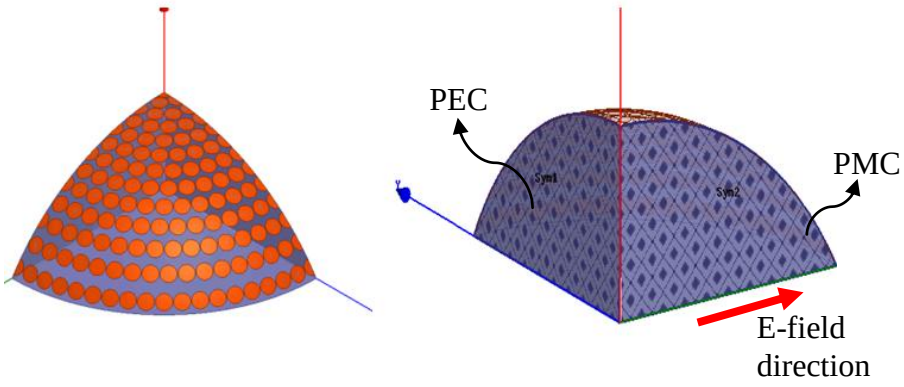

Figure 2- 9 Quarter FSS model: (a) The arrangement of FSS elements (b) Symmetry boundaries

Another alternative technique to lessen the heavy calculation load created by finite simulations can be the "semi-finite analysis" approaches. In semi-finite models, a unit cell is constructed which is finite in one dimension and infinite in other dimension. A couple of master-slave boundary condition is required since the structure is periodic in one dimension only. The finite dimension is modeled with

respect to the design requirements. For example, for a planar or singly curved cylinder FSS model, one can construct a semi-finite solution setup, i.e., periodic in one of the principle dimensions and finite in the transverse plane as shown in Figure 2- 10 and Figure 2- 11. With this model, both the effects of finite elements are observed and the simulation load is reduced dramatically with respect to the solution of a finite model. The application of semi-finite analysis is accomplished in the following chapters for both planar and curved FSS structures.

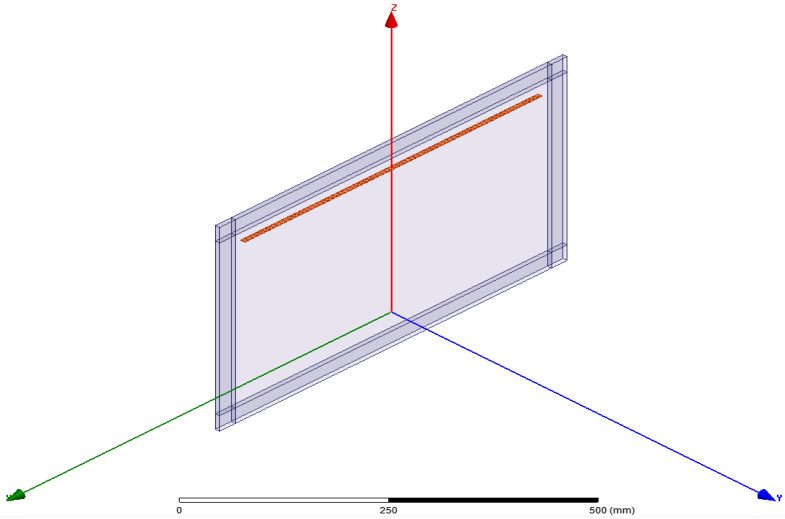

Figure 2- 10 Planar semi-finite FSS model unit cell

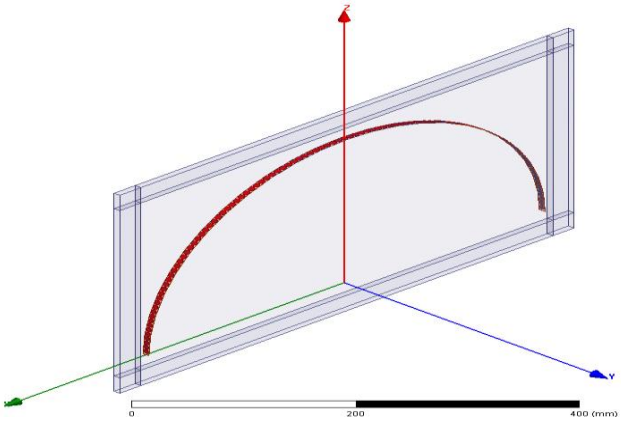

Figure 2- 11 Curved semi-finite FSS model unit cell

The construction of unit cell for the semi-finite analysis is a little different from the classical two dimensional, single element FSS unit cell. The semi-finite unit cell model consists of a single slice in the periodic direction. The construction steps of the semi-finite unit cell can be explained as follows. First of all, FSS model is built up in HFSS. Afterwards, a vacuum box covering the FSS model and standing tangent to FSS walls in periodic direction is created. The non-periodic faces of the vacuum box are chosen to assign Perfectly Matched Layers (PML) which provide open boundary conditions, i.e., they do not reflect the incoming signals (see Figure 2- 12). The PML setup user interface automatically constructs the PML objects consisting of bi-axial anisotropic materials. In HFSS, another open boundary condition for radiation problems exists, which is named "Radiation Boundary". However, PMLs are advanced boundary conditions and give more accurate results especially for radiation problems when compared to the radiation boundaries. Hence, PMLs are more useful for the analysis of semi-finite unit cell FSS model.

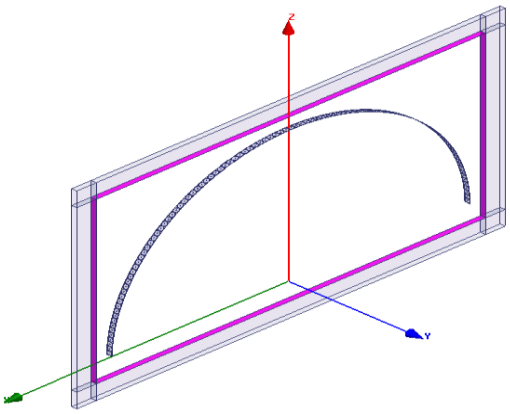

Figure 2- 12 Faces used for PML boundary identification on the curved semi-finite model

The periodicity of the semi-finite model is provided using a single master-slave boundary pair which implies one dimensional periodicity of the model in the longitudinal dimension. The critical point defining the master-slave pair for this model is that master and slave boundaries are required to cover the PMLs since they are also necessarily infinite in the periodic dimension. Therefore, two sheets

covering the corners of the outer PML boxes are created and defined as master-slave pair. On the center line of the semi-cylinder, a linear array of 31 Hertzian dipoles is used in order to illuminate the FSS radome with a Taylor distribution of 20 dB side lobe level (SLL). FSS characteristics are gathered from the knowledge of the far field datum for different frequencies. The total and incident electrical fields in the far zone are compared in terms of peak and SLLs for different frequencies. The incident electrical field data stands for the case that FSS radome does not exist.

2.2 Design Approaches for Curved FSS Structures

The conformal FSS design requires extra points to consider when compared to planar FSS applications. The model of FSS structure is critical since the good conformability properties are needed. The circular elements are generally preferred by the designers due to good conforming properties. The singly curved structures are easier compared to the doubly ones since the periodic properties can still be maintained on a singly curved body. However, for the doubly curved cases, the periodic nature of the FSS array is very difficult to be preserved. For example, on the surface of a sphere, it is impossible to arrange the FSS elements in a two dimensionally periodic sense. Thus, different approaches should be introduced to realize the FSS performance on a doubly curved structure. One of the approaches is to use an FSS model which is insensitive to shifts in the alignment of elements in multilayered structures. In the single element planar unit cell design period, the performance of the FSS model can be tested in aspects of the predefined properties. Furthermore, a different periodicity approach can be implemented which preserves the period between the inter-elements in one dimension and the subsequent sequences of FSS elements in the orthogonal dimension. Another method for the doubly curved structures can be to optimize the performance of the total structure by arranging the positions of the elements using the finite model analysis. This

method would give the most reliable results, however; it is inefficient and time-consuming compared to other approaches.

2.3 Design Methodology for Conformal Frequency Selective Surfaces

The design procedure for the conformal FSS applications starts with the determination of the unit cell model definitions as in the planar cases. The required characteristics like band pass/band stop filtering, levels of insertion loss or reflection coefficients, oblique incidence performance etc., are specified. Then, the starting points for the unit cell parameters are determined either by using circuit equivalent approach if applicable or through simulation based fast search or by scaling the known model parameters for a specific application. The starting point determination brings the designer to a feasible solution region instead of searching the final optimum sizes in the whole space. Generally, the optimum design parameters will be within the close neighborhood of these starting values. The next step is to analyze the FSS unit cell. The design is first verified for the normal incidence case with 2D infinite planar array model. Using the unit cell model shown in Figure 2- 13, FSS performance for the oblique incidence cases can also be observed and fine tuning of unit cell parameters to satisfy the design goals for oblique incidences is pursued. Oblique incidence conditions are created by applying phase differences to the periodic boundaries of the unit cell as described in this chapter.

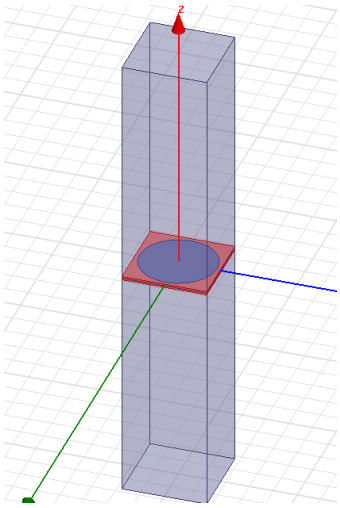

Figure 2- 13 Coupled-aperture disk hybrid FSS unit cell model

The array topology is very important for the conformal FSS applications. The placement of the elements on a doubly curved structure is not straightforward as for the planar or singly curved applications. When the surface is planar or singly curved, i.e. cylindrical surfaces, the periodicity between the FSS elements can be preserved in two dimensions. However, if the surface is doubly curved, i.e. spherical surfaces, the simple periodicity techniques are not applicable since it is impossible to maintain the periodicity in two dimensions on these surfaces. Instead, alternative techniques for the arrangement of the FSS elements are required as mentioned before in this chapter of the thesis. Therefore, the designer is strongly suggested to determine the final array parameters like inter-element spacing and array configuration. These modifications will benefit in the realization of the eventual FSS radome structure. FSS parameters can also be optimized for the new array topologies.

Verifying FSS performance using the curved models is essential since the real application surface will not be planar. The unit cell analysis of the single element is utilized for planar and infinite conditions, which does not fit the real operation conditions. The interaction between the conformal elements may be different from the planar arrays. Furthermore, the edge diffractions can be taken into account with only a finite conformal analysis. Therefore, the analysis of the FSS model with

singly or doubly curved models is required in order to observe the filtering characteristics of curved FSS elements. However, the finite models usually create a

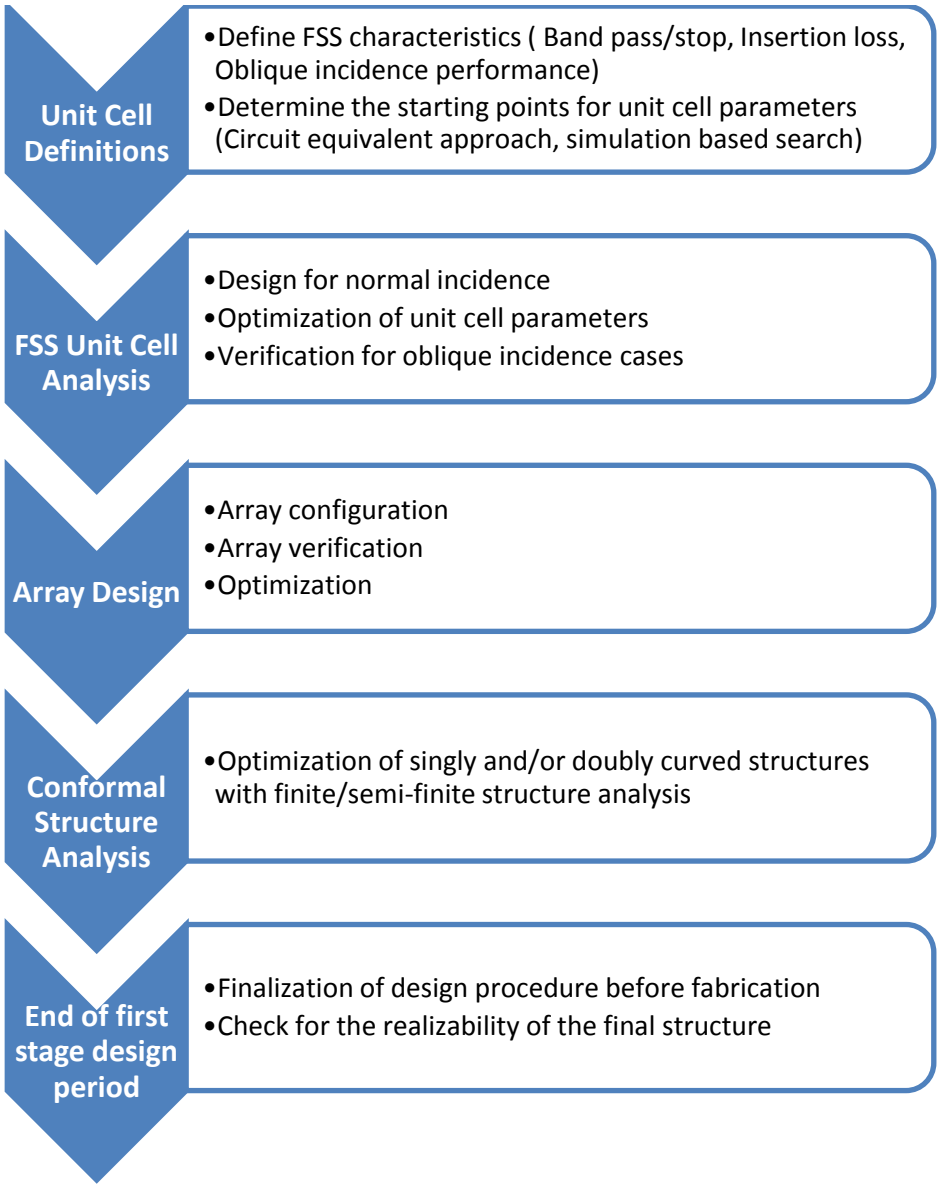

Figure 2- 14 Flowchart representation of conformal FSS design procedure

heavy calculation load which cannot be solved by even high performance work stations. To overcome this problem, a semi-finite solution is suggested in this study as mentioned in this chapter. With this solution, the edge diffractions and the performance of curved elements can be observed in the finite dimension. On the

other hand, the periodicity in the longitudinal dimension makes the problem convenient to analyze by reducing the calculation load.

When the finite or semi-finite curved FSS analysis is completed, the design procedure before fabrication is finalized. Nonetheless, the designer needs to check the final version of the FSS structure in aspects of realizability for fabrication process. The design procedure for the conformal FSS applications is also summarized with a flowchart in Figure 2- 14.

CHAPTER 3

DESIGN AND ANALYSIS OF A HYBRID CONFORMAL FREQUENCY SELECTIVE SURFACE

3.1 Design Requirements

The design requirements for the conformal application of FSS structures are more challenging with respect to planar applications. In this section, the design requirements of the FSS structure to be designed are explained. To start with the filtering behavior, FSS structure will necessarily work as a band-pass filter in Ku-band (12.4-18 GHz), which lets the transmission of the signals of the illuminating radar antenna inside the radome while reflecting the other signals of different frequencies. As another design criterion, it is required that FSS will exhibit a narrow band performance with a fast roll off in the transmission curve starting from the ends of the pass band region. The partial bandwidth of the design is 2.4% around the center frequency, f_0. It is also required that FSS will have low insertion loss in the pass-band while maintaining its performance for the oblique incidence cases. Moreover, FSS is required to be circularly polarized. The polarization requirement is determined with respect to the antenna, which will be covered by the FSS radome. The major design goals of the FSS design can also be listed as;

- High selectivity (Sharp roll-off at the edges of the boundary frequencies)
- Low insertion loss in the pass-band
- Narrow bandwidth
- Stable performance against oblique incidence
- Polarization independence

- Applicability on curved bodies

3.2 Hybrid Conformal Frequency Selective Surface Design

In order to satisfy the design requirements, a number of alternative FSS models have been examined. The typical FSS models like loaded square slot, dipole, ring elements are studied in aspects of their capabilities for the design goals. It is observed that, in general, for the doubly curved applications, disk elements are preferred due to their good conformability properties. The indispensable needs for conformability and dual polarization make the circular elements good candidates for this specific FSS design. In Figure 3- 1, some types of the circular FSS elements are shown.

Figure 3- 1 Circular FSS element models

In order to enhance the selectivity and pass-band flatness properties of the FSS elements, the number of layers used in the design is required to be increased, which will yield the designer to the hybrid FSS structures mentioned in Chapter 1. Hybrid FSSs are also superior against oblique incidence of impinging waves than the single or double layer structures. Another critical goal is the narrowband operation of FSS. To provide a narrowband filtering performance, one can make use of the coupling between the FSS layers. The application of the idea for narrow band FSS structures is first introduced by Pous and Pozar with rectangular aperture coupled elements [35]. They represented a narrowband band-pass FSS, which is also highly selective, using the coupling between the patches. The model consists of three metallic FSS layers. The outer layers are patches and the layer in the middle is a rectangular slot which is responsible for the coupling between the patches. There

are two dielectric slabs between the patches and aperture. The top and cross-sectional views of the FSS geometry Pous and Pozar used in their design are presented in Figure 3- 2.

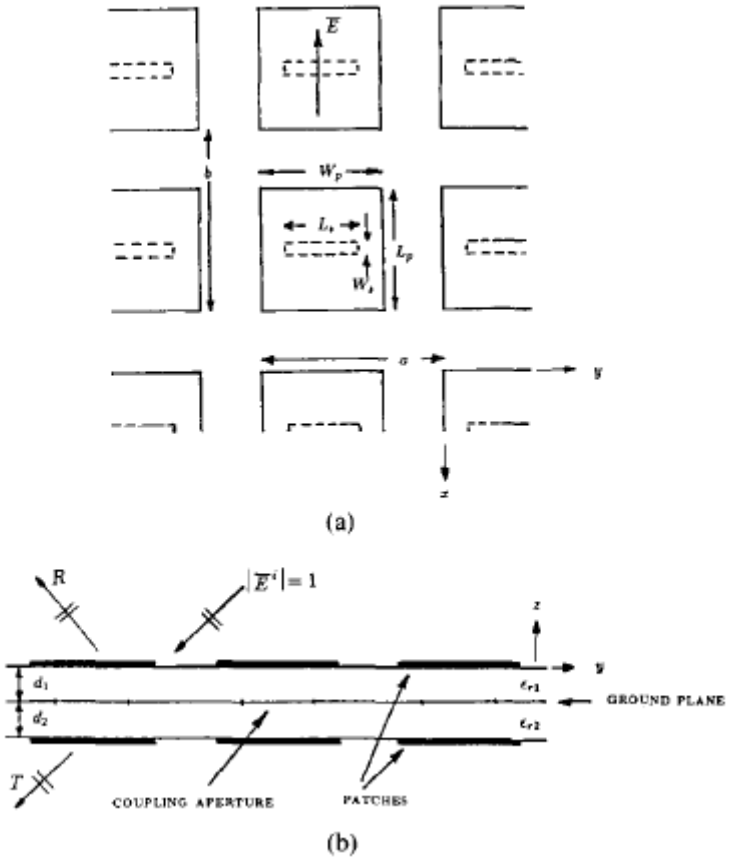

Figure 3- 2 Top (a) and cross-sectional (b) views of the rectangular aperture coupled FSS [35]

According to Pous and Pozar, the resonance frequency is mainly determined by the patch sizes, however; the width of the aperture is also crucial since it provides the coupling between the patches resulting a full transmission performance in the pass-band. If the aperture becomes very large, the level of coupling increases. When it exceeds the critical value for maximum transmission, a second resonance occurs at another frequency lower than the main resonance point. As the aperture size is increased, that second resonance moves down in frequency. The bandwidth of the structure can be controlled by the thickness and electrical properties of the substrate

material. When the thickness of the slabs is increased, the bandwidth of FSS expands. The same effect can also be created by using a material with a lower dielectric coefficient. Nevertheless, as the bandwidth is increased, the coupling level reduces which can result an undesired FSS performance.

The application of aperture coupled FSS structures using circular elements is first investigated by Hang Zhou et al. in [36]. They designed and fabricated a filter-antenna consisting of a conical frequency selective surface radome and a monopole antenna. The FSS model they proposed is composed of three metallic layers, two outer patches and one coupling aperture between the other layers. The metallic layers are separated from each other with two dielectric slabs as shown in Figure 3-3.

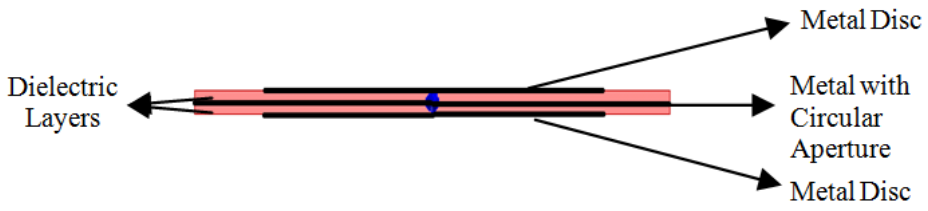

Figure 3- 3 Layers of the hybrid FSS model

They first constructed the unit cell and optimized the FSS parameters using HFSS®. After observing the unit cell model to be satisfactory in different aspects like center frequency, bandwidth and oblique incidence performances, they modeled a finite structure, a conical FSS radome with a monopole antenna (filter-antenna), to check the FSS performance under these conditions. In the finite solution, they used the symmetry property of the model and solved the problem with the quarter of the actual model as shown in Figure 3- 4. Finally, they completed their work fabricating the conical FSS and measuring its performance. The results of the measurements are observed to be consistent with the simulations. FSS radome does not significantly affect the radiation pattern of the monopole

antenna in pass-band frequencies while decreasing the RCS of the system for the out-of-band frequencies.

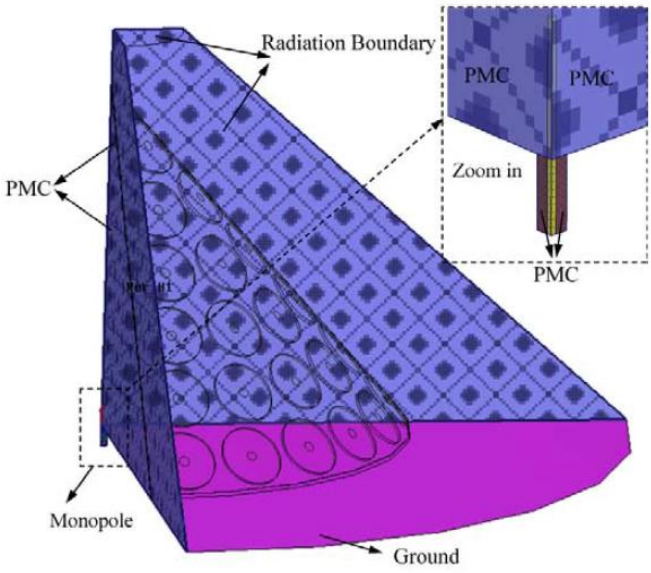

Figure 3- 4 A quarter of the filter-antenna model simulated with HFSS [36]

In this study, the aperture coupled circular hybrid FSS model of Hang Zhou et al. in [36] is utilized for a doubly-curved FSS radome design. The original model they proposed operates around 6 GHz with a bandwidth of 0.26 GHz (5.90-6.17 GHz). The parameters of the coupled aperture circular disk FSS model are scaled for the Ku-band operation. Scaling shifts the pass-band of FSS, however; there exist many discrepancies in the filtering characteristics since all the parameters have distinct effects. Therefore, the parameters are required to be optimized until the new design goals are fully met.

In order to observe the effects of different FSS parameters to the filtering characteristics, sweep analyses for each of them are performed using the single element unit cell model in HFSS®. The sweep parameters are namely, outer disk radius (r1), circular aperture radius (r0), dielectric thickness (h) and period (p) of the unit cell FSS element as shown in Figure 3- 5.

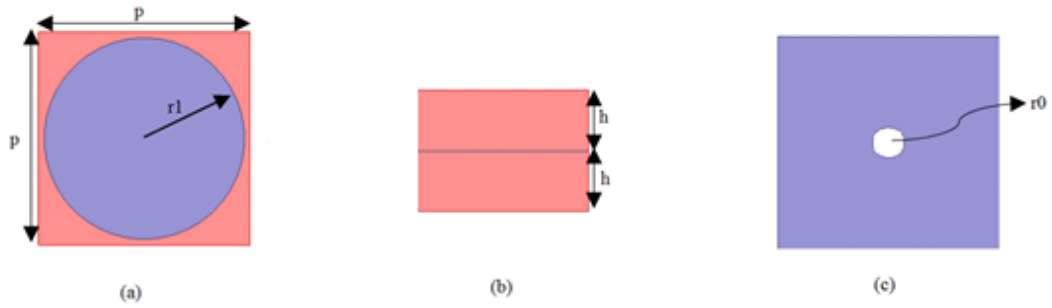

Figure 3- 5 Sweep parameters of the FSS unit cell; (a) Top view (b) Side view (c) Circular aperture metallic layer

The transmission characteristics for different FSS parameters are presented between Figure 3- 6 and Figure 3- 9. The design parameters shown in figures are given as normalized to their individual optimum values.

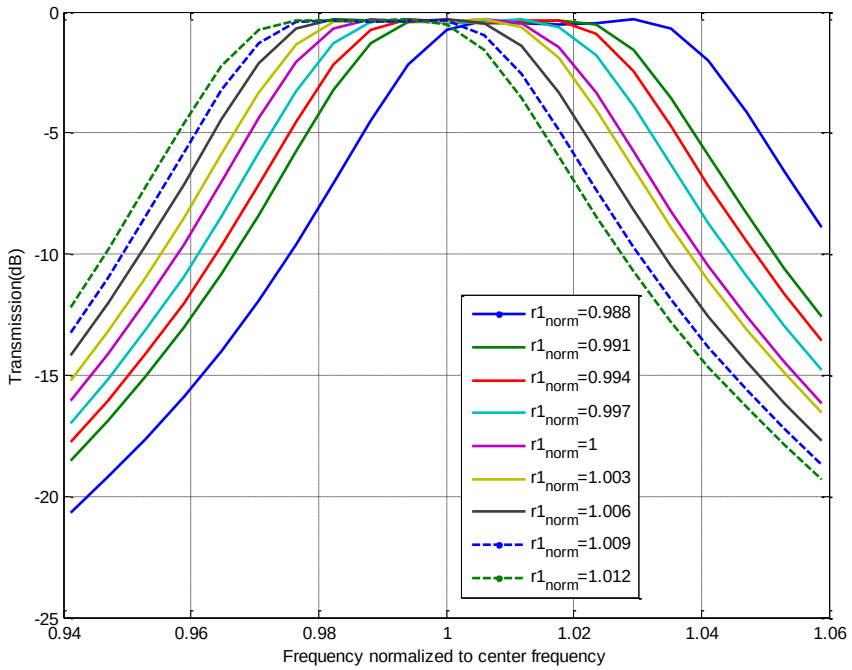

Figure 3- 6 Transmission responses of the hybrid FSS for disk radius parameter (r1) sweep

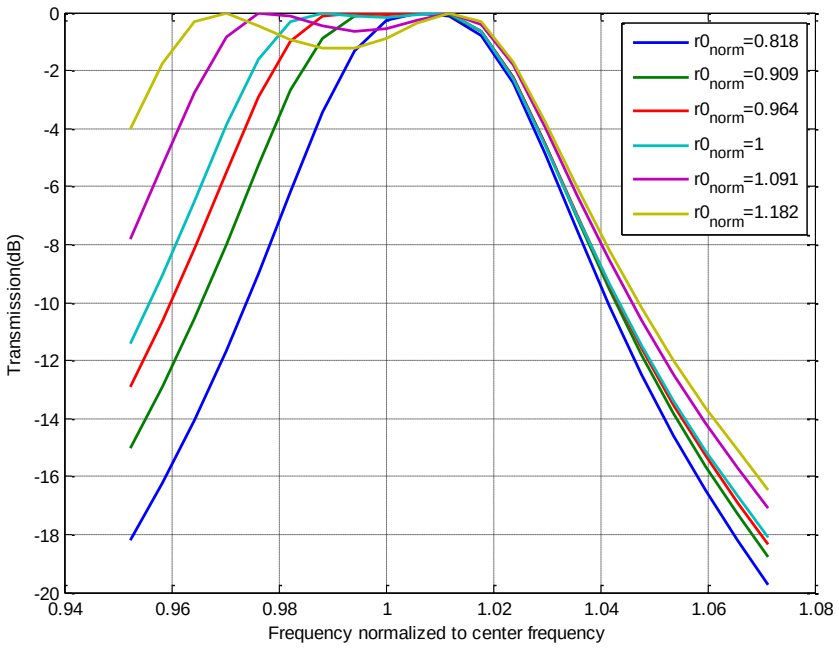

Figure 3- 7 Transmission responses of the hybrid FSS for circular aperture radius parameter (r0) sweep

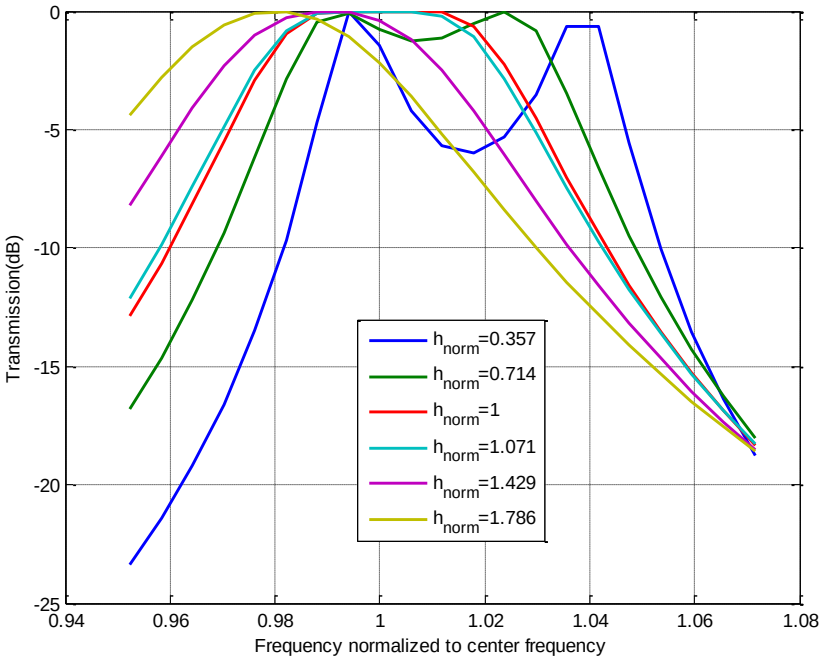

Figure 3- 8 Transmission responses of the hybrid FSS for dielectric slab thickness parameter (h) sweep

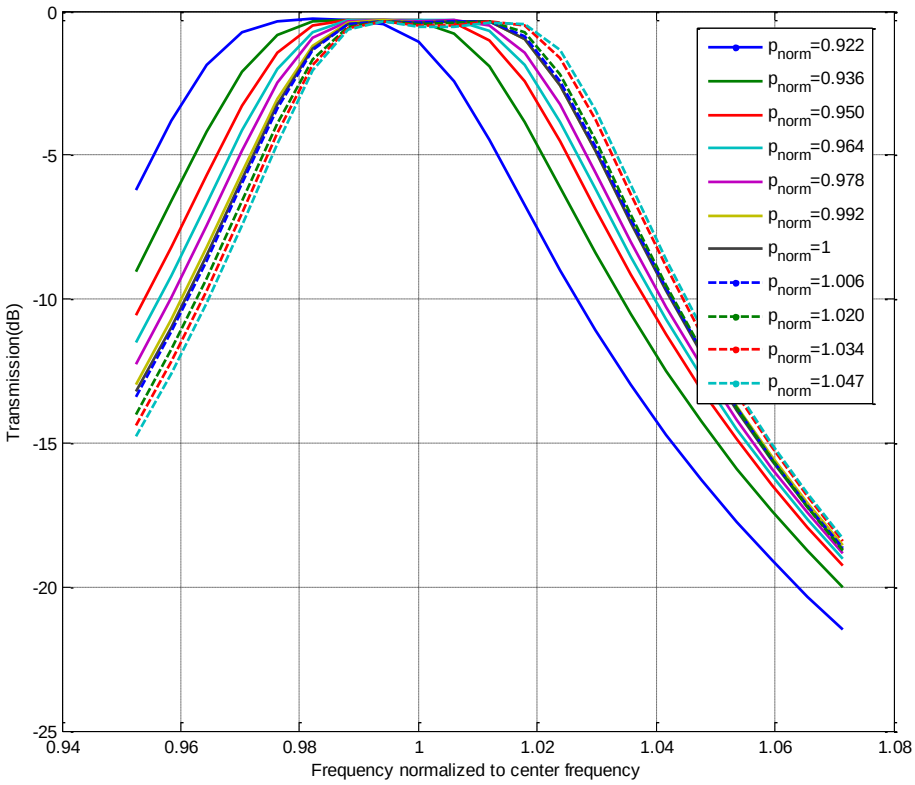

Figure 3- 9 Transmission responses of the hybrid FSS for period parameter (p) sweep

The results of the parameter sweep analyses are also summarized in Table 3- 1 to Table 3- 4 with the normalized parameter sizes, center frequencies, 3 dB frequencies and resultant fractional 3dB bandwidth values. The parameter normalizations are done with respect to the optimum values while normalization for the frequency is accomplished scaling to target center frequency of the design (f_0). As observed from Table 3- 1 and Figure 3- 6, increasing the radius of the outer disks moves the center frequency down and does not considerably affect the bandwidth of FSS.

Table 3- 1 Parameter sweep results for disk radius (r1)

r1 (Normalized)	Center Freq (Normalized)	3dB points (Normalized)		Fractional 3dB BW (%)
0,973	1,030	1,003	1,057	5,202
0,982	1,018	0,994	1,048	5,263
0,985	1,018	0,991	1,045	5,263
0,988	1,012	0,988	1,042	5,294
0,991	1,009	0,985	1,036	5,015
0,994	1,006	0,982	1,033	5,030
0,997	1,003	0,979	1,030	5,045
1,000	1,000	0,976	1,027	5,060
1,003	0,997	0,973	1,024	5,075
1,006	0,994	0,970	1,021	5,090
1,009	0,991	0,967	1,018	5,105
1,012	0,988	0,964	1,015	5,120

The transmission characteristic of the FSS model is very sensitive to the changes in aperture radius (r0) since it has the most powerful effect on the coupling between the outer patch disks. The changes on the aperture radius create bandwidth variations rather than shifting the resonant frequency of the design (see Table 3- 2).

Table 3- 2 Parameter sweep results for aperture radius (r0)

r0 (Normalized)	Center Freq (Normalized)	3dB points (Normalized)		Fractional 3dB BW (%)
0,818	1,006	0,988	1,027	3,846
0,909	1,003	0,982	1,027	4,451
0,964	1,000	0,979	1,027	4,762
1,000	1,000	0,976	1,027	5,060
1,091	0,994	0,964	1,030	6,587
1,182	0,991	0,955	1,030	7,508

Parameter sweep for the thickness of the dielectric slabs reveals that the coupling and, consequently, 3 dB bandwidth of FSS transmission response decline as the thickness is increased. The results for the thickness sweep are presented in Table 3-

3. When the thickness is decreased by more than half of the optimum value, the transmission characteristic is observed to vanish totally.

Table 3- 3 Parameter sweep results for dielectric thickness (h)

h (Normalized)	Center Freq (Normalized)	3dB points (Normalized)		Fractional 3dB BW (%)
0,357	-	-	-	-
0,714	1,009	0,982	1,036	5,310
1,000	1,000	0,976	1,027	5,060
1,071	1,000	0,973	1,024	5,060
1,429	0,991	0,967	1,012	4,505
1,786	0,982	0,958	1,003	4,545

As the period of the FSS model is changed while other parameters are kept constant, the main alteration is detected for the center frequency. Table 3- 4 exhibits the increase in the center frequency with enlarged periodicity.

Table 3- 4 Parameter sweep results for FSS period (p)

p (Normalized)	Center Freq (Normalized)	3dB points (Normalized)		Fractional 3dB BW (%)
0,922	0,982	0,961	1,009	4,848
0,936	0,991	0,967	1,015	4,805
0,950	0,997	0,970	1,021	5,075
0,964	0,997	0,973	1,021	4,776
0,978	1,000	0,973	1,024	5,060
0,992	1,000	0,976	1,027	5,060
1,000	1,000	0,976	1,027	5,060
1,006	1,000	0,976	1,027	5,060
1,020	1,003	0,979	1,027	4,748
1,034	1,003	0,979	1,030	5,045
1,047	1,006	0,979	1,030	5,030

Considering the different effects of various FSS parameters, a full performance optimization of the unit cell is implemented. The design is optimized in order to

provide sufficient transmission features up to 45^0 angle of incidence. The maximum in-band insertion loss is around 0.7 dB for both TE and TM polarizations except for 45^o TE mode incidence. Insertion loss for TE mode 45^o incidence is about 1.5 dB. The bandwidth of FSS is observed to be maintained as the angle of incidence changes. It is also successful in selectivity aspects such that it results in 10dB suppression in 400 MHz away from the upper and lower limits of pass-band region. Transmission and reflection responses of the optimized unit cell for the normal incidence are shown in Figure 3- 10.

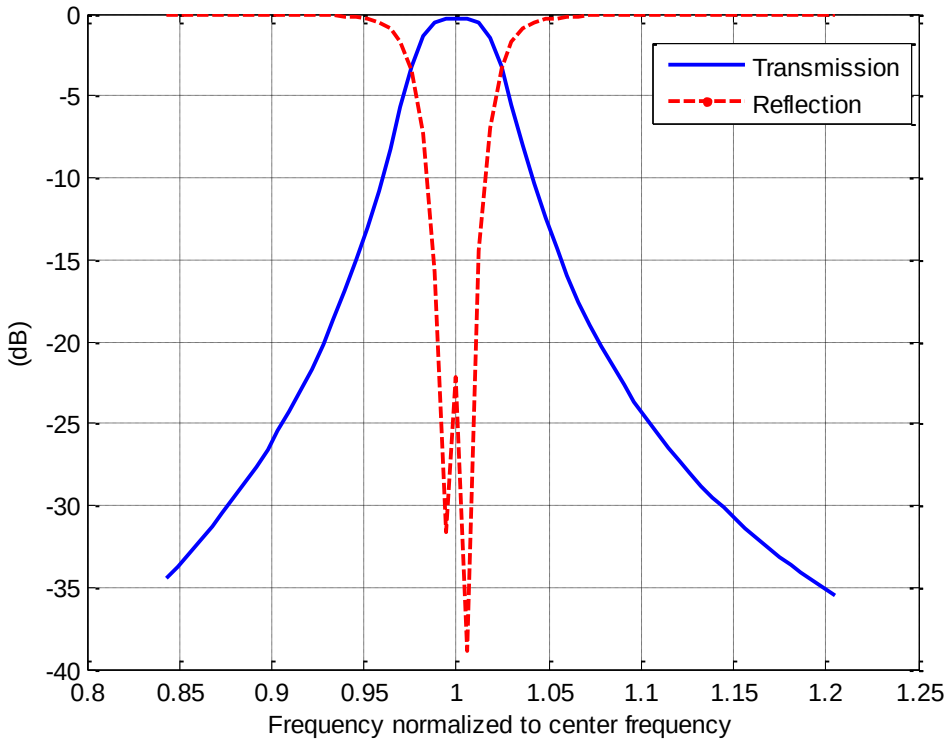

Figure 3- 10Transmission and reflection characteristics of the optimized FSS unit cell

FSS unit cell is also checked for the oblique incidence cases up to 45^0. Between Figure 3- 11 and Figure 3- 14, the transmission and reflection curves for different incident angles and polarizations (TE-TM) are demonstrated. As observed from these figures, FSS unit cell maintains the filtering performance for oblique incidence angles.

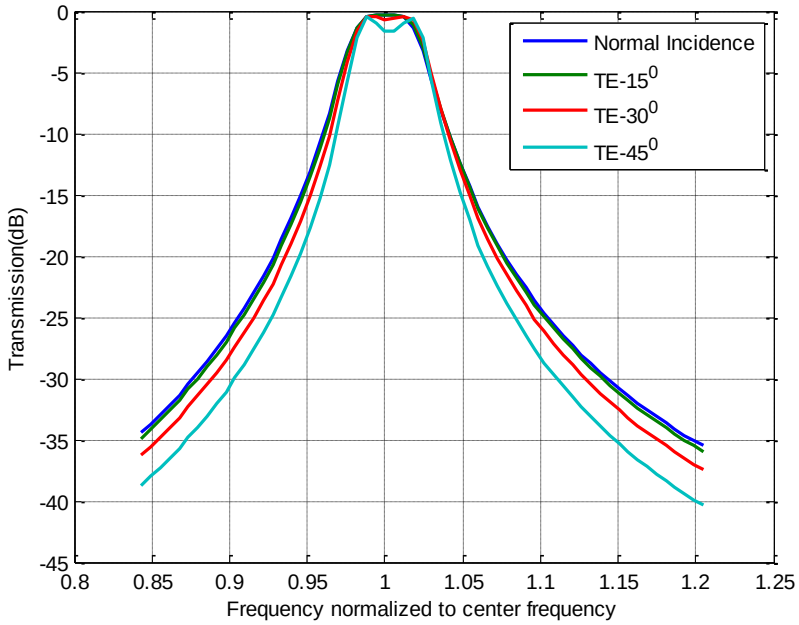

Figure 3- 11 Transmission performance of the unit cell for different angles of incidence (TE modes)

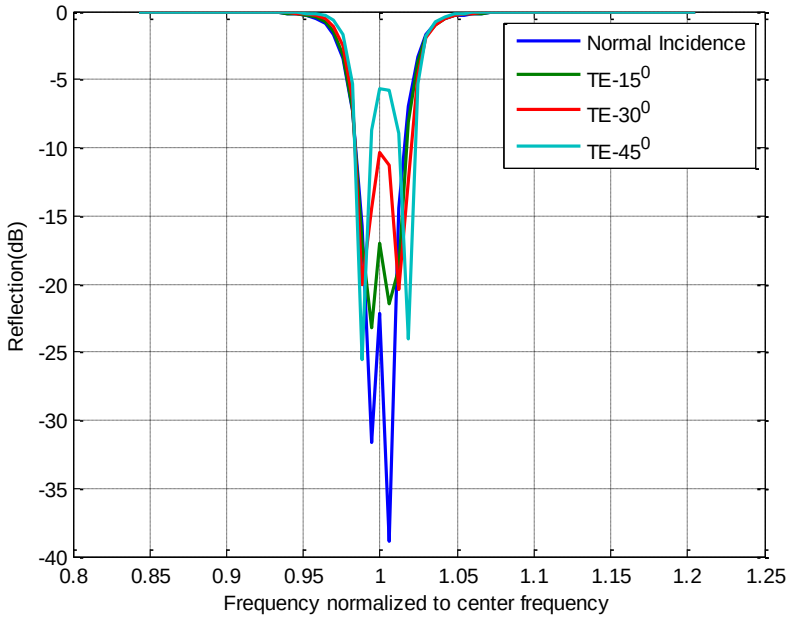

Figure 3- 12 Reflection characteristics of the unit cell for different angles of incidence (TE modes)

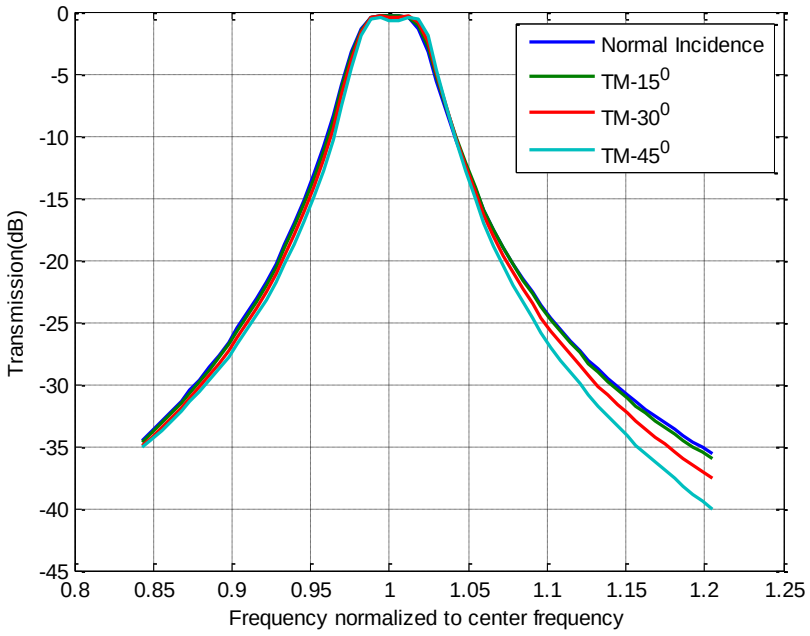

Figure 3- 13 Transmission performance of the unit cell for different angles of incidence (TM modes)

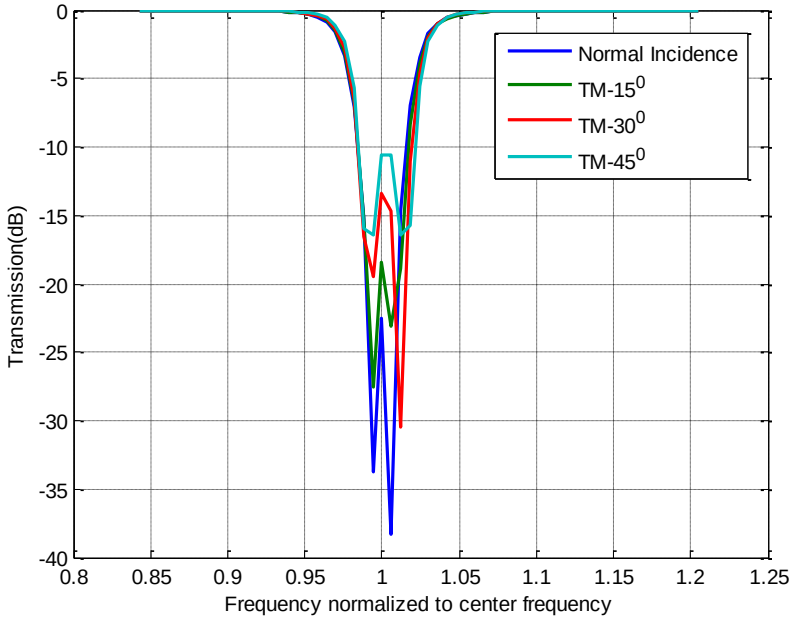

Figure 3- 14 Reflection characteristics of the unit cell for different angles of incidence (TM modes)

After the optimization of the unit cell parameters, predefined design goals are accomplished for a planar infinite-in-two-dimension array of the single FSS element. The array topology applied for this solution is rectangular, i.e., the four side walls of the single element are defined as periodic boundaries (master-slave pairs in HFSS terminology). The transmission and reflection performances of the triangular and hexagonal unit cells for different angles of incidences and polarizations are also determined using HFSS. The corresponding results are presented between Figure 3- 15 and Figure 3- 22. As observed from the figures, the properties of the rectangular array configuration do not significantly change for the different orientations of the elements. In case that an important discrepancy is observed for the new array topology, the design parameters would be optimized for that unit cell model which is very close to the final arrangement of the elements.

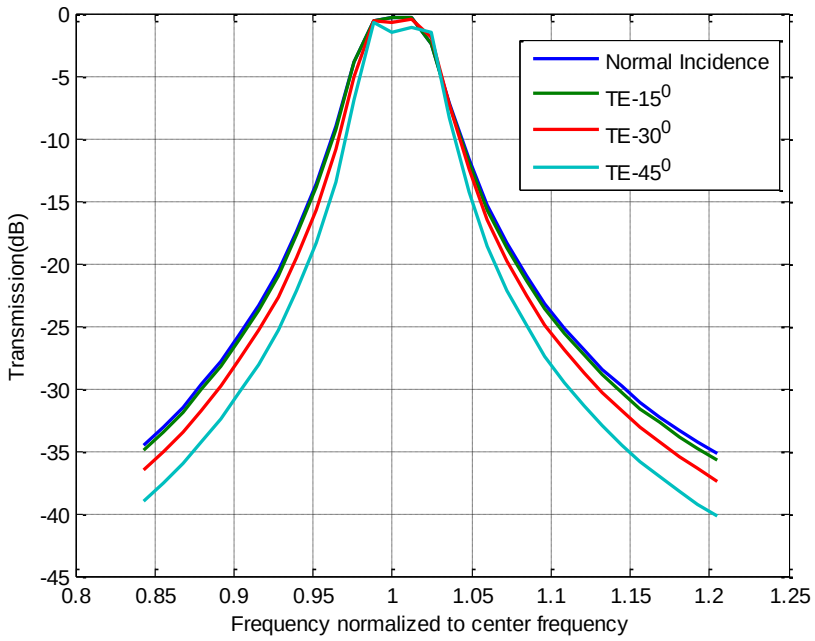

Figure 3- 15 Transmission responses of triangular array unit cell for different angle of incidences (TE modes)

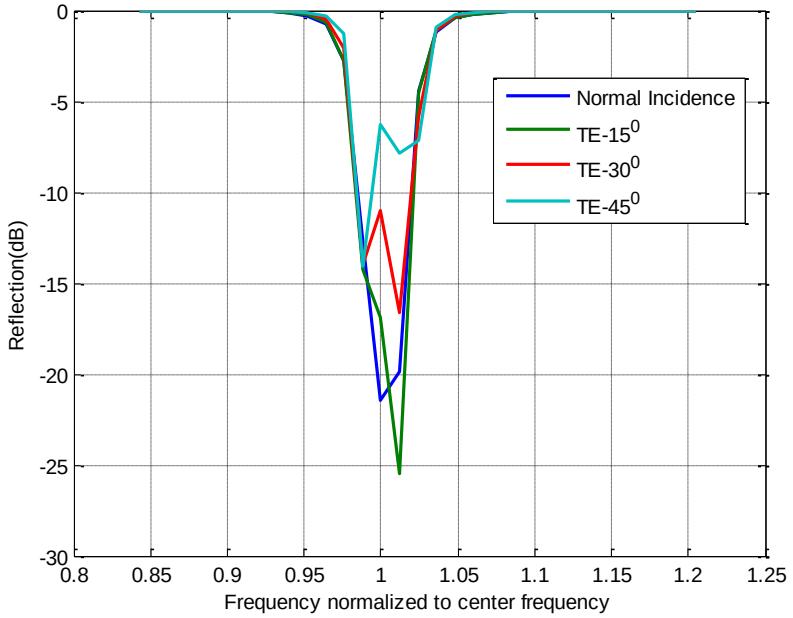

Figure 3- 16 Reflection responses of triangular array unit cell for different angle of incidences (TE modes)

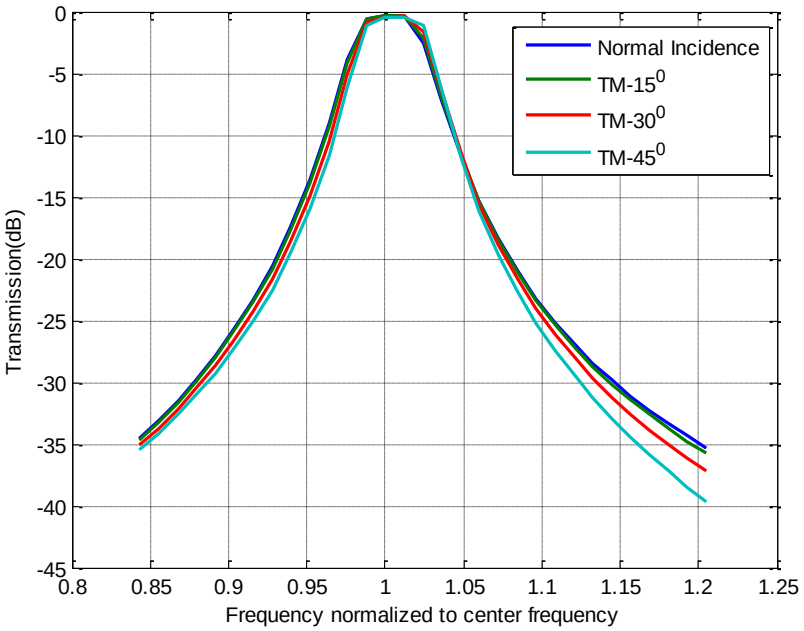

Figure 3- 17 Transmission responses of triangular array unit cell for different angle of incidences (TM modes)

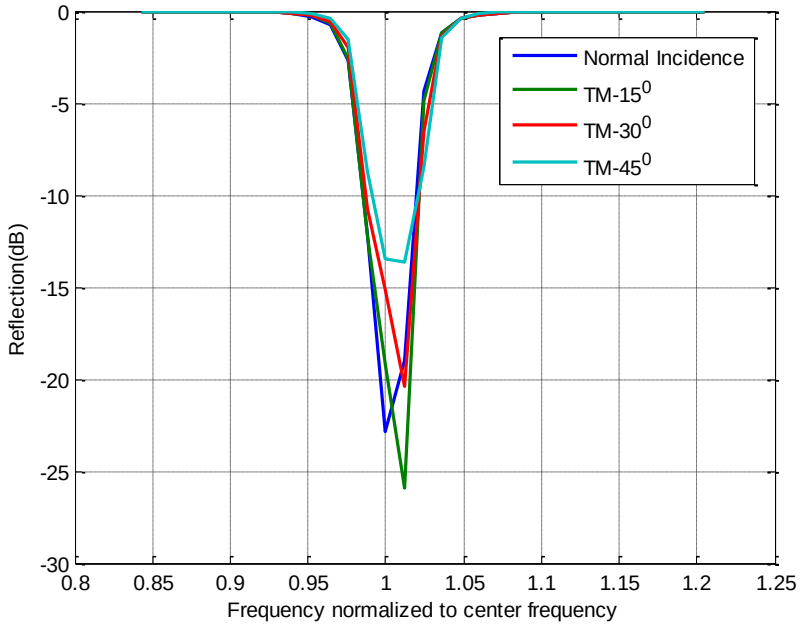

Figure 3- 18 Reflection responses of triangular array unit cell for different angle of incidences (TM modes)

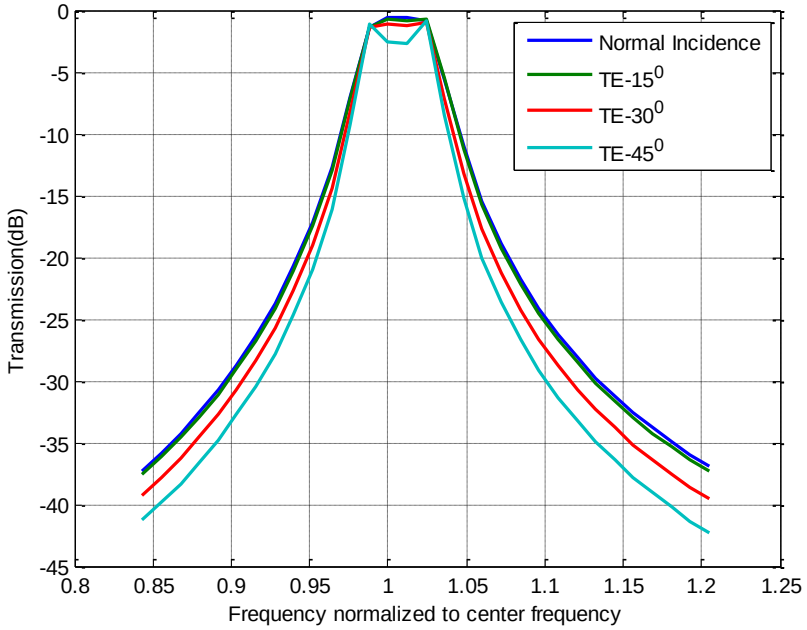

Figure 3- 19 Transmission responses of hexagonal array unit cell for different angle of incidences (TE modes)

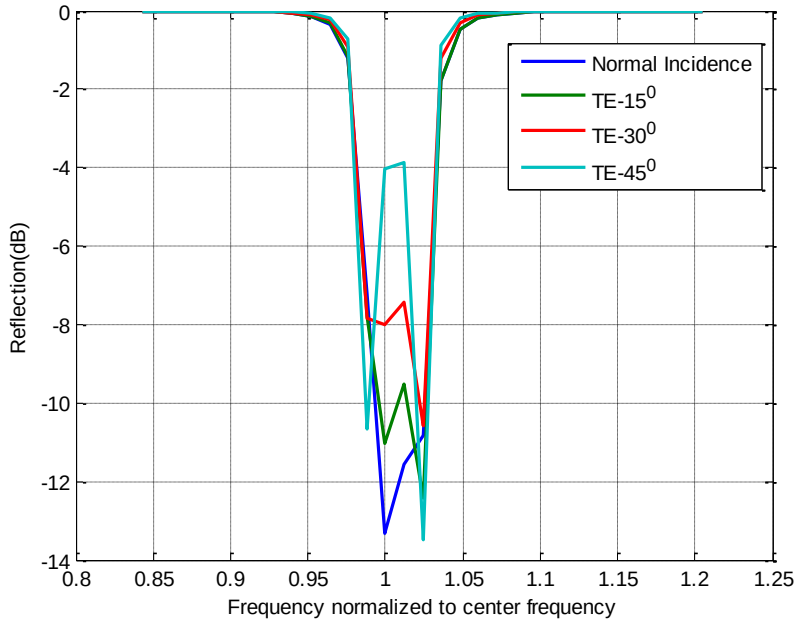

Figure 3- 20 Reflection responses of hexagonal array unit cell for different angle of incidences (TE modes)

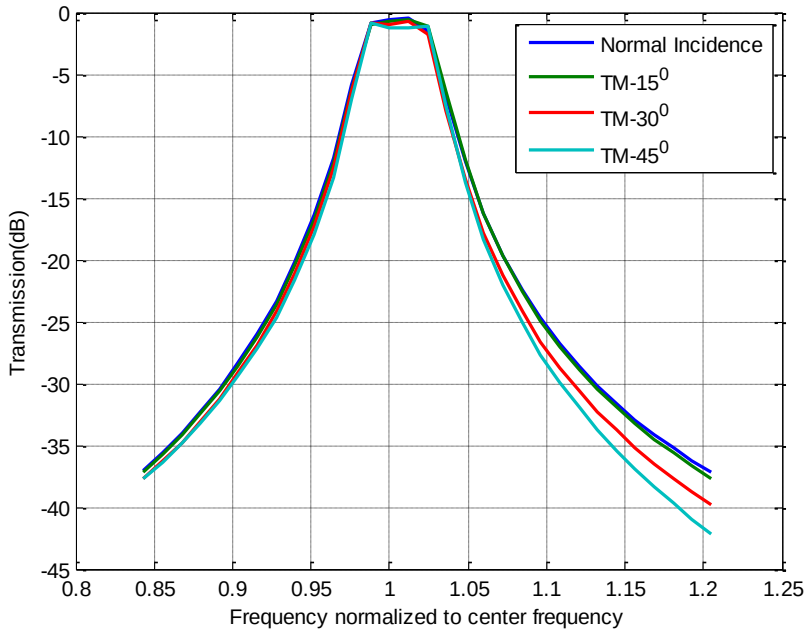

Figure 3- 21 Transmission responses of hexagonal array unit cell for different angle of incidences (TM modes)

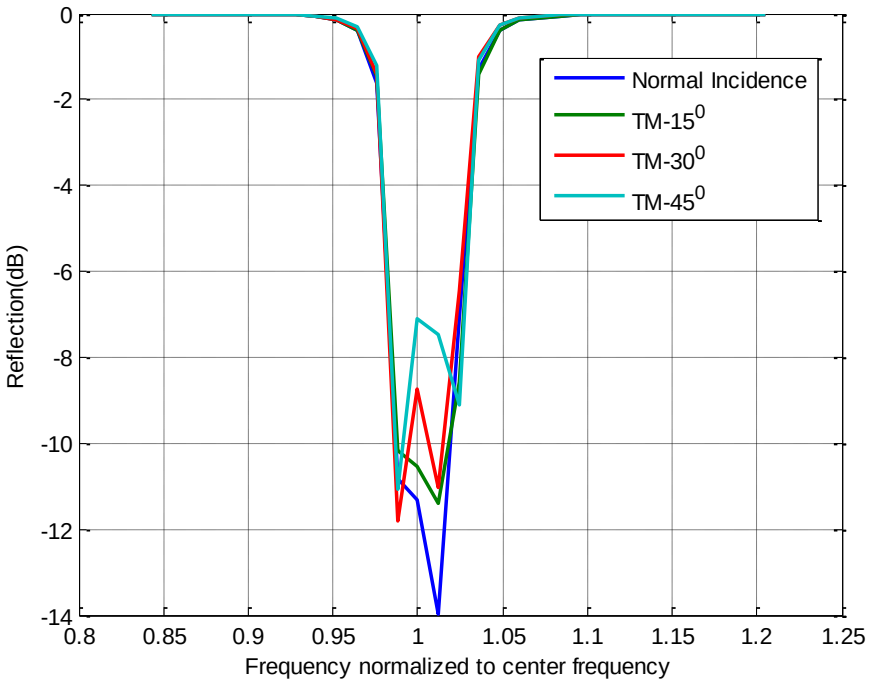

Figure 3- 22 Reflection responses of hexagonal array unit cell for different angle of incidences (TM modes)

Moreover, alternative unit cell arrangements mentioned in Chapter 2 are constructed specifically for the current problem since the placement of the elements on the final model is planned to be built in that sense (see Figure 3- 23). The same analysis procedure is implemented for these unit cells and the results are demonstrated in Figure 3- 24 and Figure 3- 25, for different amounts of shifts, which are 0, p/6, p/3 and p/2 where p is the period of the unit cell. The simulation results show that there is still no significant change in the performance of the FSS element for these unit cell models.

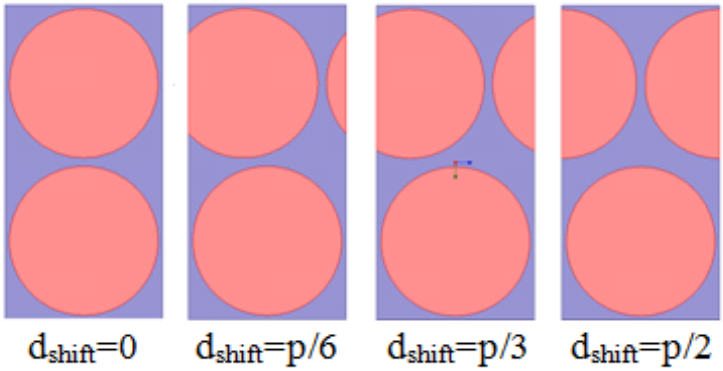

Figure 3- 23 Modified triangular array unit cells (different shifts)

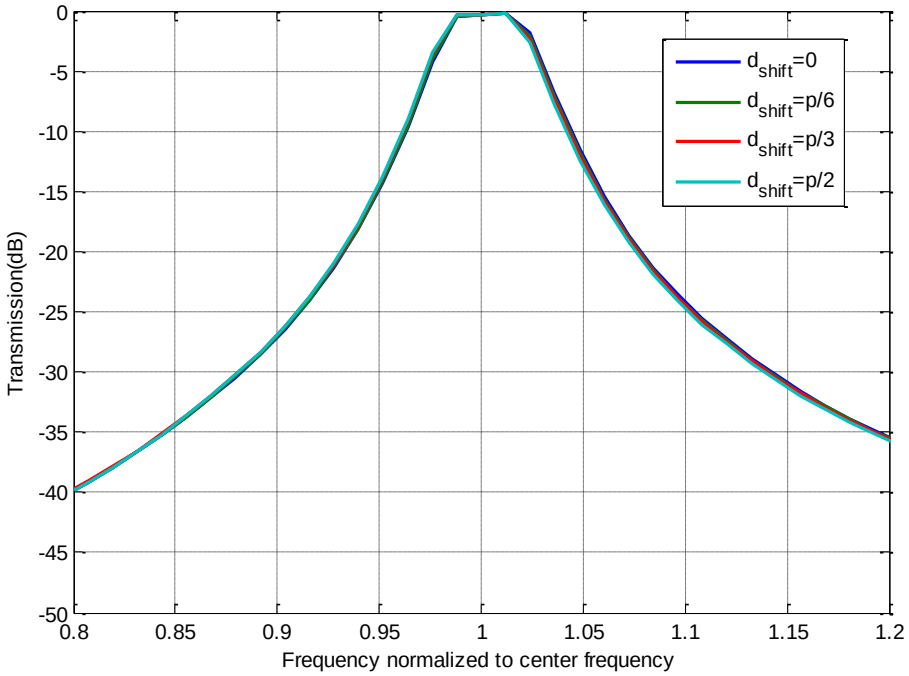

Figure 3- 24 Transmission responses of the modified triangular array unit cells

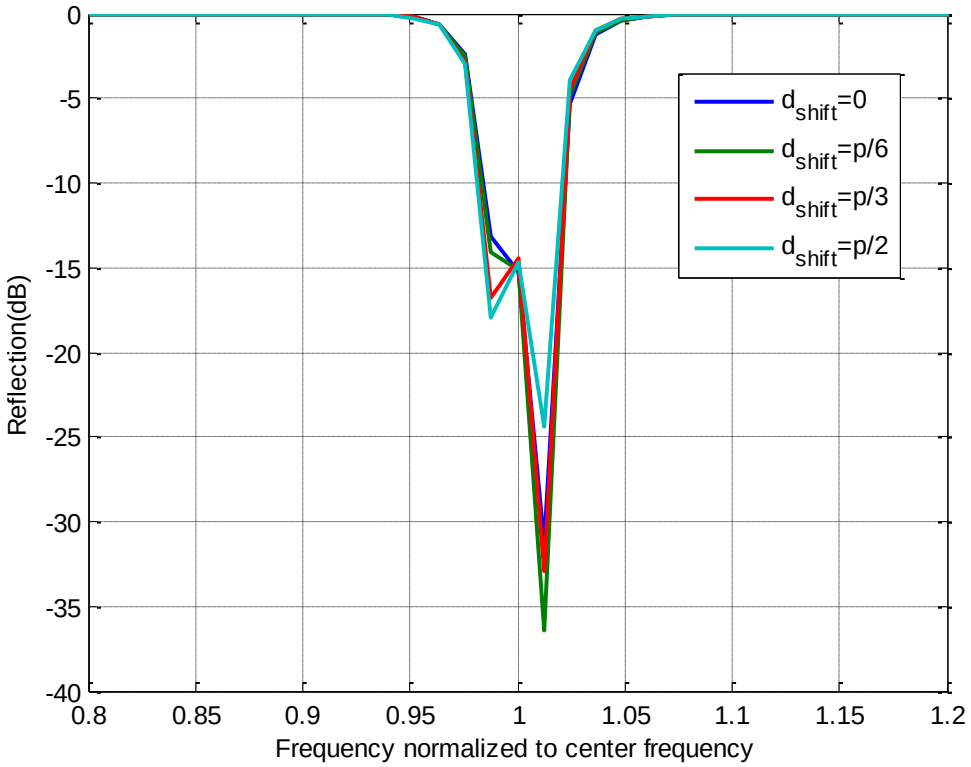

Figure 3- 25 Reflection responses of the modified triangular array unit cells

After planar single element unit cell solutions, semi-finite models with conformal and planar arrangements are constructed which are detailed in Chapter 2 (see Figure 2- 10 and Figure 2- 11). For in-band frequencies, it is observed that there is no significant change in far field patterns for the cases with and without FSS radome. When the frequencies of out-of-band region are investigated, it is observed that a total suppression of the total field occurs consistent with the filtering characteristics of the single element FSS unit cell. The total and incident fields at the far zone are demonstrated for various frequencies between Figure 3- 26 and Figure 3- 30.

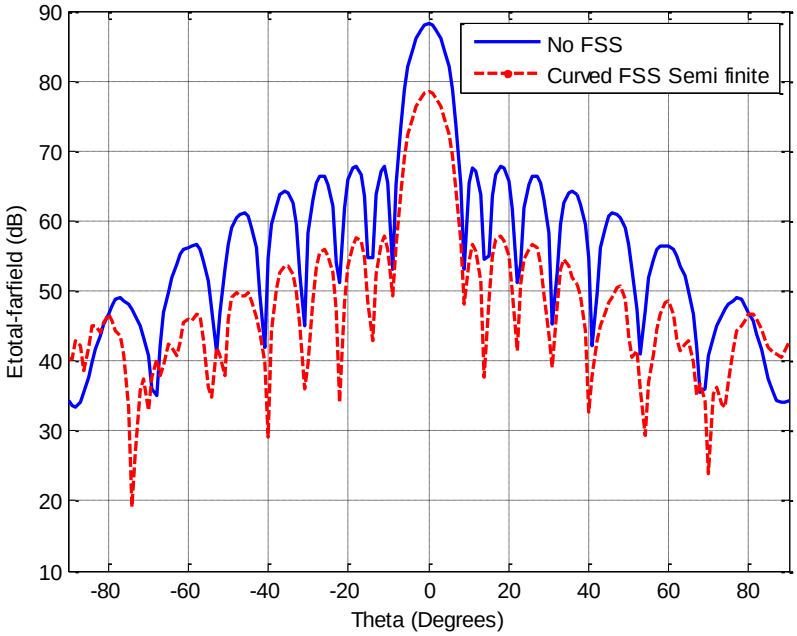

Figure 3- 26 Far field E-total patterns of 31-element source antenna array without FSS radome and with conformal FSS at $0.964*f_0$

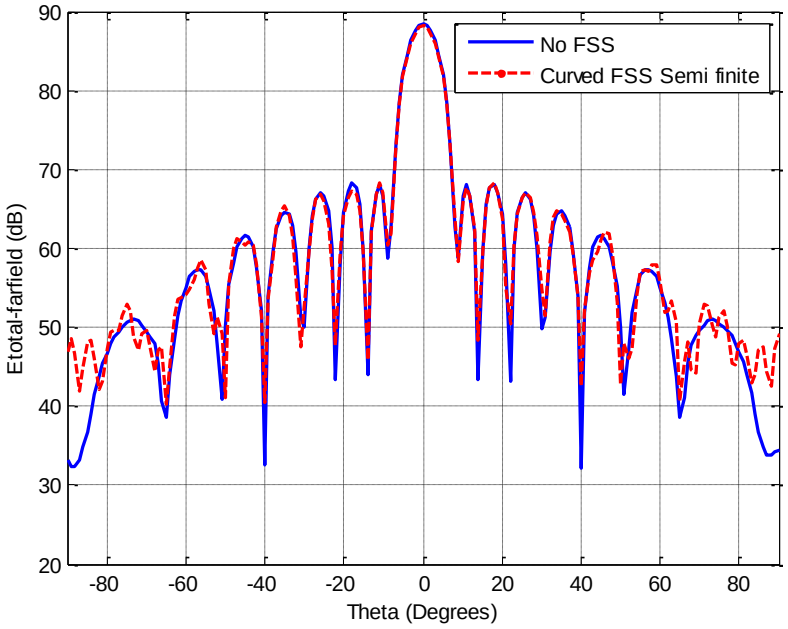

Figure 3- 27 Far field E-total patterns of 31-element source antenna array without FSS radome and with conformal FSS at $0.988*f_0$

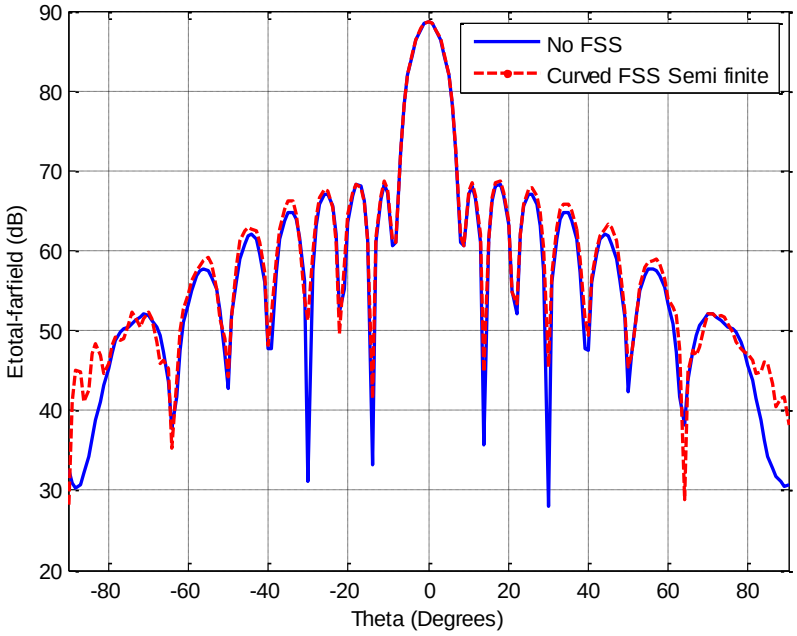

Figure 3- 28 Far field E-total patterns of 31-element source antenna array without FSS radome and with conformal FSS at f_0

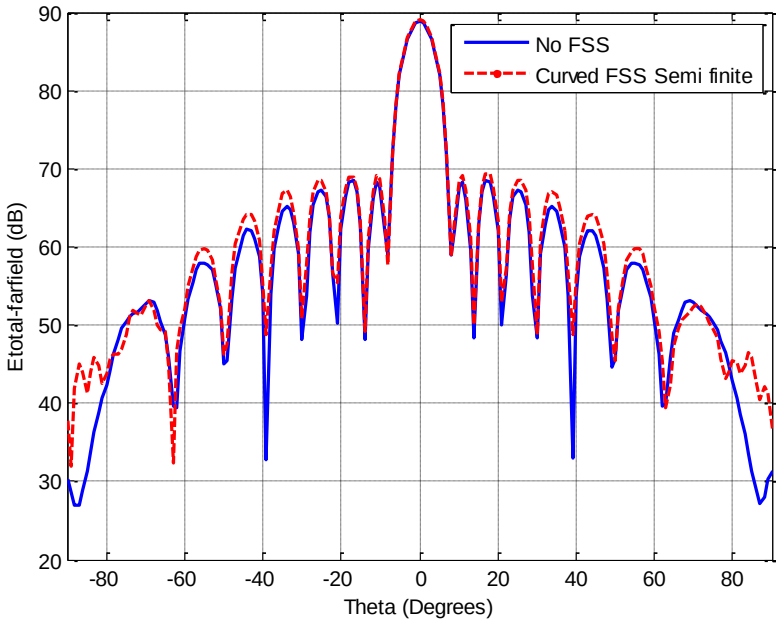

Figure 3- 29 Far field E-total patterns of 31-element source antenna array without FSS radome and with conformal FSS at $1.012*f_0$

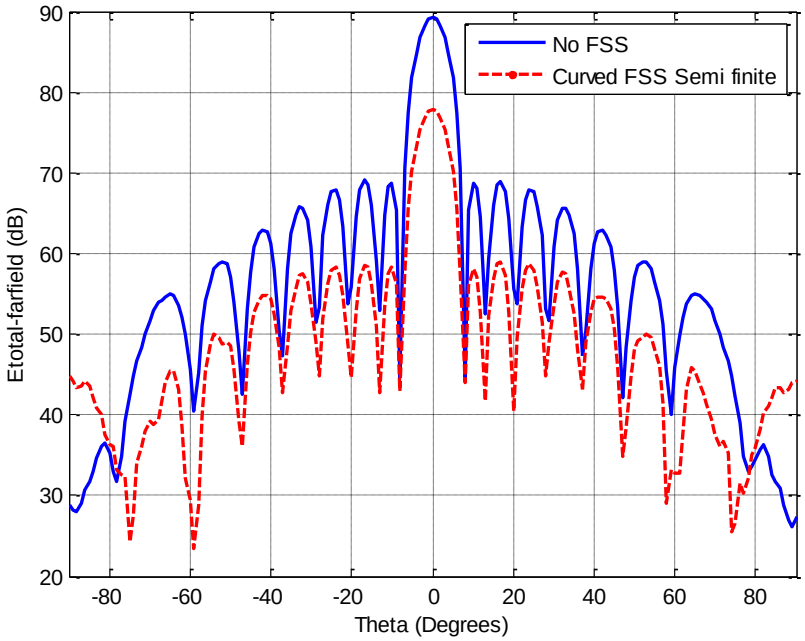

Figure 3- 30 Far field E-total patterns of 31-element source antenna array without FSS radome and with conformal FSS at $1.048*f_0$

The semi-finite FSS model is also constructed for a planar FSS sequence as described in Chapter 2 in order to compare the planar and conformal FSS structures using the same analysis method (semi-finite analysis).

Analysis results for different frequencies are given between Figure 3- 31 and Figure 3- 33 for the planar semi-finite model. The results of the cylindrical and planar models are consistent with each other and single element unit cell solution in terms of transmission characteristics. Planar model analysis clarified an important point, the shadowing effect of FSS radome over the illumination source. As observed from the figures, the transmission and suppression characteristics are valid only for the region shadowed by FSSs. For the semi-cylinder case, the dipoles are almost totally shadowed by the radome (about 160 degrees of coverage over 180 degrees). Thus, the transmission properties of FSS radome can be determined for both main lobe and side lobe regions. The planar FSS semi-finite model shadows only 70 degrees of the upper half region (180 degrees). Therefore, the results are sensible up to that point for the planar solutions.

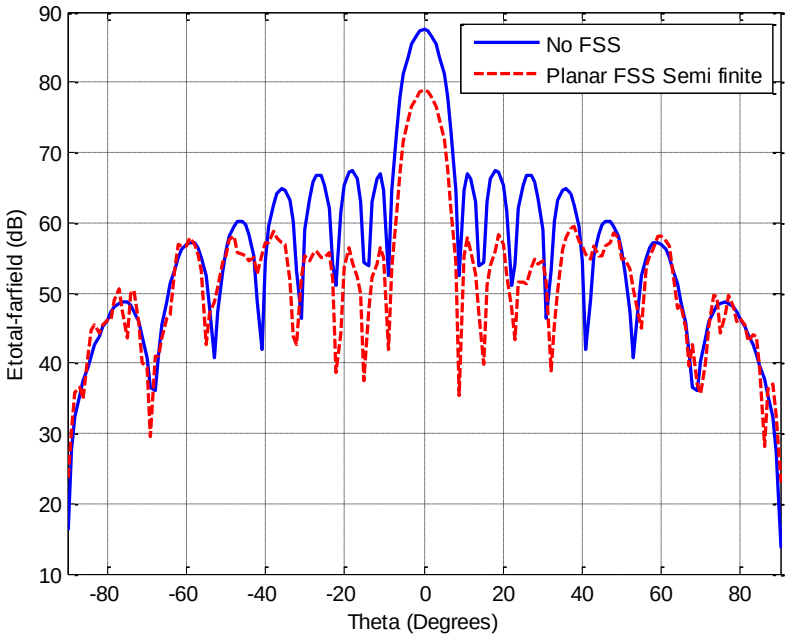

Figure 3- 31 Far field E-total patterns with and without FSS radome at $0.964*f_0$ - Planar semi-finite model

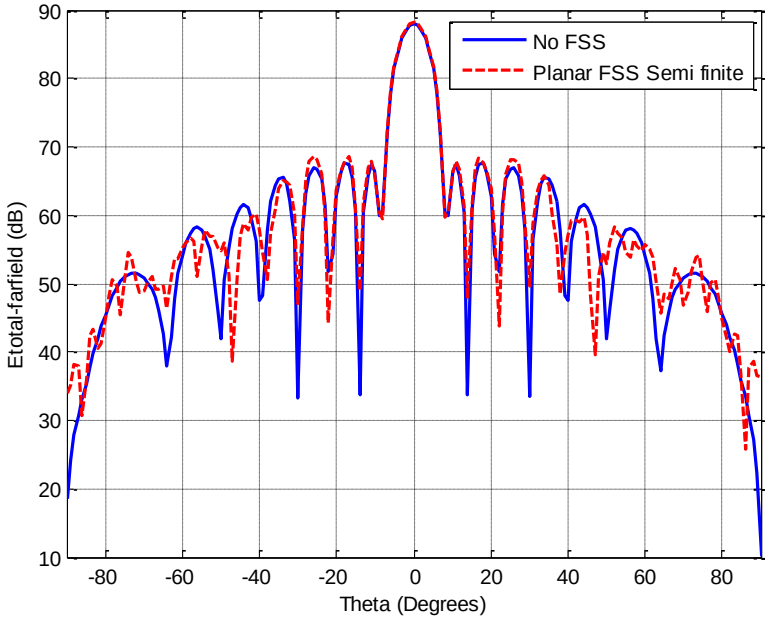

Figure 3- 32 Far field E-total patterns with and without FSS radome at f_0 - Planar semi-finite model

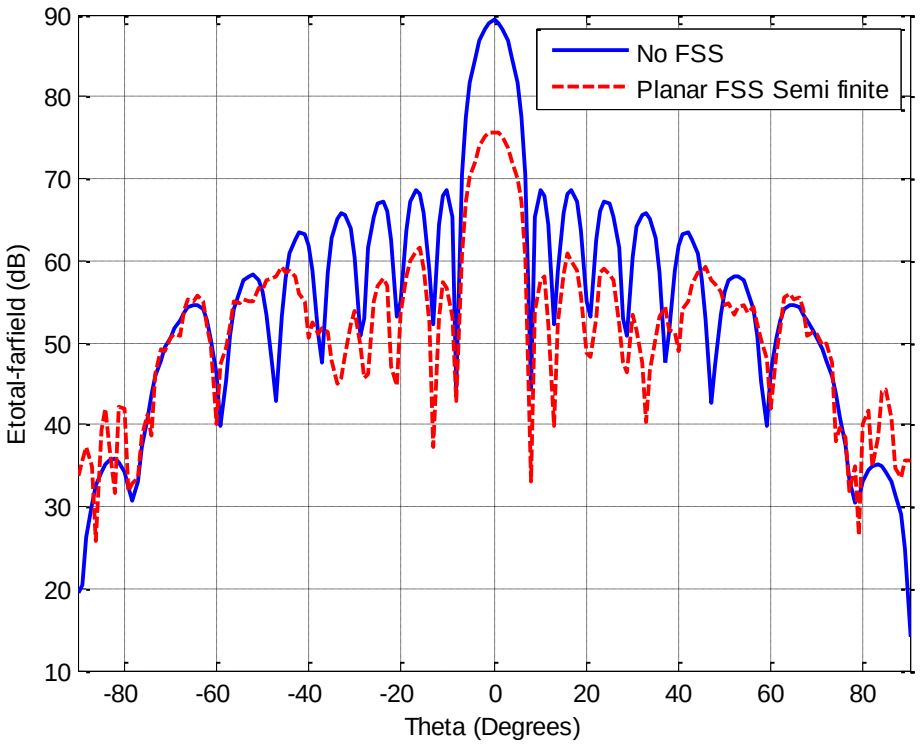

Figure 3- 33 Far field E-total patterns with and without FSS radome at $1.048*f_0$ - Planar semi-finite model

For the above solutions, a narrow-beam pattern is preferred since the final implementation of the FSS radome will be done for a highly directive antenna. In addition to that, filtering characteristics of semi-finite planar and curved models are also determined for a wide-beam illumination. Two uniformly excited Hertzian dipoles are used for this configuration. FSS models are observed to exhibit same behaviors as in the narrow-beam case. They transmit or suppress the incoming waves with respect to the frequencies and coverage region limitations. The results for the wide-beam illumination for semi-cylinder and planar models are demonstrated between Figure 3- 34 and Figure 3- 36.

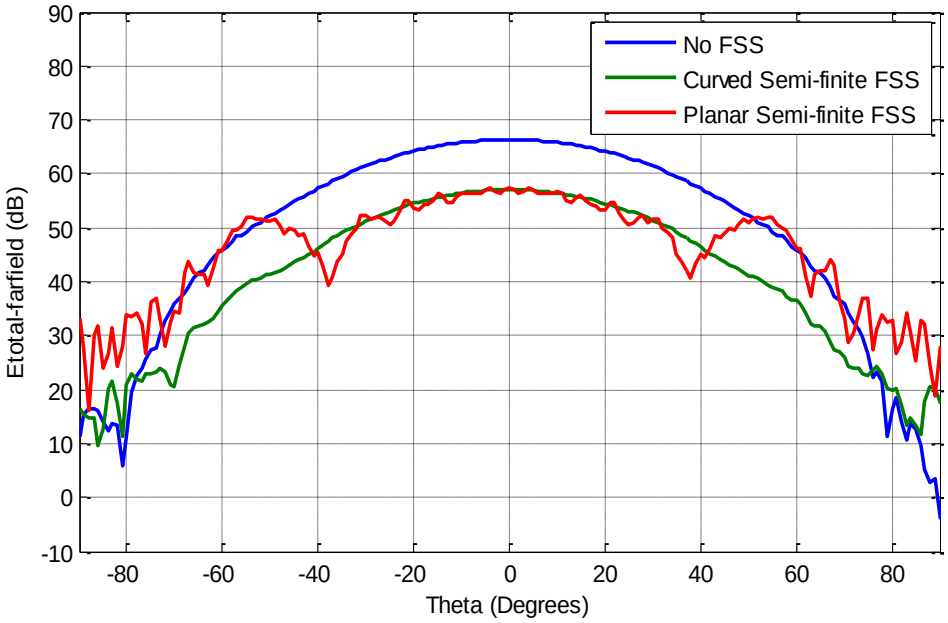

Figure 3- 34 Far field E-total patterns of 2-element source antenna array without FSS radome and with planar and conformal FSS at $0.964*f_0$

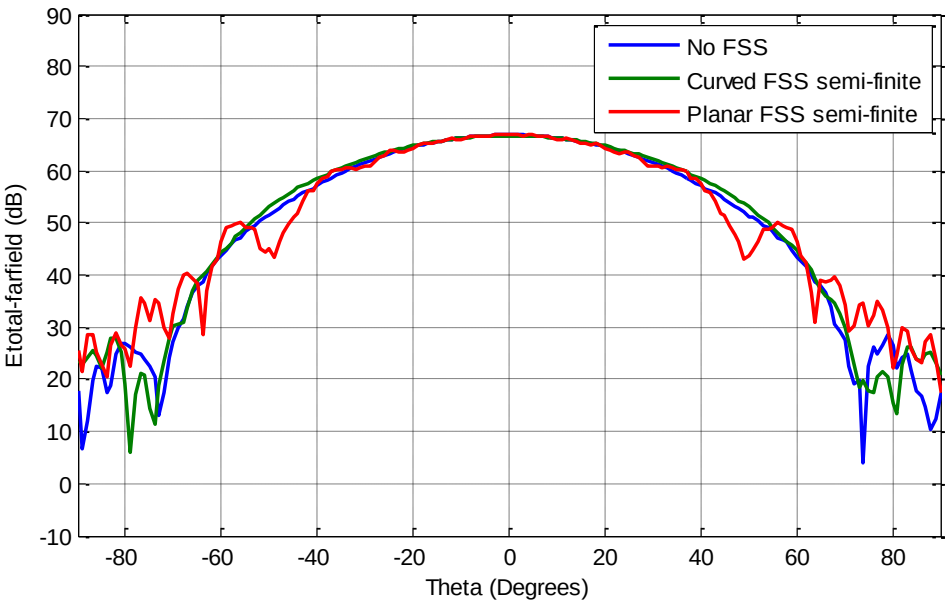

Figure 3- 35 Far field E-total patterns of 2-element source antenna array without FSS radome and with planar and conformal FSS at f_0

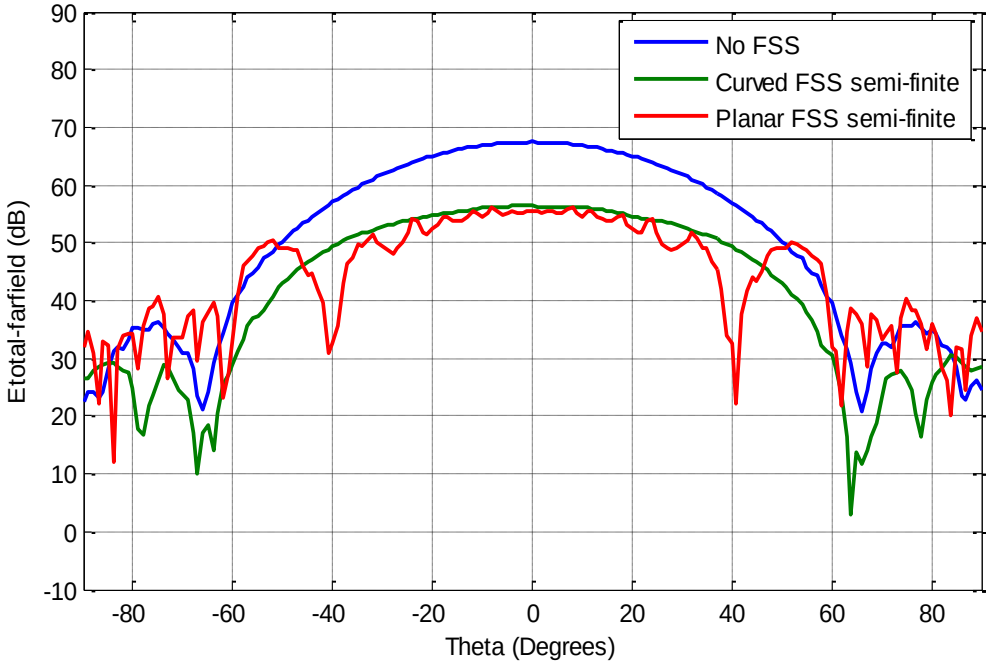

Figure 3- 36 Far field E-total patterns of 2-element source antenna array without FSS radome and with planar and conformal FSS at $1.048*f_0$

Using the results obtained from the above solutions, the transmission performances of single element unit cell, semi-finite curved and planar FSS models are compared. The transparency characteristics of the semi-finite model can be determined by the difference of the incident and total far field patterns at theta=0^0. The comparison of the transparency performances of the single element unit cell and semi-finite models both for the conformal and the planar FSS is shown in Figure 3- 37, which illustrates the good agreement between different solution techniques.

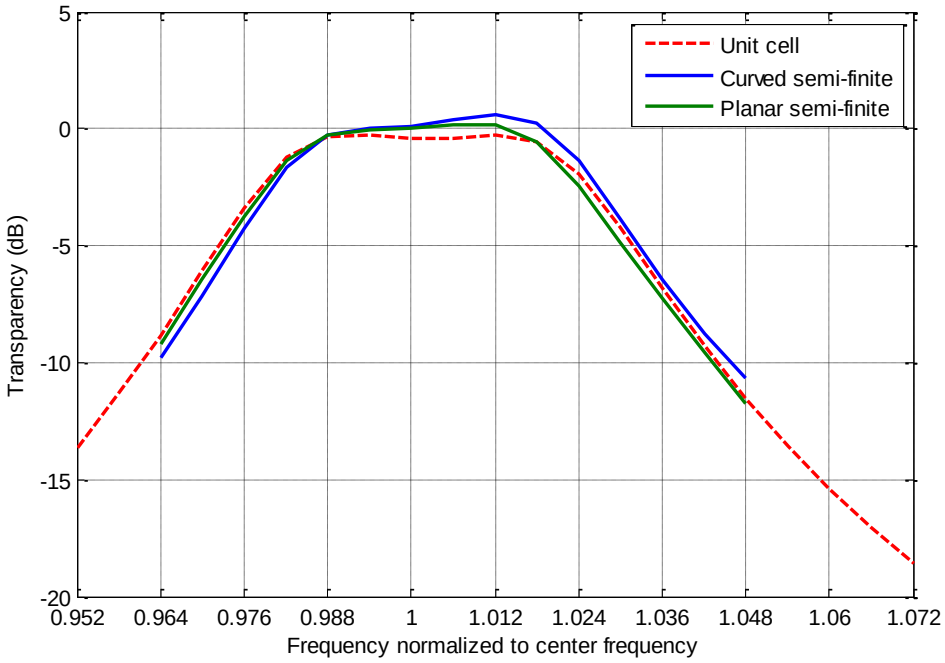

Figure 3- 37 Comparison of transmission characteristics of unit cell and semi-finite conformal and planar models

The comparison of far field patterns with and without FSS layers proves the in-band performance of FSS model. For the out-of-band characterization, the reflection properties of FSS model are required to be demonstrated. To achieve this requirement, RCS analysis can be held using the semi-finite model of the semi-cylinder FSS radome. There are two alternative techniques to compare the RCS performance of FSS radome: using PEC or dielectric cylinder of the same size as FSS radome. For the PEC cylinder configuration, the out-of-band RCS characteristics of FSS radome is expected to be similar to that of PEC cylinder. For pass-band frequencies, there must be a dramatic decrease in RCS of FSS radome. The solution approach for PEC cylinder is illustrated with Figure 3- 38. The back-scattered RCS results for FSS and PEC cylinders are given in Figure 3- 39. As seen in this figure, the RCS of the FSS radome is remarkably similar to the RCS of PEC cylinder out of the pass-band region of FSS. Moreover, the RCS of the FSS radome

significantly diminishes with respect to PEC cylinder around the center frequency in the pass-band.

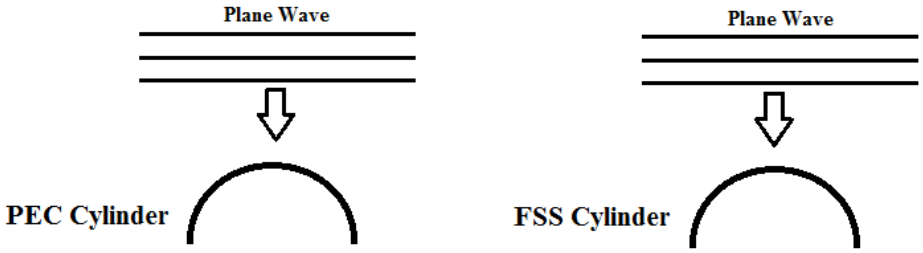

Figure 3- 38 The schematic of the RCS comparison method using PEC Cylinder

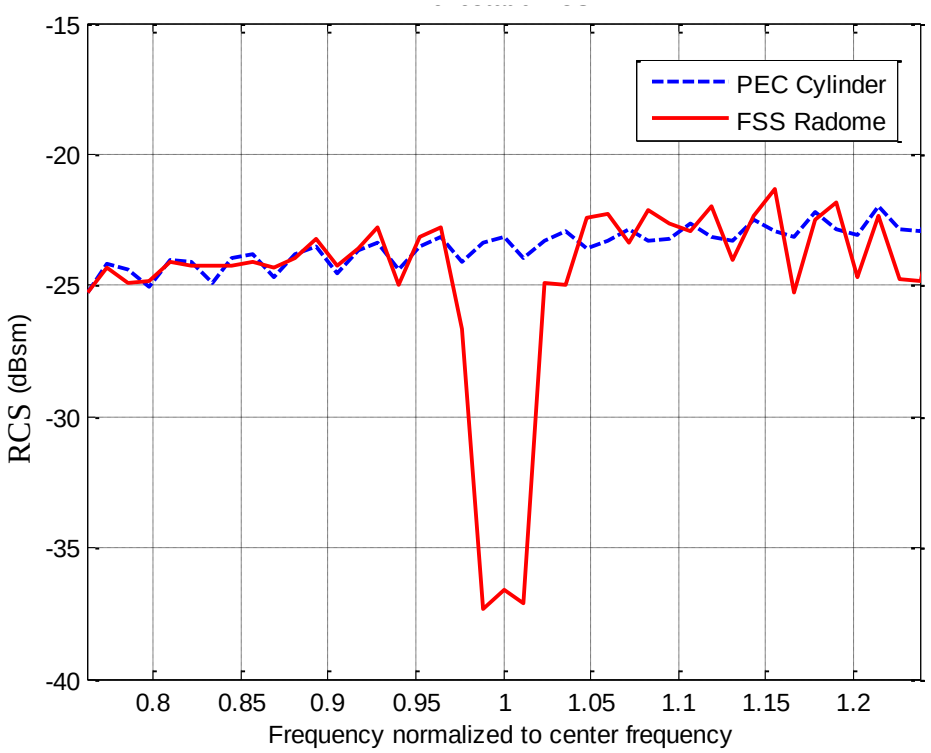

Figure 3- 39 Monostatic RCS results of FSS and PEC semi-cylinders using semi-finite analysis method

The other alternative to observe the out-of-band characteristics of FSS radome is to use a dielectric cylinder instead of PEC material. For the dielectric radome configuration, there also exists a PEC sheet representing the antenna surface used

for the illumination (see Figure 3- 40). The schematic of the configuration built for RCS comparison is given in Figure 3- 41.

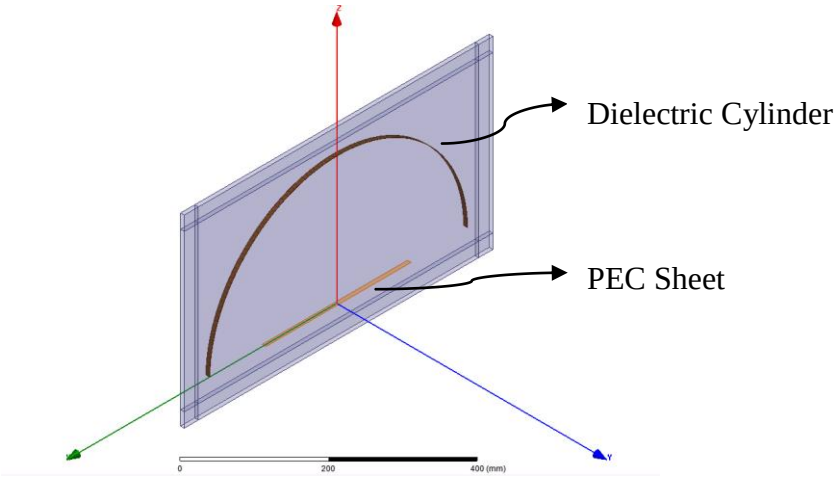

Figure 3- 40 RCS analysis using semi-finite model: Dielectric radome and PEC sheet

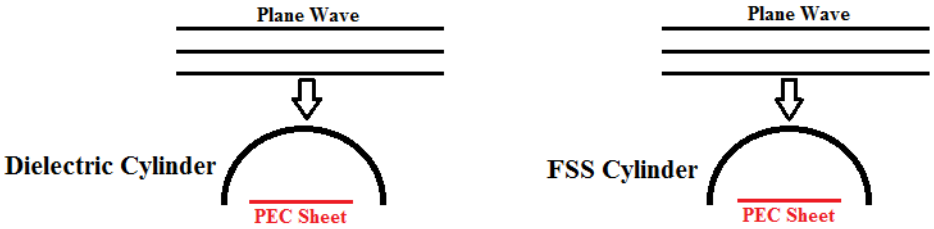

Figure 3- 41 The schematic of the RCS analysis method using dielectric cylinder and PEC planar sheet

In this approach, it is expected that monostatic RCS of the FSS cylinder must decrease dramatically for the out-of-band frequencies with respect to dielectric cylinder with PEC sheet beneath since the FSS radome reflects the incoming waves of these frequencies to different directions due to its curved surface. The analysis results indicate the expected behaviors, i.e. RCS reduction of the FSS radome with respect to dielectric radome for the band-stop regions (see Figure 3- 42).

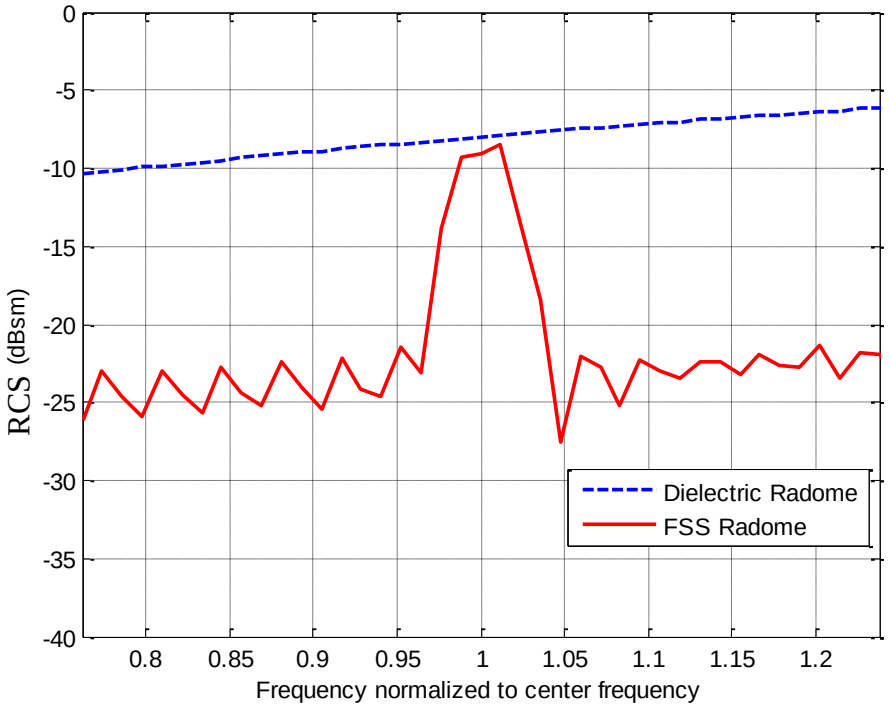

Figure 3- 42 Monostatic RCS results of FSS and dielectric semi-cylinders using semi-finite analysis method

The design process for the hybrid FSS model has been completed for both planar and conformal cases including different polarization and angle of incidence conditions. The designer may pass to fabrication steps or prove the design with a finite conformal FSS model if possible.

For this problem, a finite spherical FSS model shown in Figure 3- 43 is constructed using HFSS®. However, instead of the full spherical FSS structure, a quarter of the finite model is sufficient to analyze since there are two symmetry planes as shown in Figure 3- 44. Utilizing this property, FSS model represented in Figure 3- 44 is used to analyze the full model.

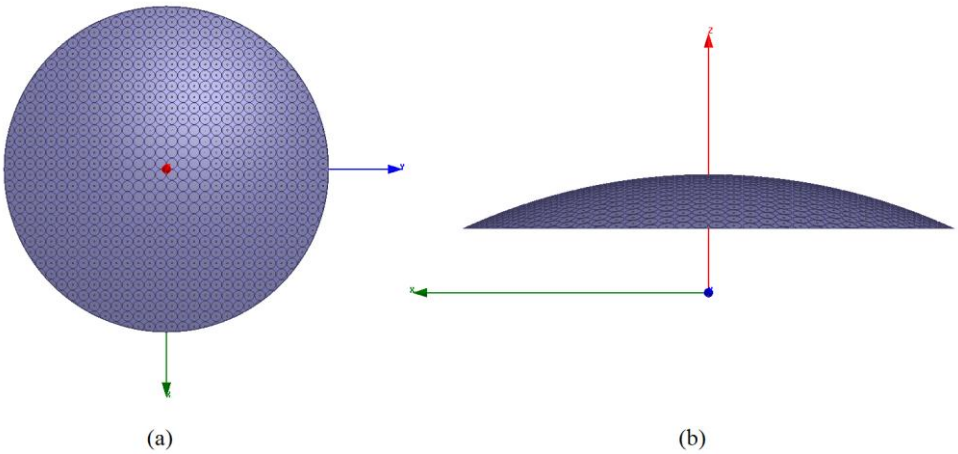

Figure 3- 43 Finite spherical FSS radome: (a) Top view (b) Side view

For illumination, a 4x1 Hertzian dipole array, which is effectively 8x2 due to symmetry planes, is used with a Taylor distribution of 20 dB side lobe level. The currents on dipoles are directed in $\hat{a}_x$-dimension. Therefore, the symmetry boundary in xz-plane is defined as PMC and the other one in yz-plane as PEC. Total electrical field patterns at far zone with and without FSS radome are compared and it is observed that FSS radome does not affect incident signals of in-band frequencies significantly, while it reflects the signals of other frequencies. Figure 3-45 to Figure 3- 47 demonstrate the filtering behavior of FSS model.

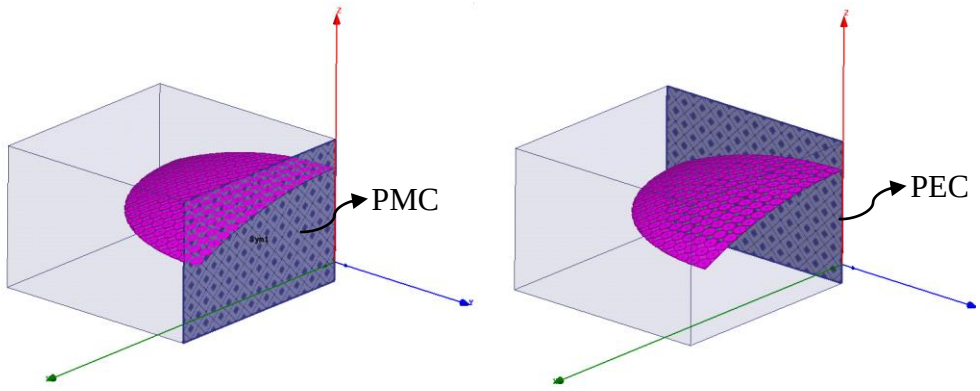

Figure 3- 44 Symmetry planes of the quarter model

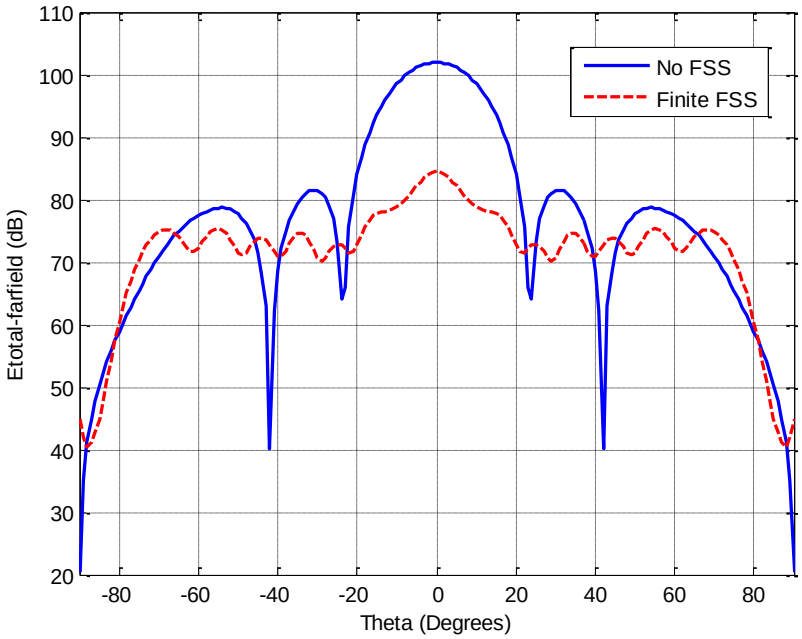

Figure 3- 45 Total E-field patterns with and without doubly curved finite FSS radome at far zone ($0.94*f_0$)

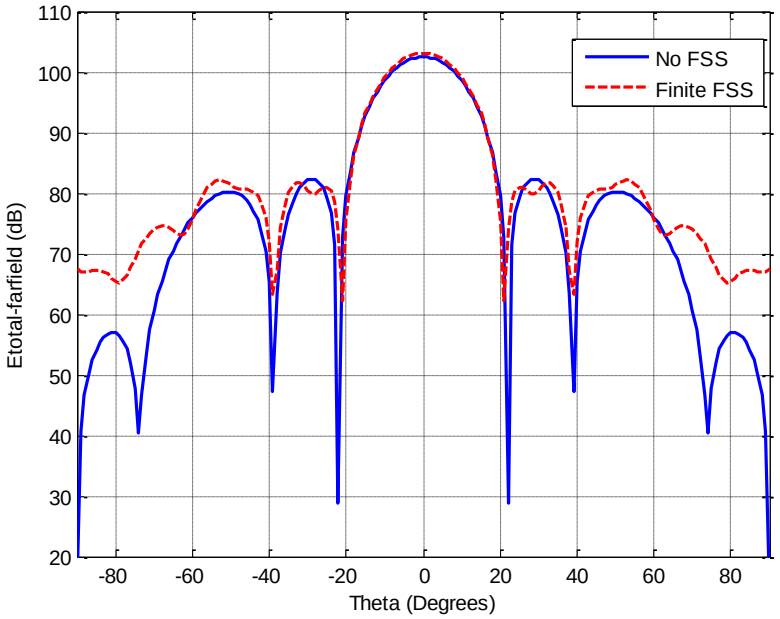

Figure 3- 46 Total E-field patterns with and without doubly curved finite FSS radome at far zone (f_0)

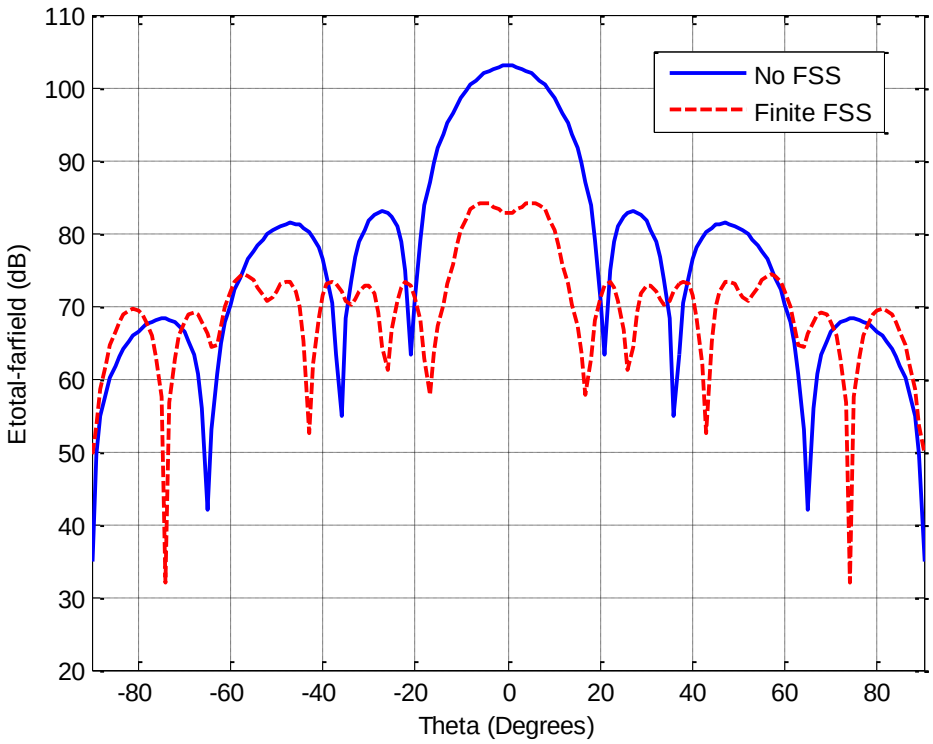

Figure 3- 47 Total E-field patterns with and without doubly curved finite FSS radome at far zone ($1.04*f_0$)

The model constructed for this finite solution is a reduced form of semi-sphere FSS radome, however; it still requires a very high memory capacity. Therefore, as explained above, if not strictly required, semi-finite solution can be accepted as the last stage of design processes since a doubly-curved finite model solutions brings a heavy calculation load and makes the approach inefficient in aspects of simulation based analyses.

As in the case of planar semi-finite model, the simulation results for the finite model imply that the FSS does not perform as expected for observation angles greater than 60^0 due to the shadowing problem associated with the coverage area of the finite structure.

CHAPTER 4

DESIGN AND ANALYSIS OF A WIDEBAND CONFORMAL FREQUENCY SELECTIVE SURFACE

4.1 Design Requirements

The general design requirements for the curved FSS applications like good conformability and stable performance against oblique incidence features, which are mentioned in details in the previous chapter, are also valid for the wideband curved FSS design. Wideband FSS structure is required to cover all X-band (8.2-12.4 GHz) frequencies with a maximum insertion loss of 0.5 dB for normal incidence. The pass-band flatness and reflection loss responses will be preserved up to 45^0 angle of incidence for both TE and TM polarizations. The principal design goals required for the wideband FSS construction can also be listed as;

- Low insertion loss in the pass-band
- Wide band operation
- Stable performance against oblique incidence
- Polarization independence
- Applicability on curved bodies

4.2 Wideband Conformal Frequency Selective Surface Design

For the conformal wide band FSS application, the ultra-wide band frequency selective surface model of H. Zhou et. al., shown in Figure 4- 1 (from [12]), is chosen as the reference model. The most distinguishing feature of this model is its stable performance against different angle of incidences. It is stated in [12] that the performance of the wide band FSS is maintained up to 30^o of incidence angle. The model consists of three metallic layers and two dielectric layers. The outer metallic patches are rectangular and the middle layer is a square grid.

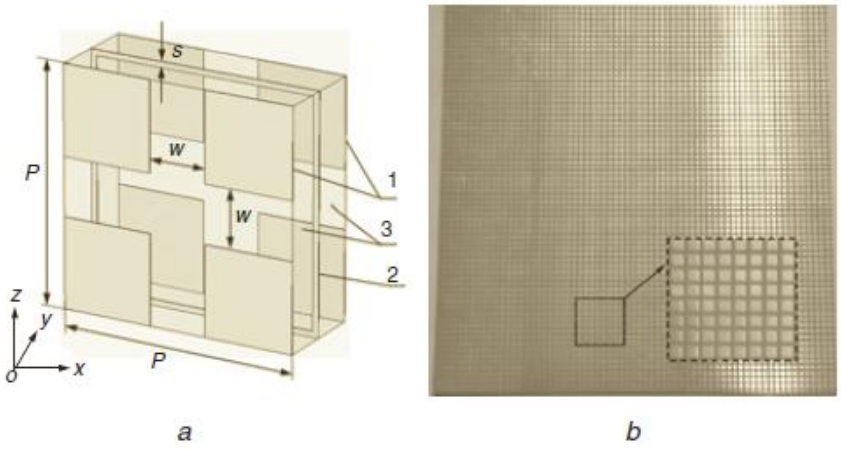

Figure 4- 1 Reference ultra-wideband FSS unit cell model: (a) Unit cell (b) Prototype of fabricated FSS [12]

The design procedure after defining the FSS model begins with the determination of starting values of the model parameters. The starting points for the optimization process are obtained by scaling the model in [12]. However, as mentioned in the previous chapters, circular elements are strongly suggested for the conformal applications due their unique properties. Therefore, the reference model is transformed to its circular counterpart, i.e. disk patches on the outer faces and circular grids between them instead of corresponding rectangular ones. Unit cell of the modified FSS model is presented in Figure 4- 2 (b). This model is analyzed

using HFSS and it is noticed that wide-band characteristics of the original FSS model is maintained without any critical change.

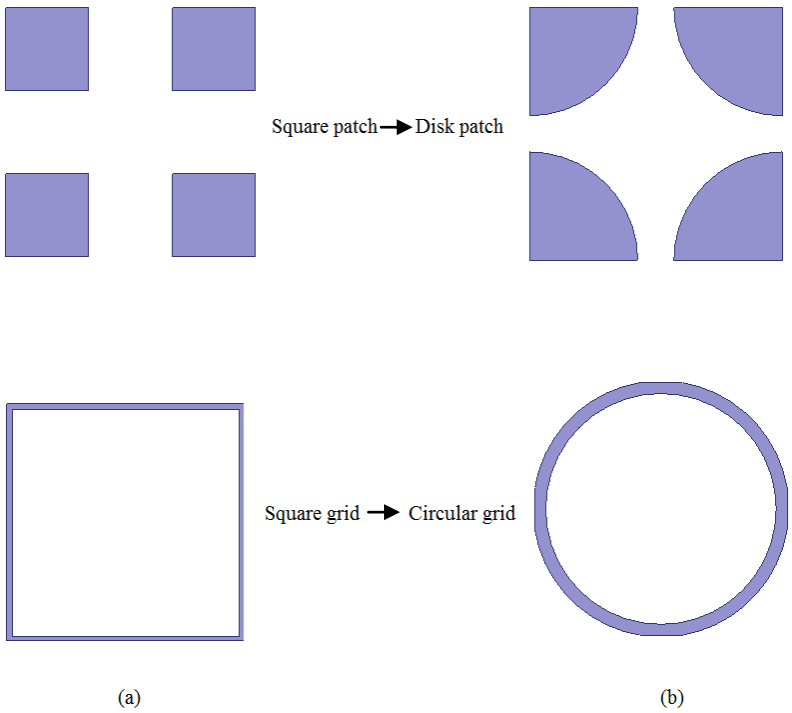

Figure 4- 2 Wideband FSS layers: (a) Original (from [12]) (b) Modified

To reach the optimum parameters ensuring the design goals, the main parameters of the modified FSS, which are period (p), dielectric thickness (h), radius of the outer disk patches (r) and width of the circular grids (s), are included in the sweep analyses. The corresponding results of different parameter sweeps are presented between Figure 4- 3 and Figure 4- 6. The values of the FSS dimensions are given as normalized to their individual optimums in the corresponding figures.

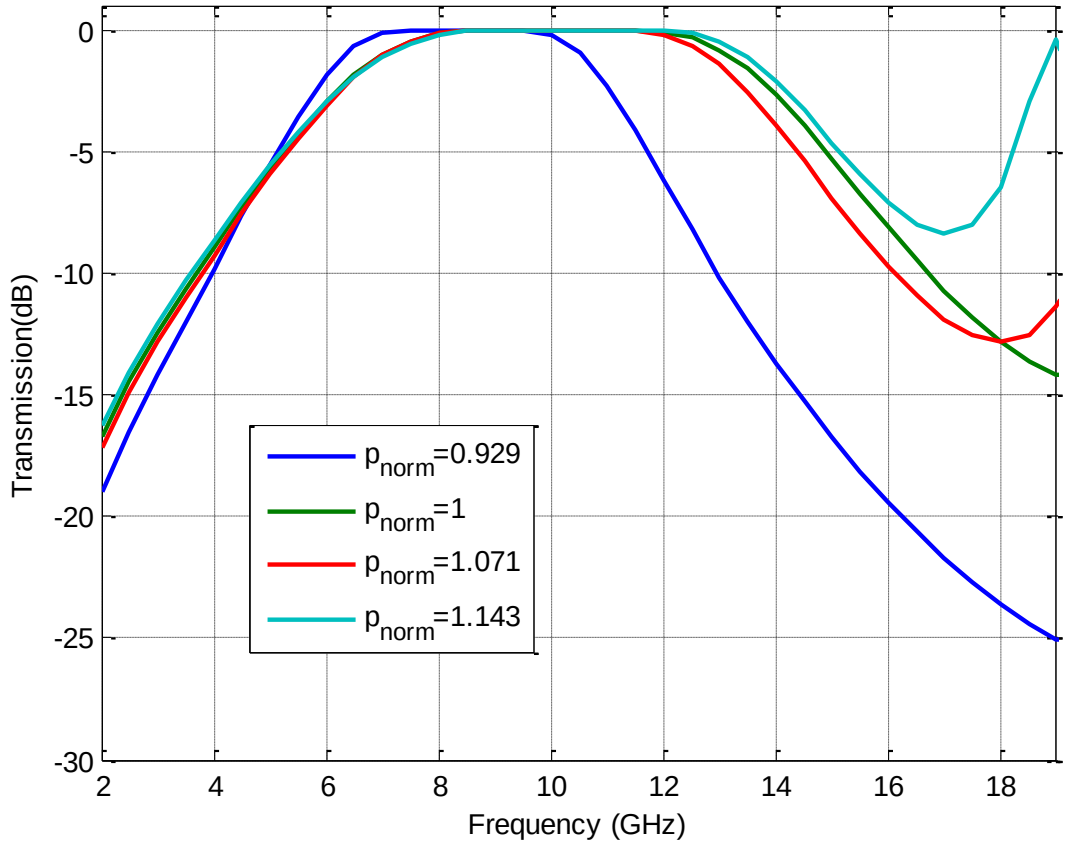

Figure 4- 3 Transmission responses for the sweep values of period parameter (p)

Variation in period parameter (p) mainly affects center frequency and bandwidth of FSS as observed from Figure 4- 3. Furthermore, a second resonance point in the upper frequency band gets closer to the operation region as period is increased while the other parameters are kept constant.

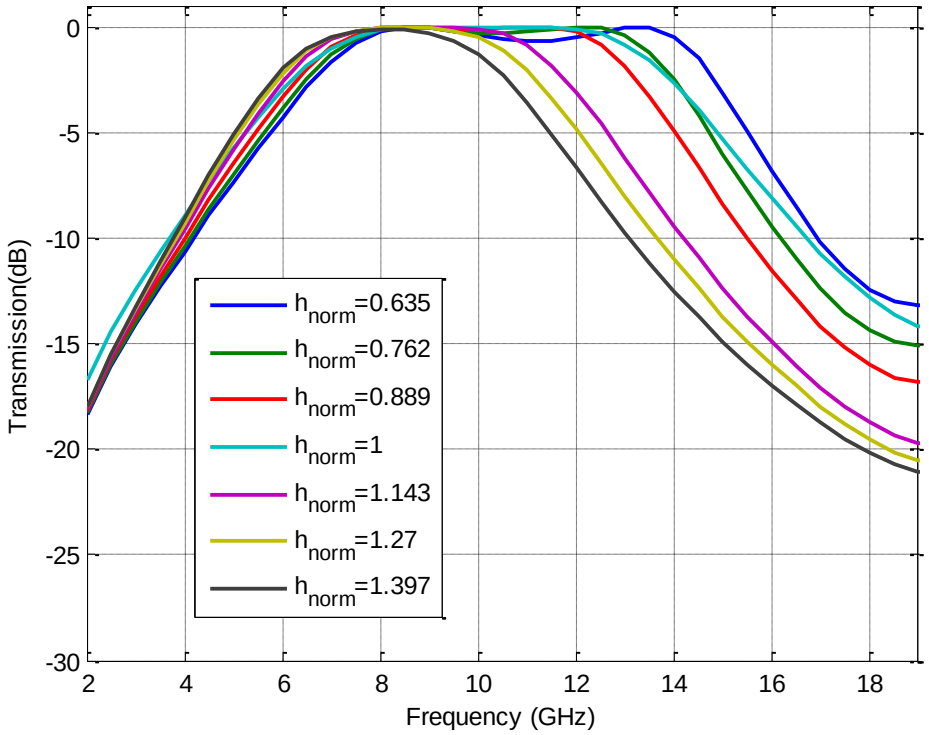

Figure 4- 4 Transmission responses for the sweep values of dielectric thickness (h)

The thickness of the double layer FSS structure effectively changes the upper limit of the pass-band region as shown in Figure 4- 4. As the thickness is increased the upper band limit decreases while the lower pass-band limit is not altered significantly.

Sweep analysis of outer disk radius parameter (r) reveals that it affects center frequency, bandwidth and selectivity features of FSS structure. As observed from Figure 4- 5, when the disk radius increases, center frequency shifts down and bandwidth decreases. Increase in disk radius also causes to weaken the selectivity performance of WB FSS.

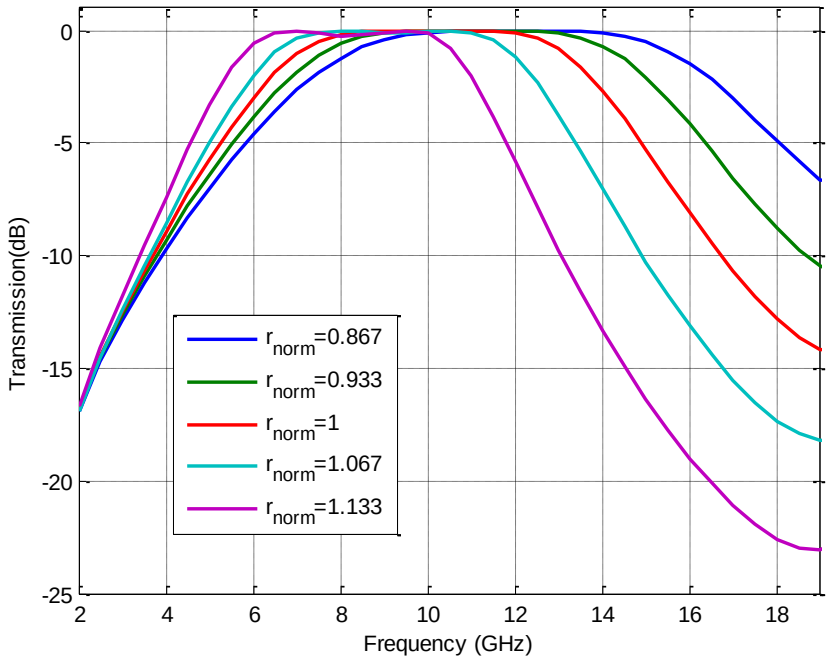

Figure 4- 5 Transmission responses for the sweep values of disk radius (r)

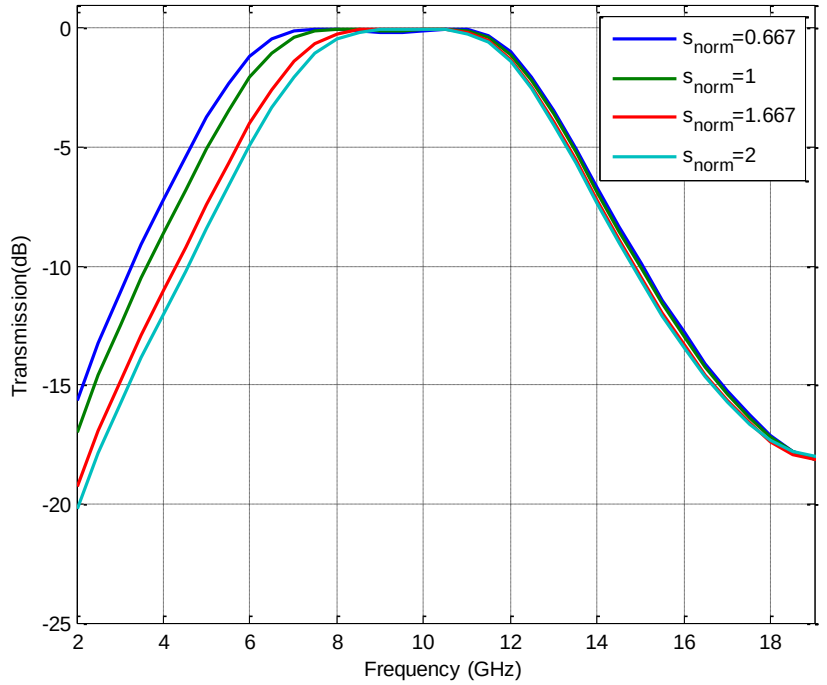

Figure 4- 6 Transmission responses for the sweep values of grid width (s)

Another swept parameter of WB FSS model is the width of metallic circular ring (s) positioned between the disk patches. Width of these rings creates alterations on the lower limit of the pass-band region mainly. Increasing ring width shifts the center frequency upwards. As the upper limit is not affected with the modifications on "s", center frequency moves upwards in frequency and, consequently, bandwidth of FSS decreases as ring width is increased as illustrated in Figure 4- 6. Utilizing the results of the parameter sweeps, the individual effects of each parameter are analyzed and the optimum values of the FSS dimensions are determined. The transmission and reflection curves of the final FSS model for normal incidence are illustrated in Figure 4- 7. The performance of the design against different incidence angles is demonstrated between Figure 4- 8 and Figure 4- 11 in terms of transmission and reflection responses.

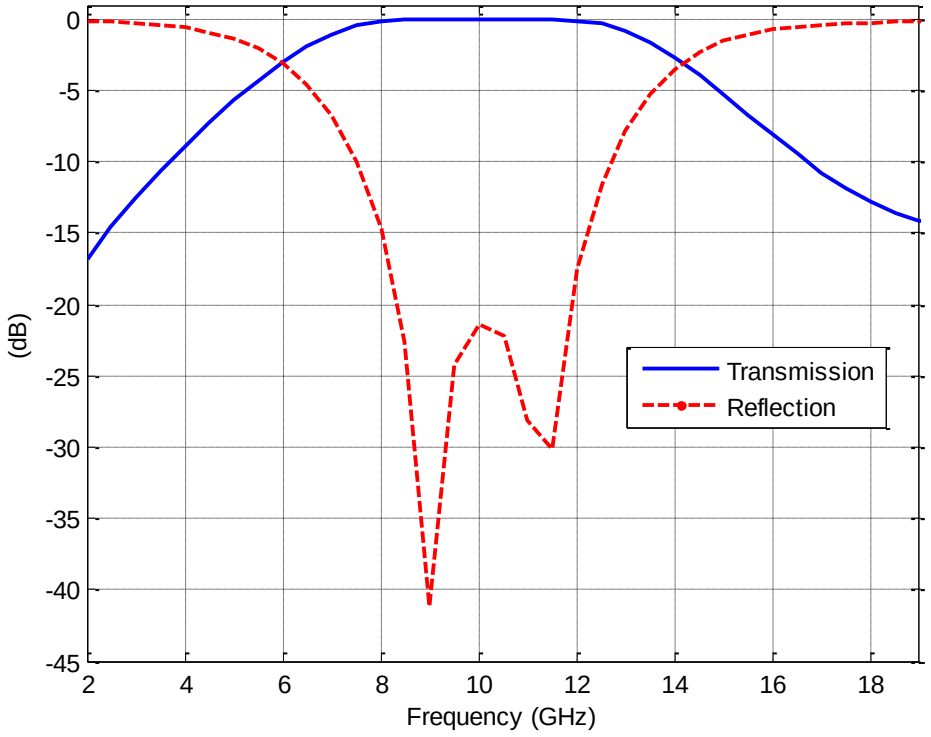

Figure 4- 7 Transmission and reflection characteristics of the optimized FSS design for the normal incidence

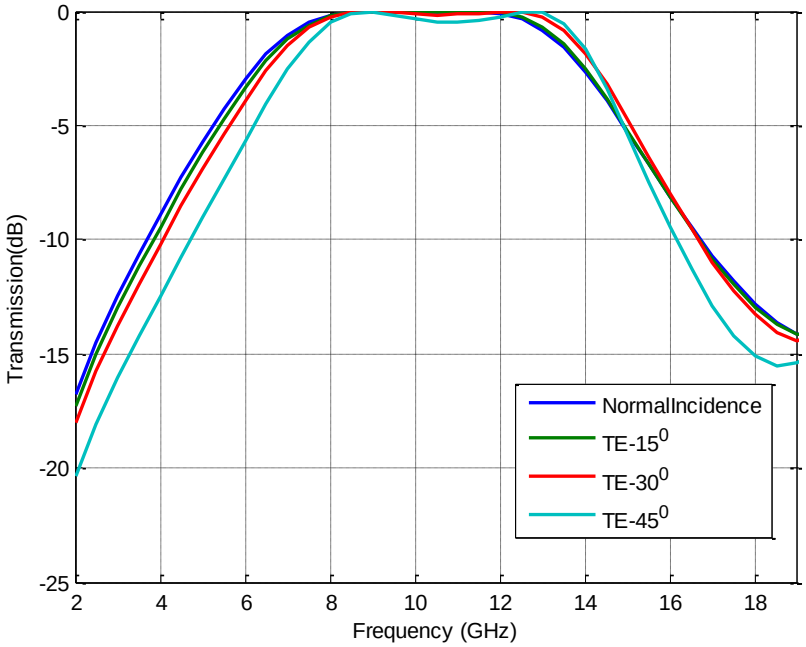

Figure 4- 8 Transmission responses of the optimized FSS design for oblique incidences (TE mode)

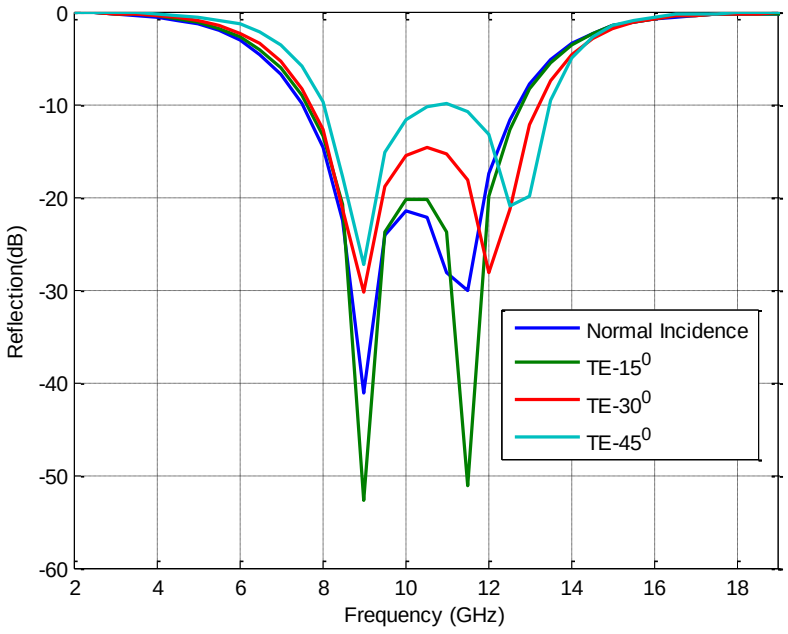

Figure 4- 9 Reflection responses of the optimized FSS design for oblique incidences (TE mode)

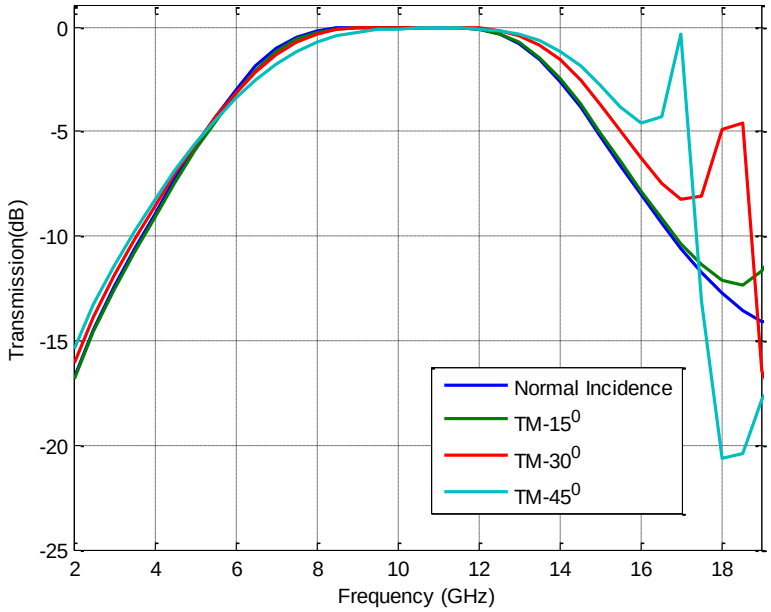

Figure 4- 10 Transmission responses of the optimized FSS design for oblique incidences (TM mode)

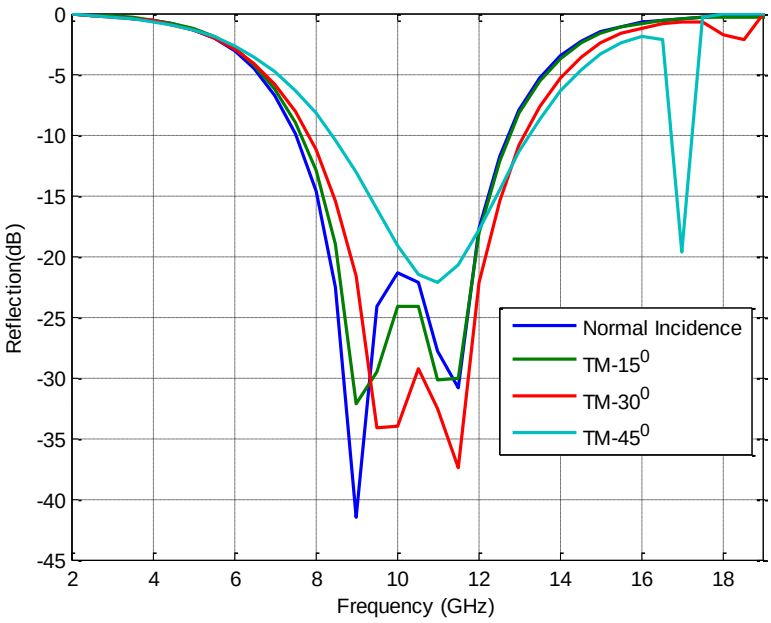

Figure 4- 11 Reflection responses of the optimized FSS design for oblique incidences (TM mode)

The wide band FSS model is optimized for the rectangular array conditions, however; the application surface may require a different array topology like triangular array. Therefore, the design is necessarily to be validated for the triangular array arrangement. The unit cell model constructed for this topology is illustrated in Figure 4- 12.

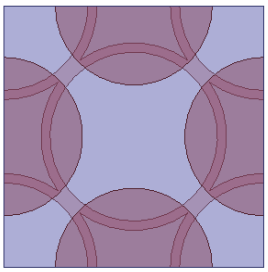

Figure 4- 12 Triangular array configuration of WB FSS model

The analysis results for the triangular array unit cell reveal the consistent performance of FSS model with rectangular array analyses. The transmission and reflection curves under different incidence angles for TE and TM modes are presented between Figure 4- 13 and Figure 4- 16.

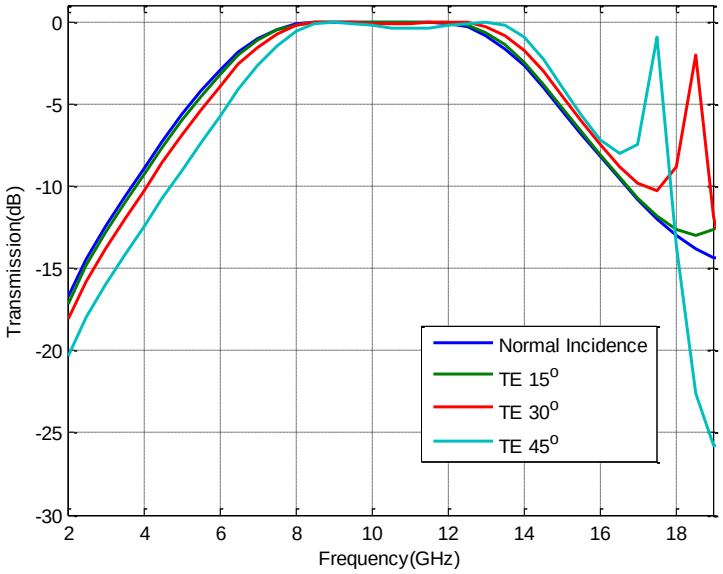

Figure 4- 13 Transmission responses of the triangular array unit cell model for oblique incidences (TE mode)

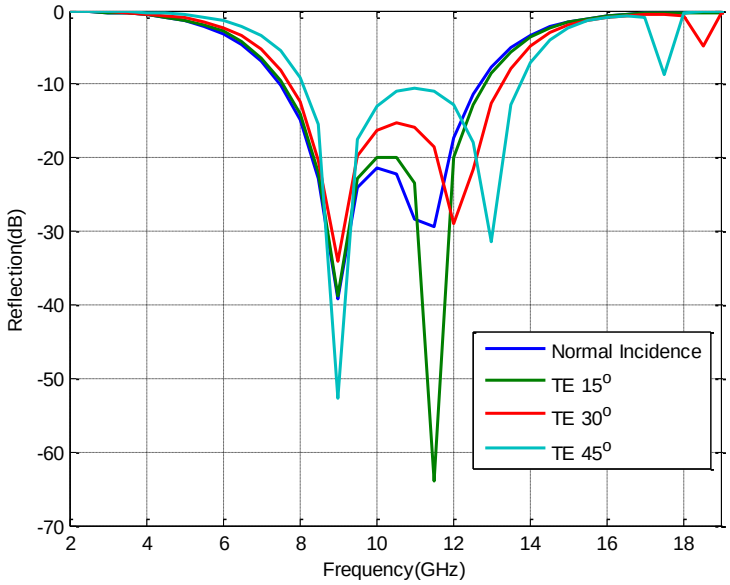

Figure 4- 14 Reflection responses of the triangular array unit cell model for oblique incidences (TE mode)

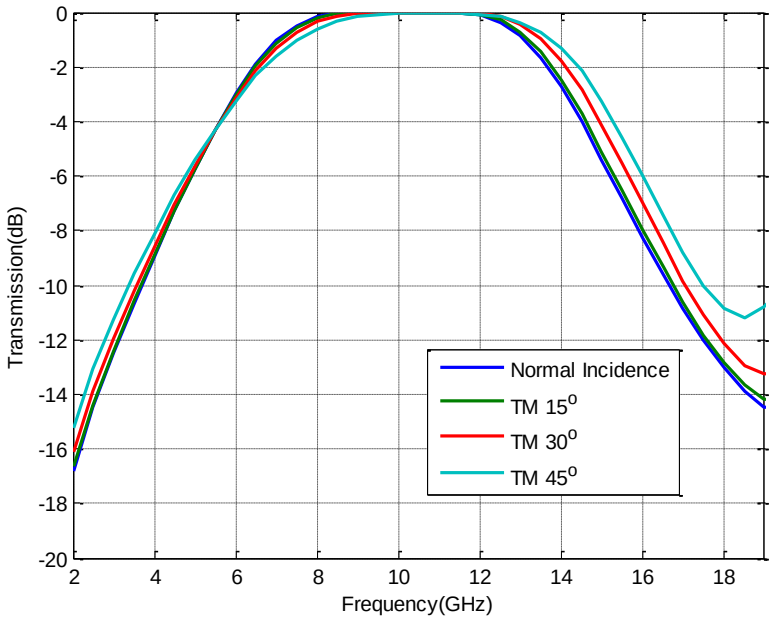

Figure 4- 15 Transmission responses of the triangular array unit cell model for oblique incidences (TM mode)

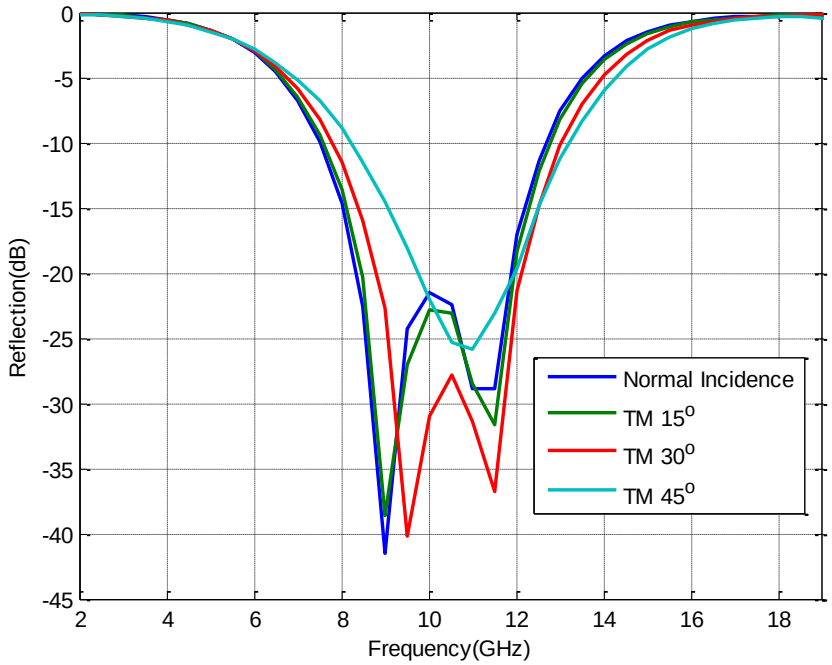

Figure 4- 16 Reflection responses of the triangular array unit cell model for oblique incidences (TM mode)

After verifying filtering performance of the FSS model with single element planar unit cell solution, the semi-finite model analysis is applied as described in Chapter 2. Between Figure 4- 17 and Figure 4- 21, the results of the semi finite analysis are presented. From these figures, it is obvious that the wide band pass characteristics of the single element planar unit cell are maintained when the elements are placed on conformal surface. Furthermore, it is observed that the edge diffractions at the end elements of the finite curved dimension do not have a significant effect on the performance of the model.

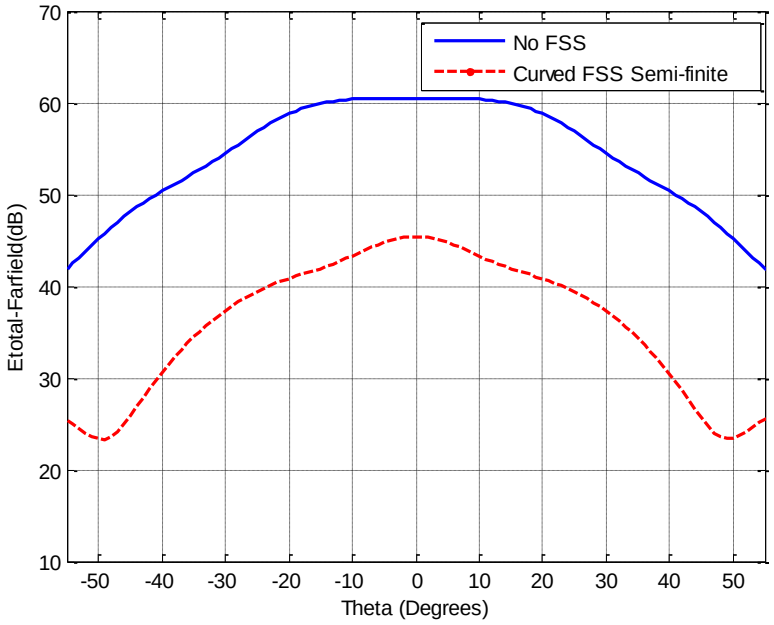

Figure 4- 17 Far field E-total patterns of 31-element source antenna array with and without wide band FSS radome at 2 GHz

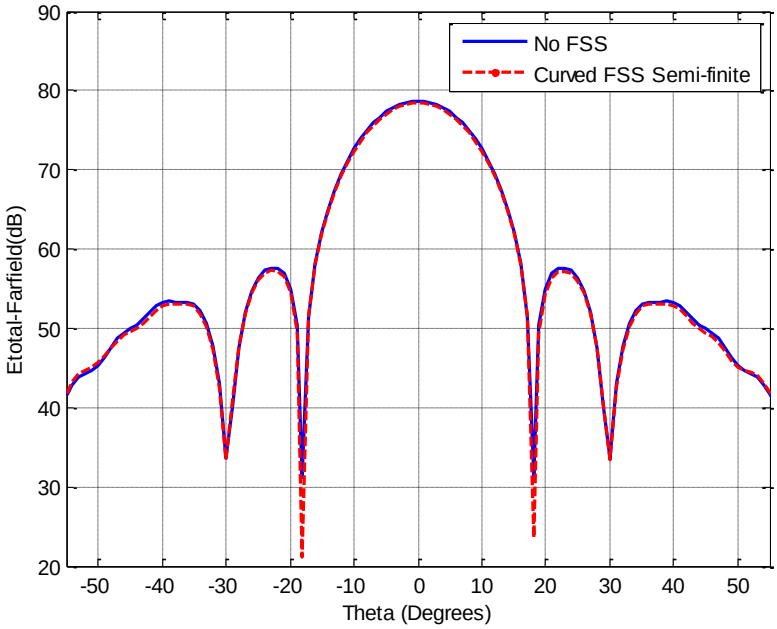

Figure 4- 18 Far field E-total patterns of 31-element source antenna array with and without wide band FSS radome at 8 GHz

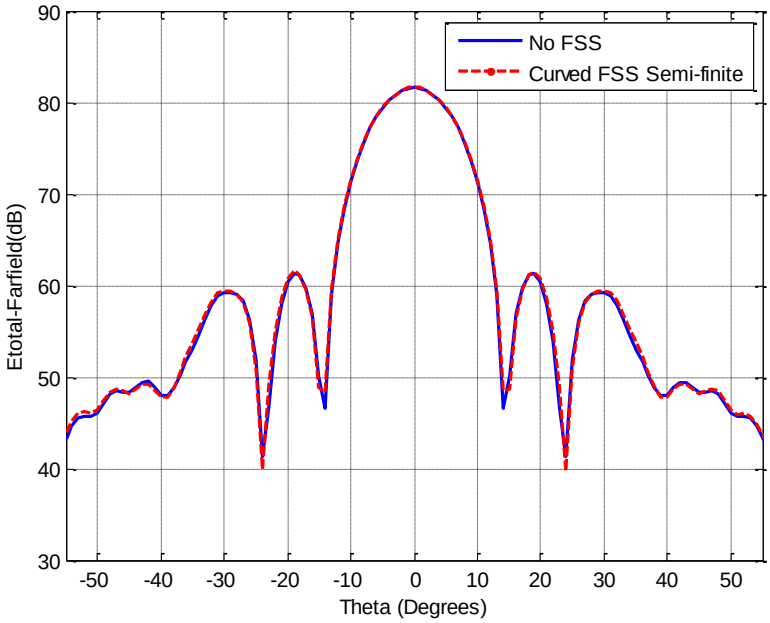

Figure 4- 19 Far field E-total patterns of 31-element source antenna array with and without wide band FSS radome at 10 GHz

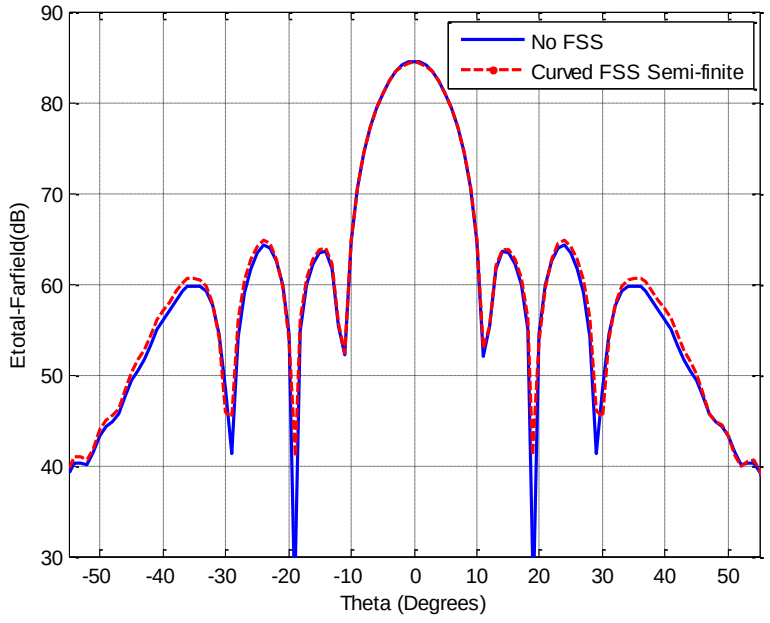

Figure 4- 20 Far field E-total patterns of 31-element source antenna array with and without wide band FSS radome at 12.5 GHz

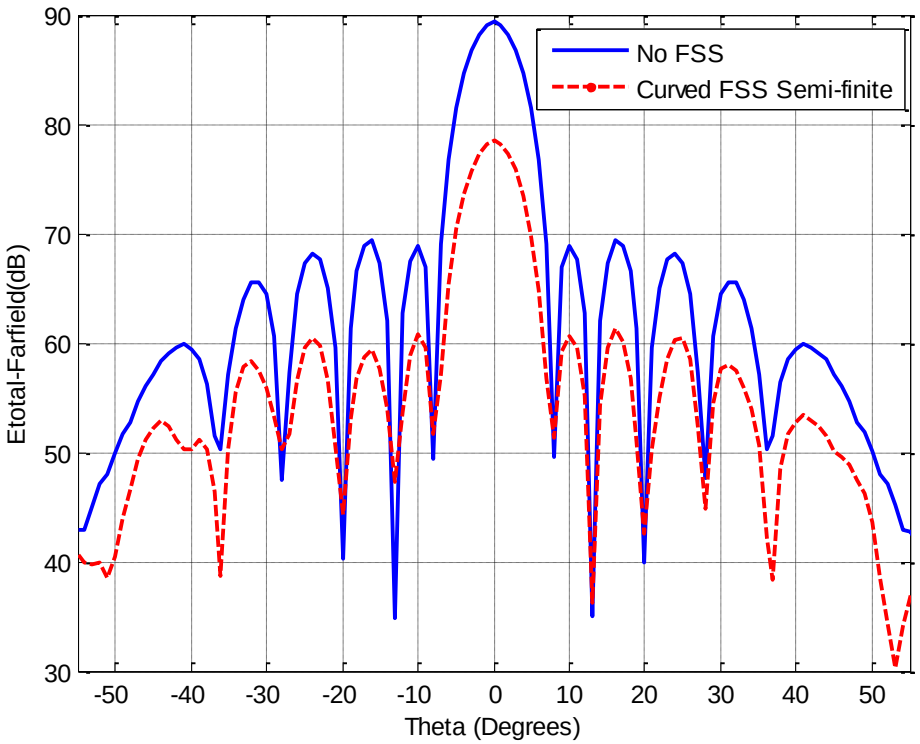

Figure 4- 21 Far field E-total patterns of 31-element source antenna array with and without wide band FSS radome at 18 GHz

Semi-finite model analysis of WB FSS structure is also implemented for planar sequence of FSS elements. Solution model is constructed as described for curved structure. Results of planar FSS semi-finite analysis show good agreement with the results of semi-cylinder FSS solution. Far field total E-field patterns with and without planar FSS sequence are shown between Figure 4- 22 and Figure 4- 24 for different frequencies.

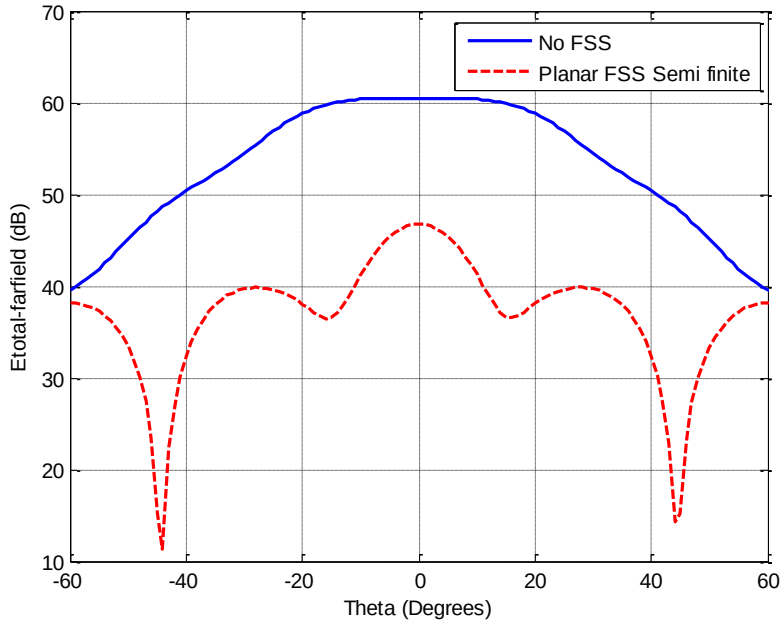

Figure 4- 22 Far field E-total patterns of 31-element source antenna array with and without planar wide band FSS radome at 2 GHz

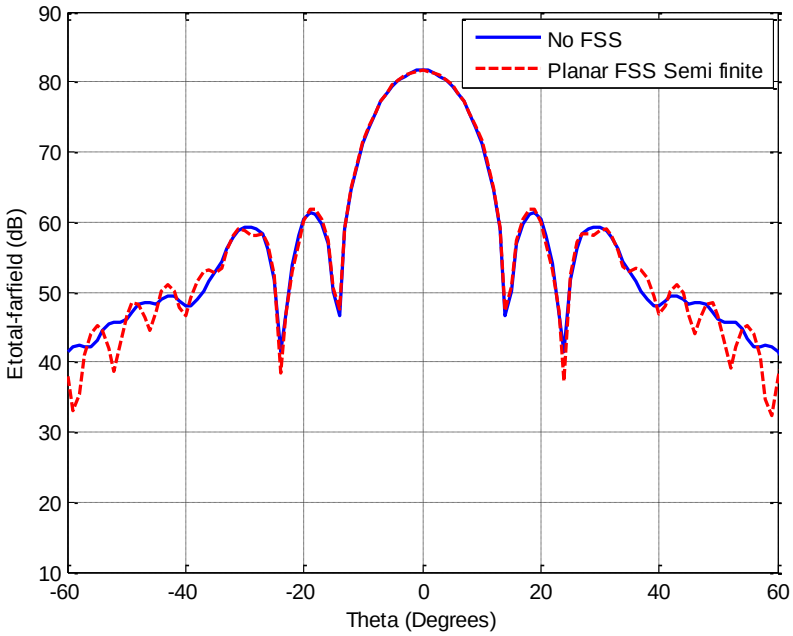

Figure 4- 23 Far field E-total patterns of 31-element source antenna array with and without planar wide band FSS radome at 10 GHz

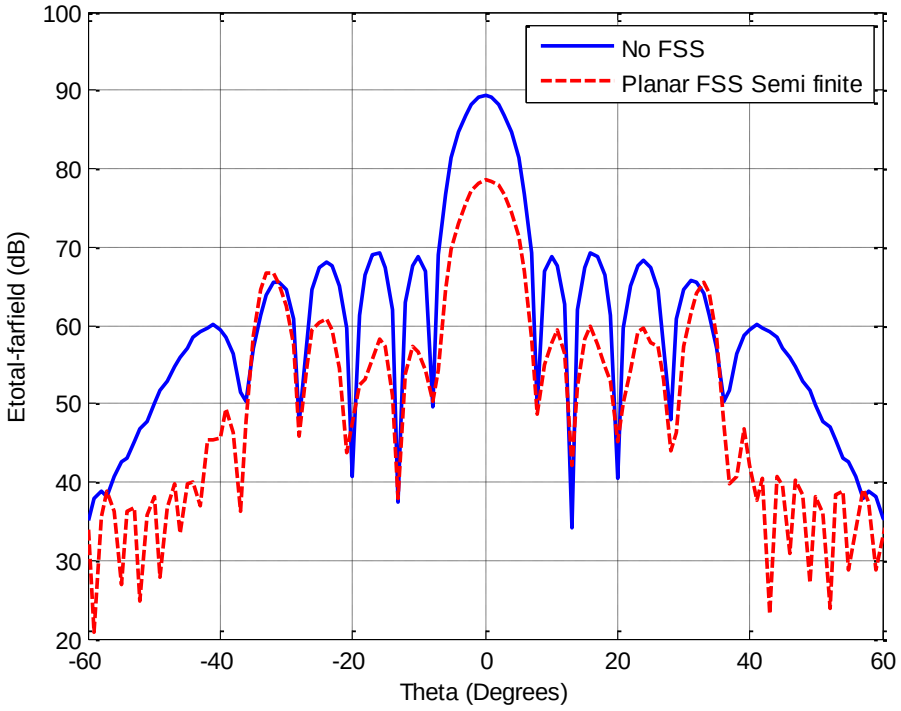

Figure 4- 24 Far field E-total patterns of 31-element source antenna array with and without planar wide band FSS radome at 18 GHz

Comparison of the analysis methods as in Chapter 3 is done for the single element unit cell solution and curved and planar semi-finite analyses. The transparency characteristics for the semi-finite models are obtained by the difference of total electric far field magnitudes of two solutions with and without FSS structure at the direction where theta equals to zero. As demonstrated in Figure 4- 25., the results of both methods are consistent with each other.

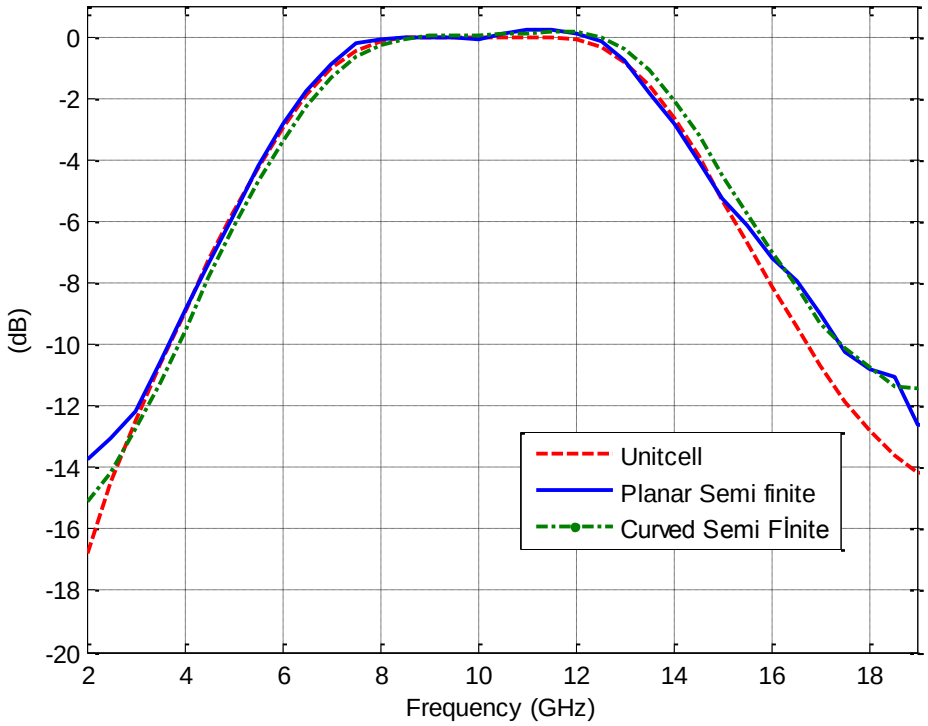

Figure 4- 25 Comparison of transmission characteristics of unit cell and semi-finite conformal and planar models

Using the semi-finite model, RCS analysis of the wide band FSS radome is implemented with two different configurations as in Chapter 3. In the first configuration, RCS of a PEC cylinder having the same radius as FSS model is compared with the RCS of the FSS radome. It is expected that RCS of the radome for the out-of-band frequencies is close to RCS of PEC cylinder while there is a great decline in RCS of FSS radome for the in-band frequencies. In Figure 4- 26, this situation is realized and expected results are determined such that semi-finite FSS radome model behaves like PEC cylinder for out-of-band frequencies.

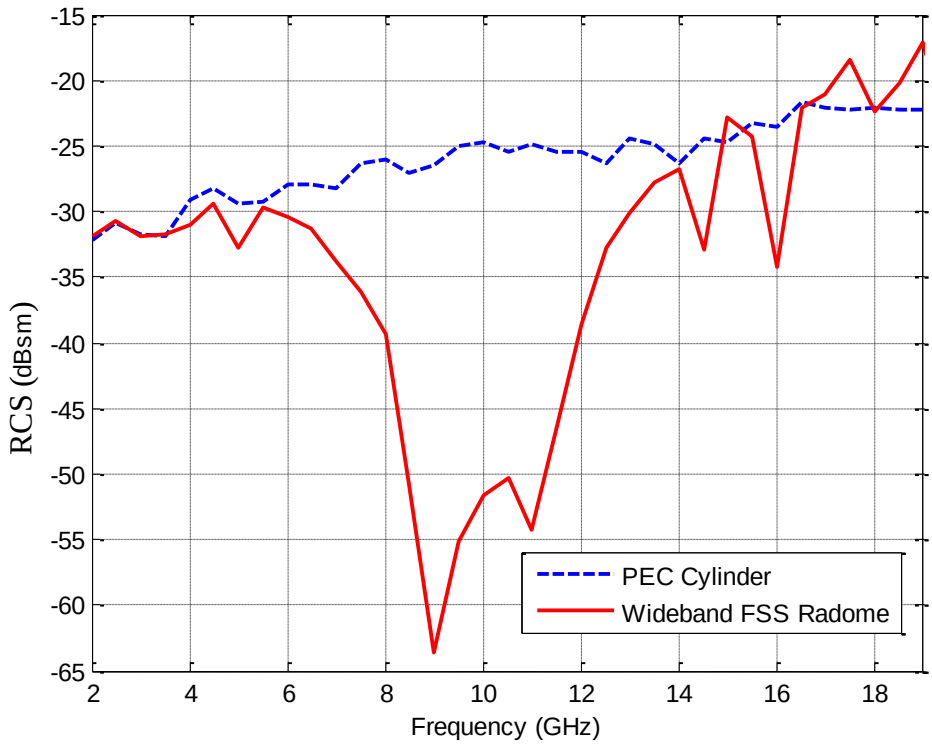

Figure 4- 26 Monostatic RCSs of WB FSS and PEC semi-cylinder using semi-finite analysis method

The other arrangement for RCS analysis includes a dielectric radome with a planar PEC sheet representing the surface of an antenna illuminating that radome. For the proper FSS operation, the monostatic RCS of the dielectric radome for in-band frequencies is close to that of FSS radome, however; there exist a huge decrease in RCS of FSS radome for out-of-band frequencies since FSS structure behaves like a conducting cylinder and scatters the incoming signals to different directions for those frequencies. RCSs of semi-finite WB FSS model and dielectric cylinder with a planar PEC sheet beneath them are demonstrated in Figure 4- 27. As expected, RCS of FSS radome is truly lower for frequencies outside of pass-band region.

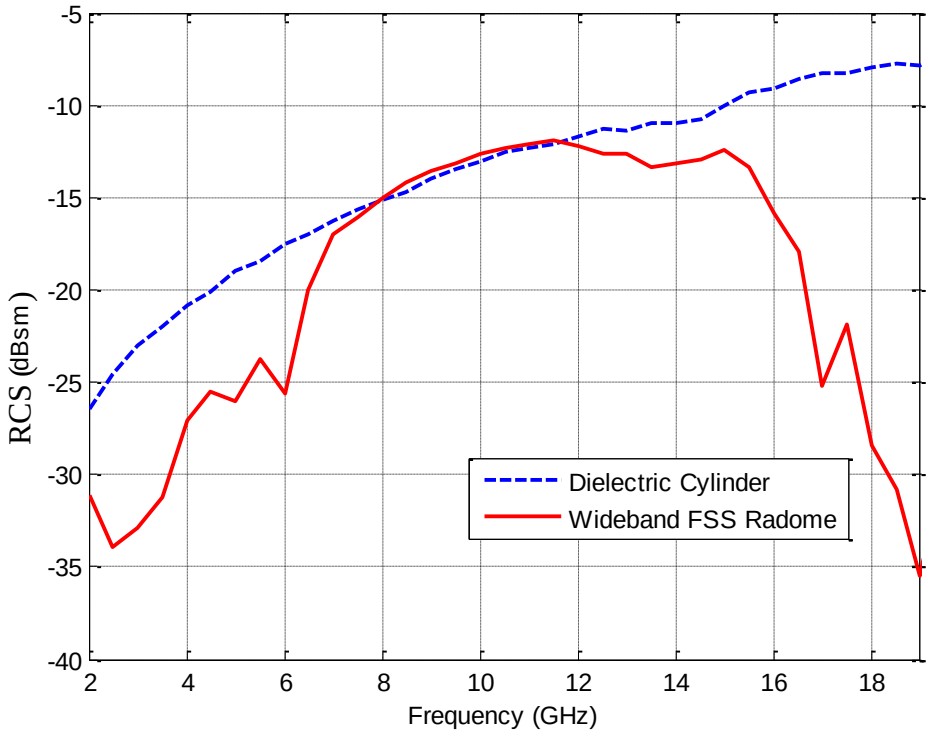

Figure 4- 27 Monostatic RCS results of FSS and dielectric semi-cylinders using semi-finite analysis method

Verification of transmission and reflection characteristics with curved semi-finite model analyses completes design and analysis processes for this specific application. After all, designer is required to check realizability of FSS model in terms of fabrication techniques and material procurement before producing FSS radome.

CHAPTER 5

FABRICATION AND MEASUREMENTS OF FREQUENCY SELECTIVE SURFACE STRUCTURES

5.1 Fabrication of the Hybrid Coupled Aperture FSS

To this point, the design methodology for the conformal FSS structures is detailed and some sample FSS models are designed. In order to prove the performance of the designed FSSs, planar prototypes are produced. The FSS model designed in Chapter 3, hybrid coupled aperture FSS, is fabricated in the facilities of ASELSAN. The layers of the FSS are fabricated as 40cm x 40cm planar sheets separately since the double layer fabrication requires an advanced production infrastructure. The material used as dielectric slab is RT/duroid® 5880 High Frequency Laminate of Rogers Corporation [40]. For the conformal implementation of the fabricated FSS structures, the base laminate material is required to be bendable on the curved surfaces. Thus, 5880 laminate is chosen due to its powerful elasticity features when compared to other PCB cards. Hybrid FSS model is a narrow-band and highly selective structure. These features are mainly characterized by the coupling mechanism of the model. Therefore, the orientation of the layers and bonding processes are very crucial in order to achieve desired filtering performances. The separate layers of the hybrid coupled aperture FSS model are demonstrated in Figure 5- 1. As observed from the figure, disk patch and coupling aperture patterns are scraped on the two sides of 5880 duroid laminate. For the other dielectric layer, the scraping of the disk pattern is implemented on one face and no metal is left on the other surface.

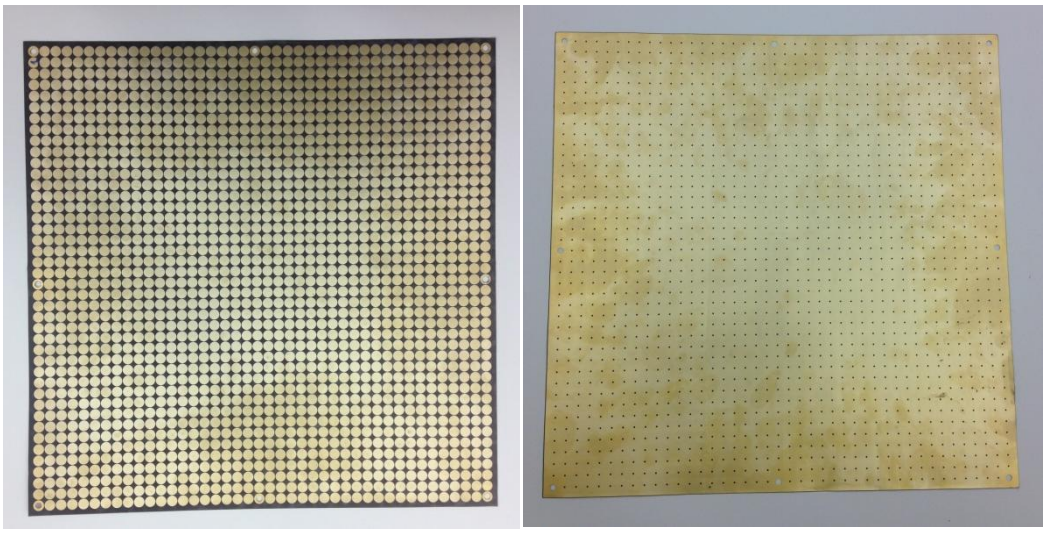

Figure 5- 1 Separate layers of the fabricated FSS Prototypes

FSS layers are bonded according to the configuration described in Chapter 3. Loctite® 401 of Henkel is used as adhesive for bonding of the layers [41]. The liquid adhesive (Loctite® 401) is spread over the empty surface of the FSS layer, single side of which is scraped only. Since these processes are done manually, a homogenous very thin layer of adhesive cannot be constructed. Instead, homogenously spread drops of the adhesive are placed on the surface of the bonding layer. Moreover, the FSS layers are also pressed manually after bonding which may create some discrepancies on the performance of the double layer FSS.

5.2 Measurements of Fabricated FSS Structures

To measure the transmission and reflection responses of FSS structures, two alternative measurement setups are prepared in order to ensure the measurement results. The first setup used for the measurements is “MMS Free Space Microwave Measurement Setup” of Antenna Technologies Department of ASELSAN Inc. [42]. The setup arranged for the FSS measurement is demonstrated in Figure 5- 2.

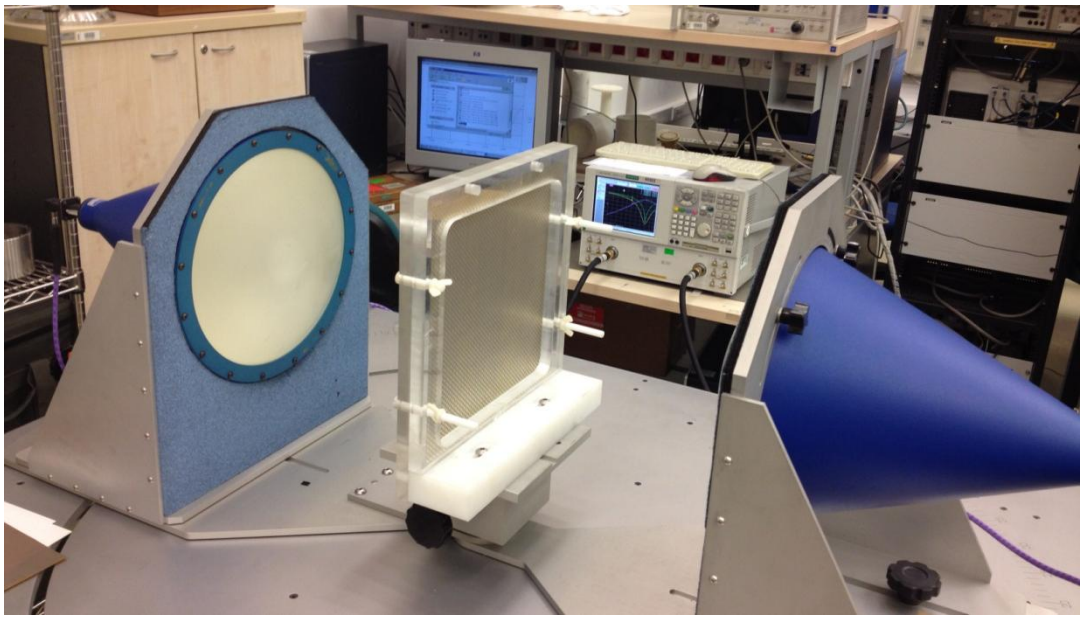

Figure 5- 2 Free Space Microwave Measurement Setup

The free space measurement setup consists of a network analyzer, sample holder and focused antenna pairs for different frequency ranges, which are namely C-band (5.6-8.2 GHz), X-band (8.2-12.4 GHz) and Ku-band (12.4-18 GHz), as shown in Figure 5- 2 above. Since the hybrid coupled FSS operates in Ku-band, the corresponding antenna pair is mounted on the setup. Before starting the measurements, the setup is required to be calibrated with the help of the software of MMS. The calibration type applied for the setup is TRL (Transmission-Reflection-Line). After the calibration is completed, FSS prototype is placed on sample holder as shown in Figure 5- 3.

The measurement of S-parameters is then accomplished using the user interface software of MMS. The total thickness of hybrid FSS is normally expected to be around 290 um, however; the measured thickness is around 330 um, which is attributed to the fabrication incapabilities. This difference is likely to be created by a combinational effect of air gaps and adhesive remainders which are not pressed appropriately. The transmission response of two fabricated prototypes, which are named as "No1" and "No2", are presented in Figure 5- 4 together with the single element unit cell solution.

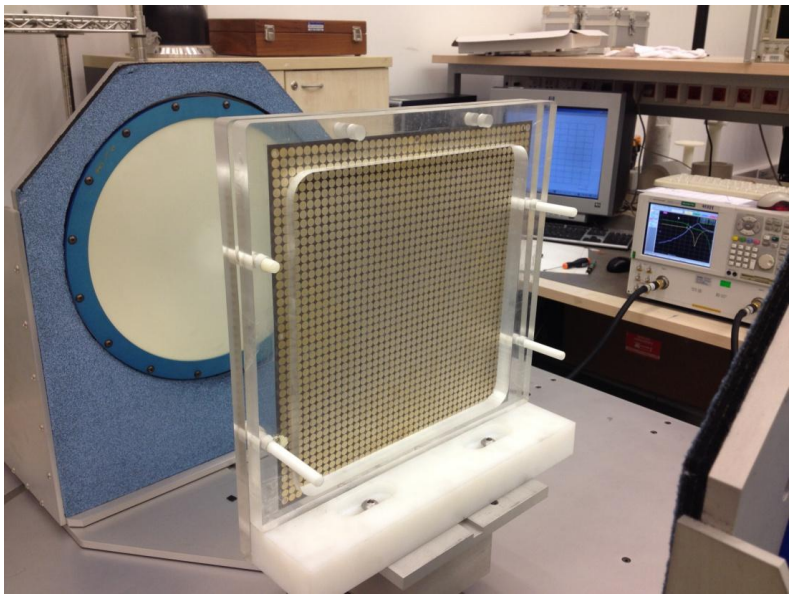

Figure 5- 3 Placement of FSS prototype on the Free Space Measurement Setup

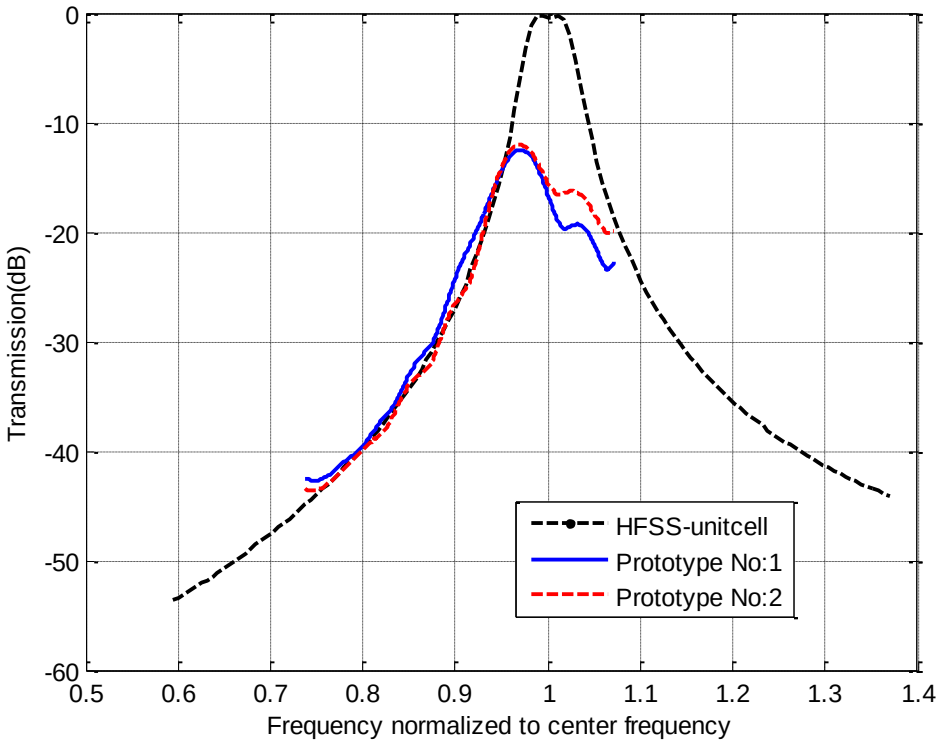

Figure 5- 4 Free Space Measurement and HFSS Unit cell results for hybrid coupled FSS prototype No.1 and No.2

The results of the free space microwave measurements are observed to be unsatisfactory in terms of transmission levels and resonance frequencies compared to the unit cell simulations. In order to reexamine the performance of the FSS prototypes, a new measurement setup is constructed using the "Arc S-parameter Measurement Setup" of Antenna Technologies Department of ASELSAN Inc. as illustrated in Figure 5- 6. The arc measurement setup is normally used for the oblique incidence reflection measurements so as to determine the performances of absorbers for different angles of incidences. Nonetheless, with a small modification, this setup becomes suitable for transmission measurements for normal incidence cases. Two apparatus are designed and constructed using 3D printer in ASELSAN (see Figure 5- 5). These components provide the horizontal positioning of horn antennas with respect to the ground, which is actually not possible with the default setup.

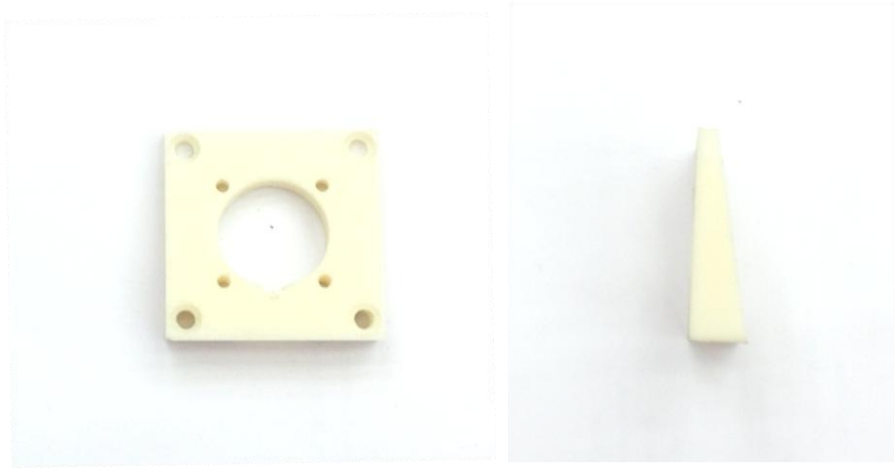

Figure 5- 5 Modification apparatus (front view on the left, side view on the right) for FSS measurements using Arc Measurement Setup

The modified setup includes two Ku-band standard gain horn antennas, sample holder, network analyzer and RF cables (see Figure 5- 6). The calibration technique for this measurement setup is different from Free Space Microwave setup. In horn measurement, time domain gating feature of the network analyzer is utilized such that the place of the FSS is determined in time and by gating this region, the

destructive effects of measurement environment on the transmission characteristics at other time instants are excluded from FSS surface. Transmission performance of FSS prototypes are determined by normalizing FSS measurements to "air" measurement. Therefore, FSS and air transmission coefficients are measured separately. Same gating definitions are applied for air and FSS prototypes.

Figure 5- 6 Modified horn antenna measurement setup

Measurement results obtained from the horn antenna setup are presented in Figure 5- 7 together with HFSS solutions, for FSS prototypes No.1 and No.2.

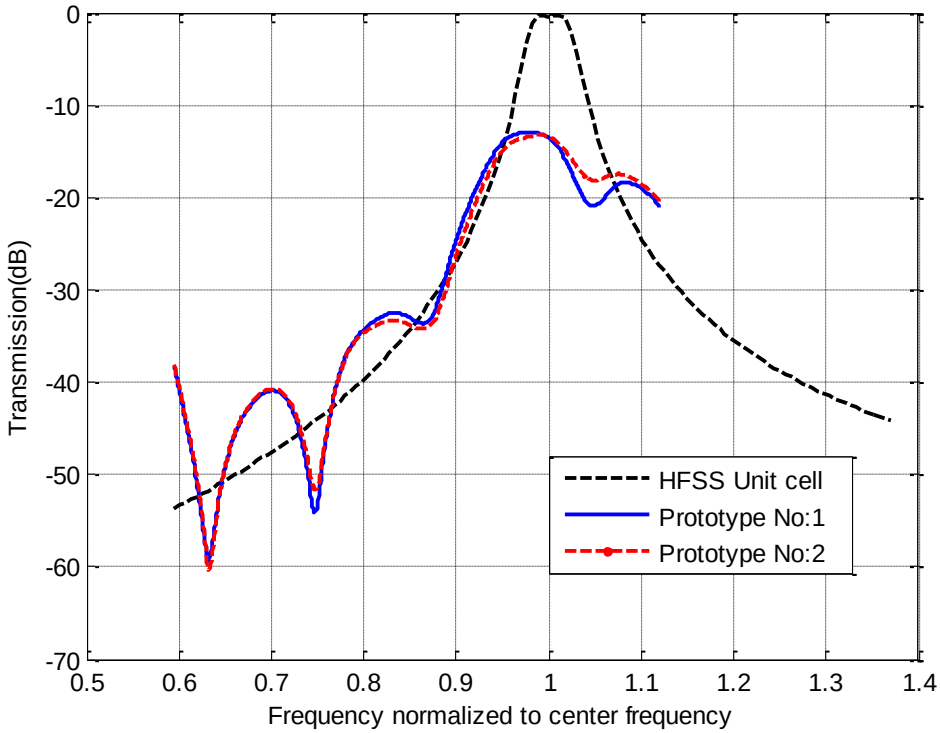

Figure 5- 7 Horn Antenna Measurement and HFSS Unit cell analysis results for hybrid coupled FSS prototype No.1 and No.2

The results of FSS measurements with two different setups are given in Figure 5- 8 and Figure 5- 9 for prototype No.1 and No.2 and it is observed that they show a good agreement with respect to each other, however; the filtering characteristics are far away from the simulation results.

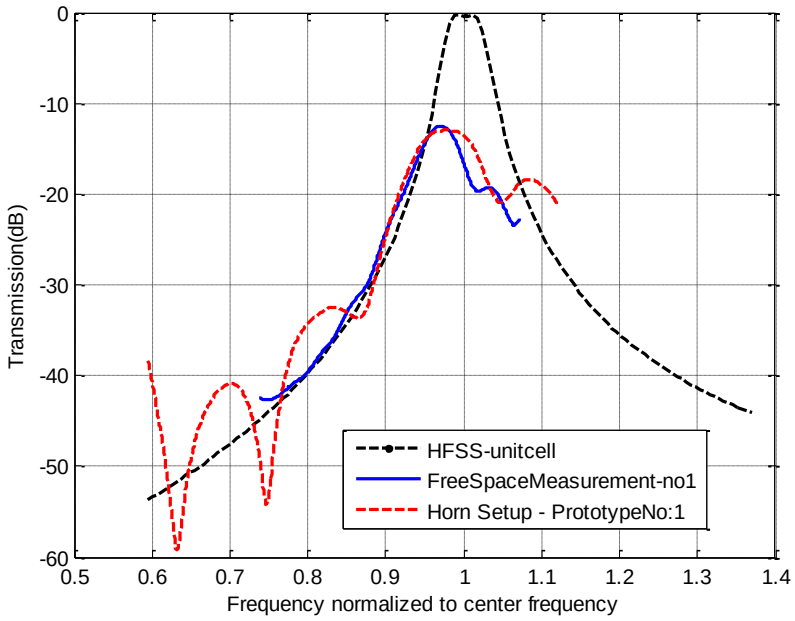

Figure 5- 8 The comparison of unit cell model analysis and measurements with Free Space Microwave and Horn Antenna setups (Prototype No.1)

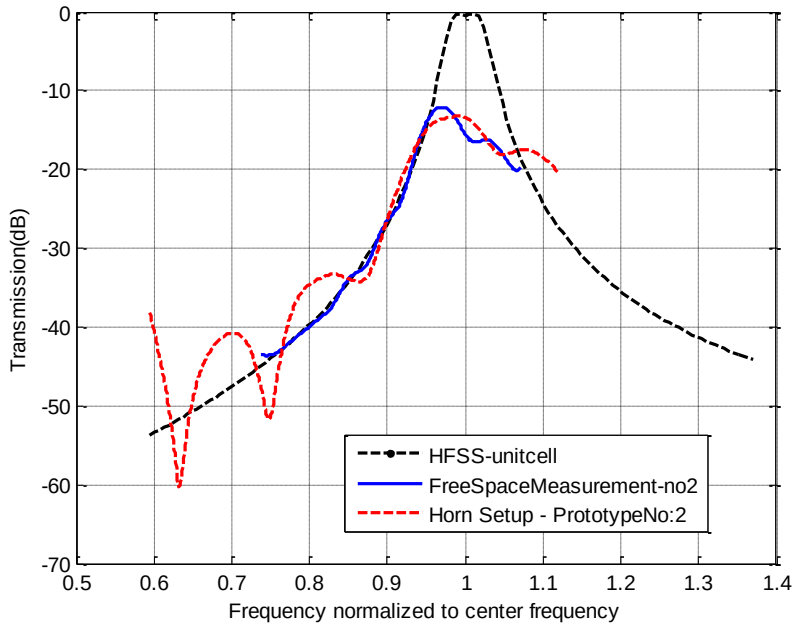

Figure 5- 9 The comparison of unit cell model analysis and measurements with Free Space Microwave and Horn Antenna setups (Prototype No.2)

Discrepancies observed in the filtering responses of the prototypes are ascribed to the lack of double layer fabrication capabilities. As mentioned before in this chapter, the measured thicknesses of prototypes are around 330um instead of the expected value of 290um. In order to determine the effect of this difference, a unit cell model having a vacuum layer of 40um thickness is constructed and analyzed in HFSS. The result of this simulation is presented in Figure 5- 10 and Figure 5- 11 together with measurement results and unit cell solution of ideal model.

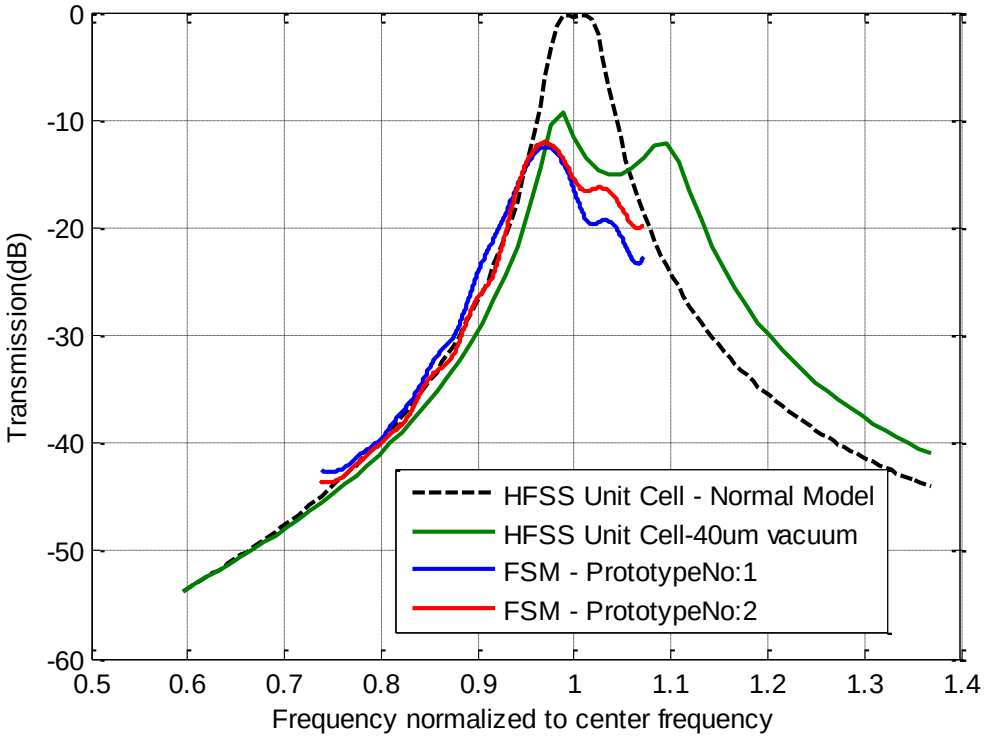

Figure 5- 10 Comparison of normal and 40um-vacuum layered unit cell analysis results with Free Space Microwave Measurements

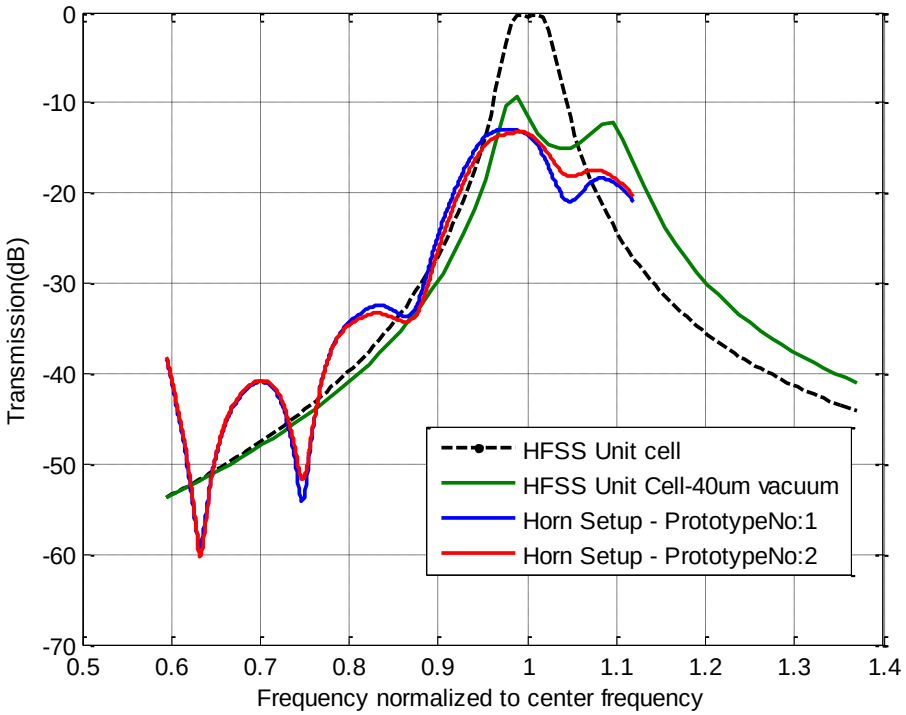

Figure 5- 11 Comparison of normal and 40um-vacuum layered unit cell analysis results with Horn Antenna Measurements

The unit cell analysis taking 40um vacuum layer into account clarified the dramatic effect of any inadequacy in fabrication processes to the realized transmission characteristics. The measurements and new unit cell analysis results are consistent with each other. The slight difference between the measurements and analysis can be attributed to the non-uniformity of the actual vacuum layer of the prototypes.

To investigate the discrepancies between the results of simulations and measurements, the effect of misalignment of FSS layers is also simulated with the unit cell model shown in Figure 5- 12.a for various shifts which is defined by d_{mis} parameter referenced to period (p). As described in Figure 5- 12.b, bottom and middle metallic layers are shifted together since they are on the same dielectric substrate. The upper disk layer is shifted in the perpendicular direction as demonstrated in Figure 5- 12.c. Simulation results show that misalignments of FSS layers cause degradation in filtering performance while the center frequency is

stable against these modifications (see Figure 5- 13). However, the shifts up to 7% of period create no significant change with respect to normal unit cell model which shows that FSS model is not sensitive to alignment errors. Therefore, the discrepancies between simulations and measurements are not attributed to alignment errors as the observed misalignments of fabricated prototypes are not larger than 7% of period.

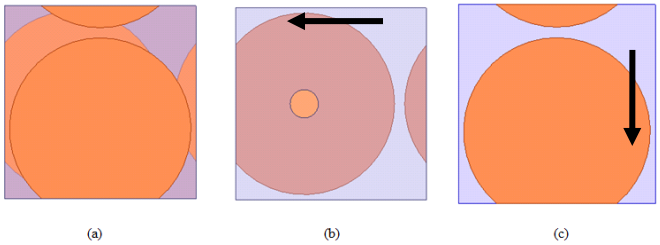

Figure 5- 12 Misalignment configuration of unit cell model a) Unit cell b) Bottom and middle FSS layer c) Upper FSS layer

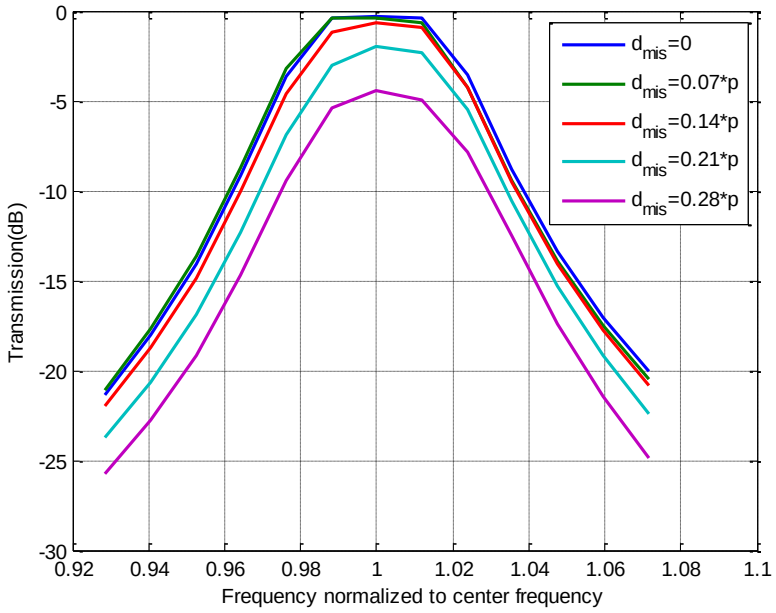

Figure 5- 13 Transmission responses for different shifts in FSS layers

As the fabrication of multi-layer coupled FSS structure is difficult in the limits of the facilities, FSS models which require no bonding can be produced easily. For

example, a complementary FSS model (see Figure 5- 14) on a single dielectric substrate can be a good candidate in order to eliminate deficiencies related to fabrication process. In this model, there are two metallic FSS layers on dielectric substrate which are complement to each other, i.e. circular grid and aperture. However, complementary FSS model is poor in terms of selectivity characteristics with respect to the coupled aperture hybrid FSS model of Chapter 3 as illustrated in Figure 5- 15. Even though the selectivity performance of this single layer design is not satisfactory, this structure will be manufactured and measured to explore whether the manufacturing capabilities are good enough for the production of single layer structures.

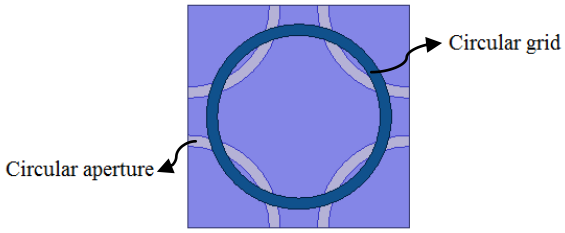

Figure 5- 14 Complementary FSS model with single dielectric substrate

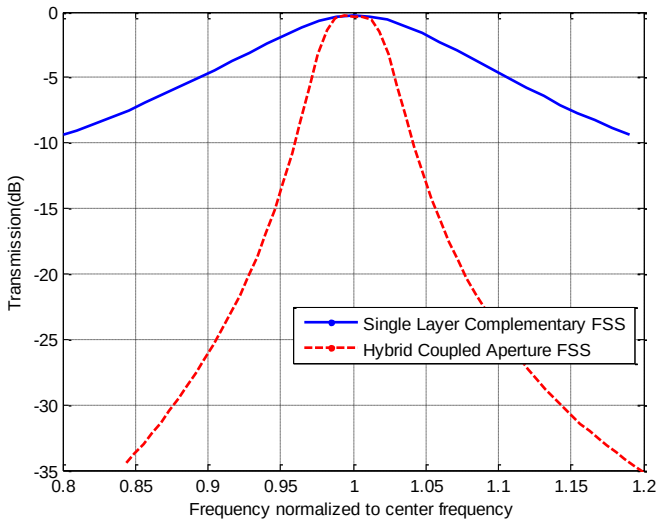

Figure 5- 15 Comparison of transmission responses of coupled aperture hybrid FSS and single layer complementary FSS with single dielectric substrate

CHAPTER 6

CONCLUSIONS

Design and analysis approaches for conformal frequency selective surface structures are investigated in this study. A design methodology starting from linear single element unit cell FSS model employing periodic features in two dimensions and advancing to determination of FSS characteristics placed on a semi-cylinder radome model which is finite in curved dimension and infinite in transverse dimension. Normally, after unit cell optimizations are accomplished, performance of FSS structure is required to be tested for finite and curved element conditions since both may have significant effects on transmission and reflection characteristics of FSS since diffractions from edge elements and interference between curved FSS elements cannot be determined from the unit cell solution of a single planar FSS structure. Nonetheless, implementations of finite model solutions are usually not practical when the desired FSS radome models are electrically very large, i.e. number of FSS elements is remarkably high, since full wave simulations of those models create heavy calculation load which is mostly impossible to be held even by high performance computers. Therefore, finite model solutions are inefficient and time consuming, in general. To overcome the disadvantages of finite model solution, a semi-finite solution approach is investigated in this study. According to this approach, a semi-finite model of FSS structure is constructed which is a semi-cylinder having a single sequence of FSS elements. Semi-finite model has periodic boundaries in the longitudinal dimension which makes it infinite in that direction. Dimension of the curved elements placed on rotational axis of cylinder is finite. Illumination of semi-finite model is carried out by a linear

array of 31 Hertzian dipoles excited with a 20 dB Taylor distribution. Due to the singly periodic nature of semi-finite model, Hertzian dipoles, in fact, constitute a 31 x *infinite* element array. As the solution environment for semi-finite models, HFSS is used. Evaluations of the solutions are done by comparing the total and incident total E-fields at far zone for different frequencies. For pass-band frequencies, incident and total far fields are expected to be similar if FSS operates appropriately for conformal configurations. Similarly, significant suppression of incident fields is necessarily to be observed for out-of-band signals since FSS model is reflective at these frequencies. Hertzian dipole configuration is capable of representing in-band characteristics of FSS model since only insertion loss of FSS radome is crucial for the source antenna. To prove out-of-band performance of semi-finite FSS model, a comparative RCS analysis is demanded. For RCS configuration, plane wave illumination is utilized. In this study, two methods to compare RCS characteristics with FSS model are employed. First method includes a PEC cylinder which is expected to have almost same RCS performance as semi-finite FSS model for out-of-band frequencies. In the second method, a semi-cylinder dielectric radome and a planar PEC sheet representing antenna surface under both dielectric and FSS radome are constructed. Out of the pass-band region, FSS radome is required to scatter the incoming waves to different directions due its curved shape and RCS of FSS radome becomes dramatically lower with respect to dielectric radome with planar PEC sheet.

Using design and analysis methodology described in this thesis, two band-pass FSS models are constructed for conformal applications. First model is a hybrid FSS structure consisting of two dielectric and three metallic layers. It operates in Ku-band and covers a narrow-band region to transmit signals. The selectivity and polarization independence properties of FSS model are favorable. Second structure is a wide band FSS comprising all X-band frequencies (8.2-12.4 GHz) with a maximum insertion loss of 0.5 dB. Both FSS models are tested with planar single element unit cell solutions in terms of different aspects like oblique incidence, dual polarization and different array topology conditions. Afterwards, aforementioned

semi-finite approach is utilized for these models both planar and curved shapes. Analysis results demonstrate filtering performances of FSS structures for in-band and out-of-band frequencies.

In order to prove the results of semi-finite solution for narrow-band FSS model of Chapter 3, a finite, doubly curved semi-sphere FSS radome model is constructed and analyzed using HFSS. Filtering properties of finite FSS model are also observed to show good agreement with single element unit cell and semi-finite solution approaches.

Fabrication and measurements of hybrid coupled FSS model are accomplished in the facilities of ASELSAN. Bonding of two dielectric layers necessitates a highly precise fabrication process since filtering mechanism of this FSS model is mainly based on the coupling supplied by the circular aperture between outer disk patches. As the bonding technique applied to fabricate double layer FSS structure is not adequate, measurements and simulation results are not consistent with each other. However, possible reasons are investigated and explained with related simulations including fabrication effects on FSS structure.

For future works, fabrication techniques for multilayer FSS structures will necessarily be improved. Moreover, new FSS types will be designed and fabricated for different conformal applications with various requirements like bandwidth, filtering characteristics, etc., using the design methodology presented in this thesis. Fabrication of FSS patterns on fabrics or composite materials is another point of interest in future plans since such kind of materials can easily be shaped into singly or doubly curved structures. Design methodology and fabrication techniques will be validated with related measurements. For future studies, numerical analysis methods for singly or doubly curved structures as in [43] can be developed in order to acquire conformal FSS characteristics of arbitrary shapes efficiently. Another research topic can be the optimization of placement of FSS elements on spherical structures at equal distances. This problem is very similar to that of electron distribution on spherical surfaces based on energy minimization principle.

REFERENCES

[1] B. A. Munk, Frequency Selective Surfaces: Theory and Design, John Wiley & Sons, Inc., 2000.

[2] C. A. Balanis, Antenna Theory - *Analysis and Design, John Wiley & Sons*, Third Edition, 2005.

[3] A. Lazaro, A. Ramos,D. Girbau, and R. Villarino, *A Novel UWB RFID Tag Using Active Frequency Selective Surface*, Antennas and Propagation, IEEE Transactions, vol.61 , pp. 1155-1165, Mar. 2013.

[4] A. S. Barlevy, D. F. Sievenpiper, Y. Rahmat-Samii, *Photonic Bandgap (PBG) Structures of Multiple Metallic Periodic Screens: Efficient Electromagnetic Characterization,* Antennas and Propagation Society International Symposium, IEEE, vol.2 , pp. 1216 – 1219, June 1998.

[5] H. Y. Chen, Y. K. Chou, *An EMI Shielding FSS for Ku-band Applications*, Antennas and Propagation Society International Symposium (APSURSI), pp. 1-2, July 2012.

[6] K.L. Ford, J. Roberts, S. Zhou, G. Fong and J. Rigelsford, *Reconfigurable Frequency Selective Surface for Use in Secure Electromagnetic Buildings*, Electronics Letters, Volume:49 , Issue: 14, pp. 861-863, July 2013.

[7] A. Chauraya, R. Seager, W. Whittow, S. Zhang, and Y. Vardaxoglou, *Embroidered Frequency Selective Surfaces on Textiles for Wearable Applications*, Antennas and Propagation Conference (LAPC), pp. 388-391, Nov. 2013.

[8] G. Marconi and C.S. Franklin, Reflector for use in wireless telegraphy and telephony, U.S. Patent, 1,301,473 1919.

[9] James S. Yee, Frequency Selective Surface (FSS), U.S. Patent, 5,208,603 , 1993.

[10] F. Bayatpur, *Metamaterial-Inspired Frequency-Selective Surfaces*, Doctorate Thesis, 2009.

[11] Benedikt A. Munk, Periodic Surface for Large Scan Angles, U.S. Patent, 3,789,404 1974.

[12] H. Zhou, S.-B. Qu, J.-F. Wang, B.-Q. Lin, H. Ma, Z. Xu, P. Bai and W.-D. Peng, Ultra-wideband Frequency Selective Surface, Electronics Letters, vol. 48, no. 1, Jan. 2012.

[13] R. J. Langley and E. A. Parker, *Double-Square Frequency-Selective Surfaces and Their Equivalent Circuit*, Electronic Letters, vol.19, no.17, pp. 675-677, 1983.

[14] D. H. Kim and J. I. Choi, Design of a Multiband Frequency Selective Surface, ETRI Journal, vol. 28, no. 4, pp.506-508, Aug. 2006.

[15] Romeu, J., Rahmat-Samii, Y., *Dual band FSS with fractal elements*, Electronics Letters, 35(9):702-703, April 1999.

[16] D. H. Werner and R. Mittra, Eds., *Frontiers in Electromagnetics*, Piscataway, NJ: IEEE Press, ch. 1–3, 1999.

[17] Romeu, J., Rahmat-Samii, Y., *Fractal Elements and Their Applications to Frequency Selective Surfaces*, Aerospace Conference Proceedings, vol. 5, pp. 77-81, 2000.

[18] Benedikt A. Munk, Space Filters, U.S. Patent, 4,125,841 1978.

[19] Z. Sipus, M. Bosiljevac and S. Skokic, *Analysis of Curved Frequency Selective Surfaces*,Final Report, May 2008.

[20] G. Gerini and L. Zappelli, *Multilayer Array Antennas With Integrated Frequency Selective Surfaces Conformal to a Circular Cylindrical Surface*, IEEE Transactions On Antennas And Propagation, vol. 53, vo. 6, June 2005.

[21] I. M. Ehrenberg, S. E. Sarma and B. Wu, *Fully Conformal FSS via Rapid 3D Prototyping* Antennas and Propagation Society International Symposium (APSURSI), July 2012.

[22] G. Sen, S. Mahato, T. Mandal, S. Mondal, S. Majumdar and P.P. Sarkar, *Design of a Wide Band Frequency Selective Surface (FSS) for Multiband Operation of Reflector Antenna*, 5th International Conference on Computers and Devices for Communication (CODEC), Dec. 2012

[23] ANSYS HFSS®, <http://www.ansys.com/hfss>, Last visited on March 2014.

[24] A. Wexler, *Solution of Waveguide Discontinuities by Modal Analysis*, IEEE Trans. Microwave Theory Tech., vol. 15, no. 9, pp. 508–517, Sept. 1967.

[25] H. Loui, *Modal Analysis and Design of Compound Gratings and Frequency Selective Surfaces*, Doctorate Thesis, 2006.

[26] N. Don, A. Kirilenko, M. Bozzi, L. Perregrini , *Numerical Simulation of Frequency Selective Surfaces Perforated with Arbitrarily Shaped Apertures*, Physics and Engineering of Millimeter and Sub-Millimeter Waves (MSMW) Symposium Proceedings, pp. 301-303, 2007.

[27] I. Anderson, *On the theory of self-resonant grids*, Bell Syst. Tech. J., vol. 54, no. 10, pp. 1725-1731, Dec. 1975.

[28] C. K. Lee and R. J. Langley, *Equivalent circuit models for frequency selective surfaces at oblique angles of incidence*, IEE Proc. H, vol. 132, no. 6, pp. 395–399, Oct. 1985.

[29] X. Yao, M. Bai and J. Miao, *Equivalent Circuit Method for Analyzing Frequency Selective Surface With Ring Patch in Oblique Angles of Incidence*, Antennas and Wireless Propagation Letters, IEEE, vol. 10, pp. 820-823, Aug. 2011.

[30] R. F. Harrington, *Field Computation by Moment Methods*, New York, NY: Macmillan, 1968.

[31] R. Mittra, C. H. Chan, and T. Cwik, *Techniques for analyzing frequency selective surfaces - a review*, Proceedings of the IEEE, vol. 76, no. 12, pp. 1593–1615, Dec. 1988.

[32] I. Bardi, R. Remski, D. Perry, and Z. Cendes, *Plane Wave Scattering From Frequency-Selective Surfaces by the Finite-Element Method*, IEEE Transactions On Magnetics, vol. 38, no. 2, pp. 641-644, Mar. 2002.

[33] D. B. Davidson, A. G. Smith, and J. J. van Tonder, *The analysis, measurement and design of frequency selective surfaces*, in Proc. 10th International Conference on Antennas and Propagation, vol. 1, pp. 156–160, Apr. 1997.

[34] CST Microwave Studio ® <https://www.cst.com/Products/CSTMWS>, Last visited on March 2014.

[35] R. Pous and D. M. Pozar, *A frequency-selective surface using coupled microstrip patches*, IEEE Trans. Antennas Propag., vol. 39, no. 12, pp. 1763–1769, 1991.

[36] H. Zhou, S. Qu, B. Lin, J. Wang, H. Ma, Z. Xu, W. Peng, and P. Bai, *Filter-Antenna Consisting of Conical FSS Radome and Monopole Antenna*, IEEE Transactions on Antennas and Propagation, vol. 60, no. 6, June 2012.

[37] H. Zhou, S. Qu, Z. Pei, J. Zhang, B. Lin, J. Wang, H. Ma and C. Gu, Narrowband Frequency Selective Surface Based On Substrate Integrated Waveguide Technology, Progress In Electromagnetics Research Letters, Vol. 22, pp. 19-28, 2011.

[38] J. P. McKay and Y. Rahmat-Samii, *Multi-Ring Planar Array Feeds for Reducing DiffractionEffects in the Compact Range*, AMTA Proceedings, pp. 7-3–7-8, Columbus, OH, Oct. 1992.

[39] B. R. Mahafza, *Radar Systems Analysis and Design Using MATLAB*, Chapman and Hall / CR, 2000.

[40] Data Sheet, *RT/duroid® 5870 /5880 High Frequency Laminates*, ROGERS Corporation

[41] Technical Data Sheet, Loctite® 401™, Henkel Technologies, June 2007.

[42] MMS – Microwave Measurement Systems < http://www.mmstech.com/free-space-systems.aspx>, Last visited on May 2014.

[43] C. Pelletti, G. Bianconi, R. Mittra and A. Monorchio, *Analysis of Finite Conformal Frequency Selective Surfaces via the Characteristic Basis Function Method and Spectral Rotation Approaches*, IEEE Antennas and Propagation Letters, vol. 12, pp. 1403-1407, 2013.